Schädler, G., Berg, P., Düthmann, D., Feldmann, H., Ihringer, J., Kunstmann, H., Liebert, J., Merz, B., Ott, I., Wagner, S.

Flood Hazards in a Changing Climate

Project Report

Center for Disaster Management and Risk Reduction Technology

KIT - University of the State of Baden-Wuerttemberg and
National Research Center of the Helmholtz Association

Helmholtz Centre Potsdam
GFZ German Research Centre for Geosciences

Flood Hazards in a Changing Climate

G. Schädler [*] , P. Berg [*], D. Düthmann [†] ,
H. Feldmann [*], J. Ihringer [‡] , H. Kunstmann [§] ,
J. Liebert [‡], B. Merz [†], I. Ott [§],
and S. Wagner [§]

January 2012

[*]Institute for Meteorology and Climate Research (IMK-TRO), KIT, Hermann-von-Helmholtz-Platz 1, Bldg. 435, 76344 Eggenstein-Leopoldshafen, Germany
[†]Deutsches GeoForschungsZentrum GFZ (Sektion 5.4, Hydrologie), Telegrafenberg, C4 2.14, 14473 Potsdam
[‡]Institut für Wasser und Gewässerentwicklung (Bereich Wasserwirtschaft und Kulturtechnik), Geb. 10.81, Otto-Amman-Platz 1, 76131 Karlsruhe
[§]Institute for Meteorology and Climate Research (IMK-IFU), KIT, Kreuzeckbahnstraße 19, 82467 Garmisch-Partenkirchen, Germany

Center for Disaster Management and Risk Reduction Technology (CEDIM)

Contents

1 Introduction

The climate is changing all over the world, and due to the inertia of the climate system, the rate of change will be beyond the reach of any mitigation effort for the next few decades. Adaptation to the changing climate is the remaining option. However, not all regions of the world are affected to the same degree, and local assessments of changes are thus necessary to plan for adaptation of infrastructure in order to maintain current safety standards. Projected changes in temperature and precipitation make it plausible to assume an increase in the risk of extreme flood events. Global projections of future climate at global and regional scales have, however, large uncertainties, which must be assessed to provide a better informed basis for adaptation decisions. This project aims to contribute such information.

1.1 Climate Change in Germany

Over the 20th century, temperature has increased at a higher rate in Germany than the global mean, with largest increase in winter [Arbeitskreis KLIWA, Heft 5]. Connected to these temperature trends are an increase of hot days (maximum temperature above 30°C) and a reduction of ice days (maximum temperature below 0°C). Therefore, it is very likely that the potential evapotranspiration will increase in summer. Furthermore, duration and thickness of snow cover in winter are expected to decrease further. This can have an impact on the timing and amount of runoff due to snowmelt.

It is expected that the above average warming in Germany will continue into the near future with stronger increases in winter than in summer [Christensen et al., 2007]. Temperature is projected to increase during the 21st century for all of Europe with higher rates than the global mean temperature [Christensen et al., 2007]. The changes projected by different GCMs for temperature are more homogeneous than for precipitation.

For precipitation, the past changes in Germany are difficult to assess. A large inter-annual variability makes it difficult to extract statistically significant trends for mean precipitation. In general, slight increasing trends are found in winter over large parts of Germany, wheras in summer the trends are more heterogeneous with mostly no change or a slight decrease [Arbeitskreis KLIWA, Heft 5]. Trends for precipitation extremes are stronger, however the changes depend on the season and region studied [Trömel and Schönwiese, 2007, Zolina et al., 2008, Arbeitskreis KLIWA, Heft 8].

For the 21st century, mean precipitation is expected to increase in the north and decrease in the south of Europe. This expectation is based on a climate projection from an ensemble study with GCMs, carried out in connection to the AR4 IPCC-report [Christensen et al., 2007]. It was also shown that the ensemble not only produces such a pattern over Europe, but that the individual members agree significantly on the sign of the changes in the north and south respectively. The transition zone between increase and decreases, which includes central Europe and Germany, shows only weak changes and the GCMs do not even agree on the sign of the change.

Whereas mean precipitation shows only weak changes for central Europe, there are significant changes to the distributions of precipitation intensities projected [Boberg et al., 2010]. These changes are such that there is a decrease in the weaker intensities, and a corresponding increase

of the higher intensities. In other words, the precipitation events are becoming more intense. Note that this intensification of precipitation has been found also for regions where precipitation overall decreases [Christensen and Christensen, 2004, Frei et al., 2006]. RCM studies of Germany have shown that the variability of precipitation is increasing for the next few decades, with larger changes for more extreme events than for more moderate events [Schädler et al., 2010, Feldmann et al., 2011].

1.2 Changes in Flood Discharges

Flood discharges are sensitive not only to changes in precipitation amounts and the distribution over the year, but also to changes in precipitation intensities and the timing of snow melt. There are several possible drivers for trends in flood frequency. Besides changes in climate, changes in flood discharges may also be caused by land use and land cover shifts, river training works or the construction of dams and reservoirs, and it is challenging to clearly attribute changes in flood hazards to its drivers [Merz et al., 2012]. Longer records and inventories of historical flood events show distinct phases of increased and reduced flood frequency (e.g. [Sturm et al., 2001]), i.e. there is a clear natural variability in the flood records. Such natural variability can further complicate the attribution of trends to the climate change phenomenon.

For the 20th century, studies of changes in flood discharges over Germany mostly showed that there are only few gauges with significant trends in very long time series, however, more significant increasing trends are found if the time period being studied is constricted to the last 40–50 years [Bormann et al., 2011, Villarini et al., 2011]. Using a common time period (1951–2002) for catchments larger than 500 km^2, the spatial characteristics of the trends have been studied [Petrow and Merz, 2009]. Increases in the annual maximum flood trends were found for a third of the gauges in western and southern Germany. In winter, increasing trends were found in a diagonal band from northwest to the southeast of Germany, whereas in summer there were decreasing trends for eastern Germany and increasing trends for southern Germany.

For the 21st century, studies using single model projections have shown heterogeneous results for extreme flood events in Germany [Dankers and Feyen, 2008, Linde et al., 2010, Hurksman et al., 2010, Menzel and Burger, 2002]. As these studies only made use of one or few projections, and a different one in the different studies, the results from each single study might be overconfident. Larger projects have investigated changes in the river discharges using multi-model projections, including different GCMs, RCMs, HMs, and initializations [Kay et al., 2009, Veijalainen et al., 2010, Graham et al., 2007, Wilby and Harris, 2006]. The general result from such studies is that the GCM and natural variability have a large impact on the results, followed by the RCM, HM and finally the emission scenario used, although the HM and RCM position in the scale differs between studies. In general, and for Germany in particular, there is a lack of such multi-model simulations of discharge assessments, however with this project and the ongoing BfG (Federal Institute of Hydrology) project KLIWAS (http://www.kliwas.de/) this is beginning to change.

1.3 Outline of the Project

Focusing on changes in flood discharge, this pilot study aims at promoting the use of ensembles combining climate and hydrological models for scenario based projections, in order to assess the involved uncertainties. The near future time period of study (2021–2050) was chosen such that it conforms with that of the planning horizons of local water resource management systems, i.e. at about 30–50 years. Three focus catchments of medium and small size were selected: Ammer, Mulde and Ruhr. Such smaller catchments have faster response times to meteorological events,

and thus put high demands on the meteorological input data. High resolution RCM simulations were therefore carried out.

The ensemble, built with global climate models, regional climate models and hydrological models, was constructed such that the main sources of uncertainty are sampled. From earlier projects there are clear results that the emission scenario has a small impact on the results for the near future. This is because the different scenarios of the IPCC start to differ significantly only after about year 2050. Thus only the A1B scenario is used in this project. Physical models of nature, such as GCMs, RCMs and HMs, are ultimately limited by our understanding of the physical processes. Differences between similar models and the way they are handled, e.g. GCMs, yield different descriptions of the world, and it is often not possible to determine which one is more correct. The main idea behind model ensemble studies is that multiple models will produce a distribution of plausible results, which encapsulates the real world result.

This report has the following structure: the focus catchments are described in chapter 2, general information about the models used (GCMs, RCMs, HMs) are given in chapter 3, results of the RCM and HM simulations are shown in chapter 4, and the report ends with discussion and conclusions in chapter 5.

2 Catchment Descriptions

Three catchment areas were studied in this project. They represent the different flood regimes in Germany as described by Beurton and Thieken [2009]: dominant winter floods in the Ruhr as typical for central and western Germany, winter but also spring and summer floods in the Mulde as typical for north and east Germany, and summer floods in the Ammer as typical for southern Germany. The Mulde and the Ruhr catchments are medium sized and include low mountain ranges, whereas the Ammer is smaller with more alpine characteristics, see fig. 2.1. Such catchments react faster to heavy precipitation than large catchments and thus present a more immediate flood risk. The following sections describe each catchment in more detail.

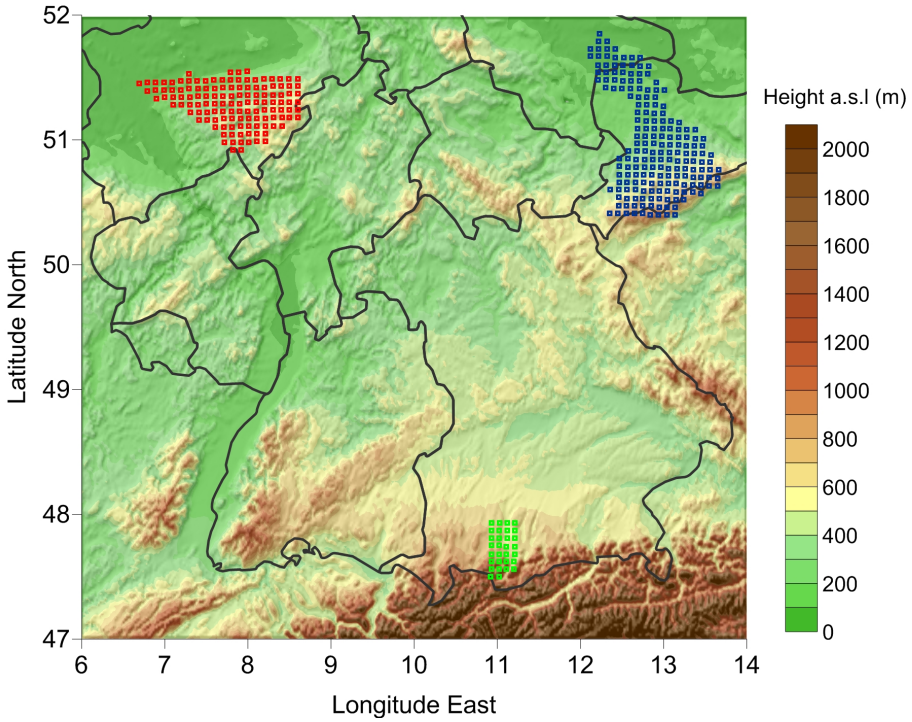

Figure 2.1: Map of the topography of Germany, with the catchment locations marked as red (Ruhr), blue (Mulde) and green (Ammer).

2.1 Ammer

The Ammer catchment is located around 50 km south-west of the Bavarian capital city Munich and covers an area of 710 km^2. It is part of the Danubian river system. The Ammer is the most important tributary for the Lake Ammersee, which discharges into the Amper and finally disembogues into the River Isar. An overview of the catchment and its subcatchment areas is shown in fig. 2.2 (left).

The transition from an alpine to a prealpine landscape causes distinctive heterogeneity in hydrological reactions results. The elevation of the outflow into Lake Ammersee is at 533 m

altitude, the highest altitude within the catchment area is the Kreuzspitze at 2185 m asl. (see fig. 2.2(right)). This elevation difference causes high spatial geological and pedological variability, a complex terrain and also various climatological conditions [Marx et al., 2006].

The two main landscape units, the Swabian-Upper Bavarian foothills of the Alps and the prealpine hilly countryside with moorland contain four geological units: the limestone-alpine and the flysch zone in the southern part of the catchment area followed by molasses and unfolded molasses in the northern part. The whole region is shaped by glacial deposition and selective glacial erosion creating lake basins as side effect [Taschner, 2003].

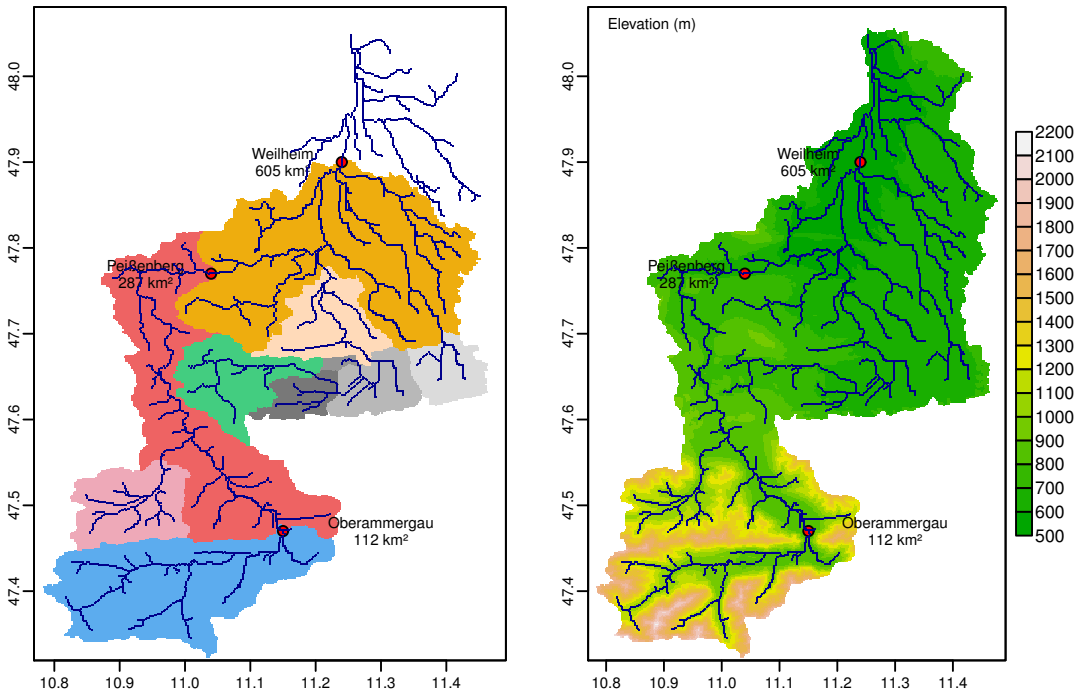

Figure 2.2: Subcatchments of the Ammer catchment with selected gauging stations (left) and orography of the Ammer catchment (right).

The soil formation in the Ammer catchment started in the Late Glacial. Due to lack of development time the present soils are in an initial stadium. The thickness of the soils is furthermore determined by slope and erosive processes [Ludwig, 2000]. The major vegetation units are grassland and woodland (mostly coniferous forest), with increasing percentage of forest in the southern part of the drainage basin. Especially the prealpine area is characterized by agricultural cultivation. The climate is cool-temperate and humid with a maximum of precipitation in the summer months (about 65% of yearly rainfall). The average precipitation amount is 1300 mm per year, in the southern part up to 2000 mm can occur. On a monthly scale, maximum precipitation in the alpine region reaches values of more than 200 mm in July compared to the prealpine zone with 150 mm in June [Kunstmann et al., 2004]. Snow cover occurs during approximately 130 days per year. The average temperature varies between 7–8 °C but can drop to 4.5 °C in the high mountain areas of the southern catchment. Due to the relief all climate variables have altitude-dependent gradients.

The geological conditions of the Ammer catchment area cause a very heterogeneous flow density. Accordingly the surface drainage of the gravel field in the northern part of the basin is very low, in contrast it is comparatively high at the ground moraine overlayed molasses. Further, it is assumed that in the southeast of the catchment, water drains subterraneously into

the adjacent drainage basin of the Loisach River [Kunstmann et al., 2006b].

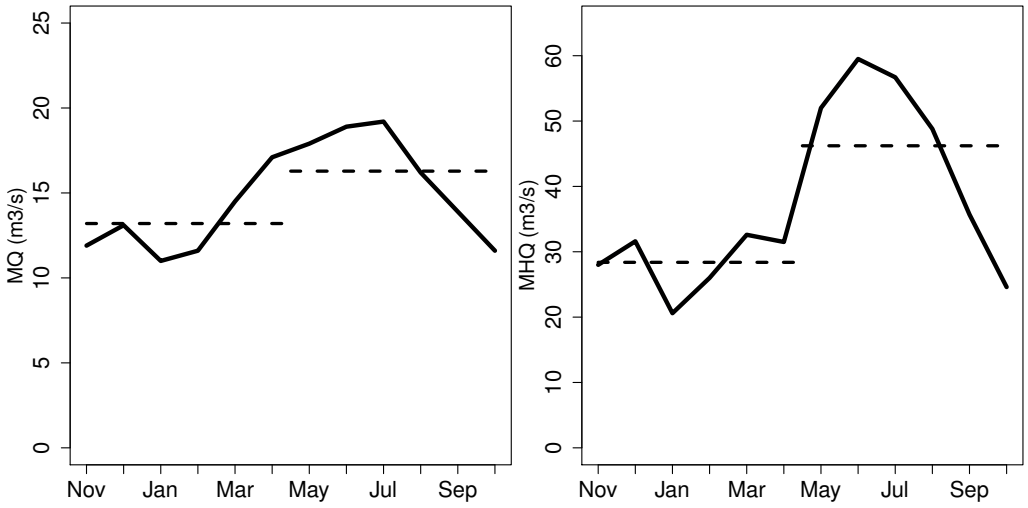

Figure 2.3: Mean monthly discharge (left) and mean maximum monthly discharge (right) for gauging station Weilheim, time series 1971-2000.

The flow regime of the River Ammer is influenced by two factors: On the one hand by the summer precipitation maximum and on the other hand by snow melt in spring. According to this, maximum monthly discharge values occur in May in alpine subcatchments and in June and July for the downstream subcatchments. Characteristic discharge curves (MQ and MHQ) for the time period 1971-2000 at the gauge Weilheim are shown in fig. 2.3.

The Bavarian flood information agency (Hochwassernachrichtendienst HND) characterizes the extent of inundation by four flood levels. They specify suitable water levels for every gauge which can be converted to discharge volume. Level 1: Little overflowing. Level 2: Agricultural land and forest areas are flooded or minor traffic obstruction on main and rural roads. Level 3: Several built-up areas are flooded or blocking of supra-local transport links or sporadic activation of dyke associations or rescue units is necessary. Level 4: Built-up areas are flooded to a greater extent or activation of dyke associations or rescue units is required on a large scale (NaDiNe 2011)[1].

In recent years the highest flood warning level four has been reached a few times in the Ammer catchment. At the gauge Oberammergau with an average discharge of 3.72 m^3/s, gauge level four means a runoff of at least 167 m^3/s. Maximum discharge values of 181 m^3/s during the flood in August 2005 and 168 m^3/s in May 1999 were measured. The downstream gauge Weilheim has an average discharge of 15.4 m^3/s. The highest flood level implies a runoff of 334 m^3/s. This level was recently exceeded in 1970 (38 m^3/s), 1999 (650 m^3/s) and in 2005 (550 m^3/s). Table 2.1 shows the flood levels and historical flood events for three gauges in the Ammer catchment area (source HND[2]).

[1]Natural Disasters Networking Platform, Gauge levels.
http://nadine.helmholtzeos.de/risks/flood/info/glossary/gauge_levels_en.html (08.07.2011)
[2]Hochwassernachrichtendienst HND: http://www.hnd.bayern.de/ (01.07.2011)

$[m^3/s]$		Oberam-mergau		Peißen-berg		Weil-heim
Average discharge		3.72		8.93		15.4
Level 1		38		105		146
Level 2		49		134		-
Level 3		-		167		212
Level 4		167		274		334
Historical flood events	Date					
	Jun. 1959	126	Aug. 1970	286	May 1940	400
	Jul. 1966	135	Jul. 1993	192	Jul. 1946	461
	May 1999	168	May 1999	365	Aug. 1970	338
	Aug. 2002	125	Aug. 2000	201	May 1999	649
	Aug. 2005	181	Aug. 2005	314	Aug. 2005	549

Table 2.1: Flood level definitions and historical floods for the Ammer catchment.

2.2 Mulde

The Mulde River is located in Eastern Germany. It drains the northern part of the Ore Mountains and is a tributary of the Elbe River. The catchment area up to the gauge Bad Dueben is 6171 km^2. The largest subbasins in the upper part are, from West to East, the Zwickauer Mulde, the Zschopau and the Freiburger Mulde. After confluence of these rivers over a relatively short river stretch they form the Vereinigte Mulde in the lower part of the catchment (fig. 2.4 left). The southern part of the catchment is mountainous and elevations reach up to 1244 m, to the north elevations decrease (fig. 2.4 right). The land cover is 30% forest, 52% arable, 7% grassland, and 9% residential. However, these are not equally distributed: forest areas are concentrated in the mountainous part of the catchment, and in the lowlands the dominant land use is agriculture. Mean annual precipitation increases from values around 600 mm in the lowlands to more than 1000 mm in the Ore mountains, where it increases from the eastern to the western part. Resevoirs in the Mulde catchment (14 reservoirs above an ordinary storage of 1 million m^3 or a flood protection storage of 0.1 million m^3, [LfULG, 2009]) are mainly used for drinking water supply, but also serve for flood protection.

The monthly discharge regime is characterized by high flows in March/April caused by rain and snowmelt, and minimum flows during the summer months (fig. 2.5). Monthly maximum flows mostly show two peaks in spring and in summer. Floods in summer occur less often than in spring but can be very severe. Petrow et al. [2007] assigned circulation patterns to all events of the annual maximum series of 15 gauges in the Mulde catchment. They showed that the frequent small flood events in winter are often caused by westerly cyclonic conditions. Several of the large summer floods (e.g. 1954, 2002) are caused by a Vb circulation pattern. It is characterized by a low pressure system moving from the Mediterranean Northeast towards Central and Eastern Europe, and leads to intensive rainfall in the Northern part of the Alps and Central and Eastern Europe.

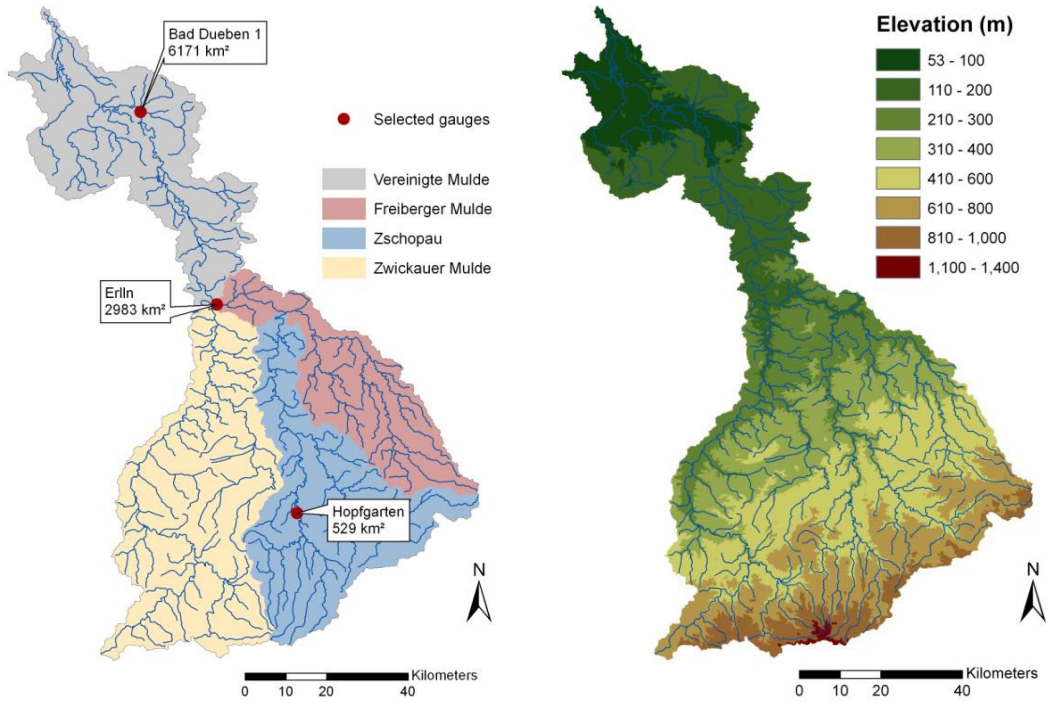

Figure 2.4: Subcatchments of the Mulde catchment with selected gauging stations (left) and orography of the Mulde catchment (right).

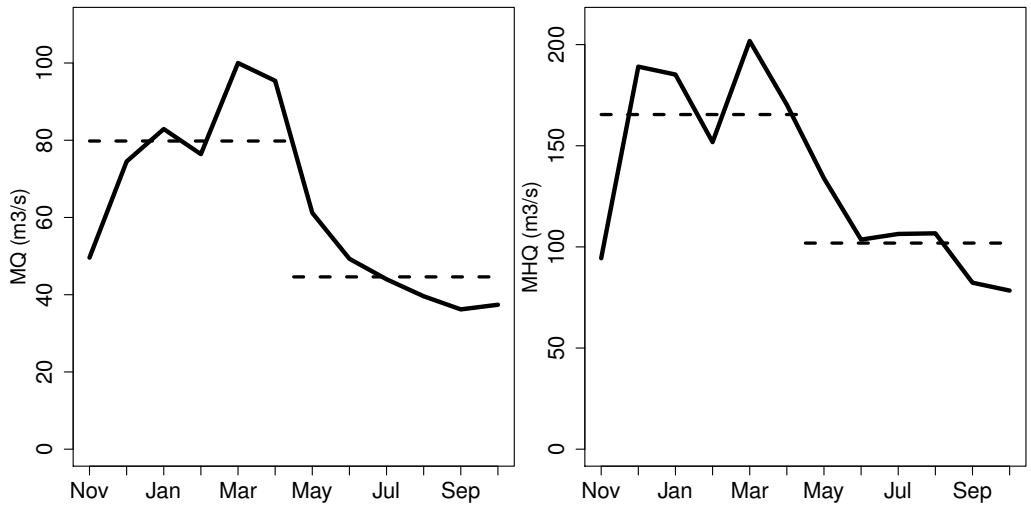

Figure 2.5: Mean monthly discharge (left) and mean maximum monthly discharge (right) for gauging station Bad Dueben, time series 1971-2000.

The most severe known flood in the Mulde catchment was the August 2002 flood. Total losses in Germany caused by the 2002 flood were estimated to be 11.6 billion euro [Thieken et al., 2006].Towns in the Mulde catchment which were very severly affected are for example Eilenburg and Grimma, where the whole historic center was flooded. Return intervals up to 180 years were assigned in the Zwickauer Mulde, and return intervals above 200 years and up to over 400

years were attributed to most gauges in the Freiberger Mulde, Zschopau and Vereinigte Mulde [LfULG, 2009]. The return periods were calculated based on summer and winter events and time series including the 2002 event; if time series excluding the 2002 event are used, much more extreme return intervals are estimated [LfULG, 2009, Schumann, 2005].

Petrow and Merz [2009] analyzed trends in flood frequency over all of Germany for the period 1951–2002. While increasing trends were detected for the annual maximum flood for many gauges clustered in southern and western Germany, hardly any trends were detected for north-eastern Germany (Elbe and tributaries and Aller). Within the Mulde catchment this study included eight gauges. None of these showed a trend for the annual maximum flood; at two gauges an increasing trend in the winter maximum flood and at another two gauges a decreasing trend in the summer maximum flood was observed. Petrow et al. [2007] additionally also performed a regional trend analysis for 15 gauges in the Mulde catchment with normalized annual maximum series, where data from 1936–2002 were included for 13 gauges and data from 1961–2002 were included for another two gauges. This resulted in a slightly positive trend, if the 2002 event was included, and else a slightly negative trend. No trend was found using individual tests for these 15 gauges.

2.3 Ruhr

The Ruhr is a right tributary of the Rhine located in North Rhine-Westphalia. The catchment size is 4485 km^2. The headwaters of the Ruhr are situated in the north-west range of the Rothaargebirge in the Hochsauerland region. The maximum heights in the catchment are up to 850 m. The major sub-catchments are Möhne, Lenne and Volme. The Ruhr basin has a mainly mountainous character and wide parts are covered by forest. Extensive urban areas are located in the lower and outlet part of the catchment. To serve the varied needs in the Ruhr catchment there is a complex water supply and management system with six larger reservoirs and water export in operation [Brudy-Zippelius, 2003].

For the purposes of this project, three representative gauges in the Ruhr catchments were chosen. The criteria for the selection of gauges were aspects of flood relevance, impact through the water management system and the availability of data. The selected gauges are Bamenohl at the upper Lenne above the large Bigge reservoir, Hagen-Hohenlimburg located at the Lenne outlet, and Wetter at the lower Ruhr. There are further gauges, but most of them are not capable of representing the natural hydrological processes in the catchment due to direct effects of the diverse water resources management objectives. For calibration and validation of the hydrological model the other gauges are used as well.

The monthly discharge regime at the Ruhr shows a typical (sub-)mountainous seasonal cycle. High flows in December to March are caused by intensive rainfalls during the winter period (generally due to the frequent westerly cyclonic weather conditions). Snow, respectively snowmelt, are not unusual for flood situations. During the summer months (May–October), distinct low flow conditions dominate. In critical low flow situations (natural and/or through industrial water export) at the lower Ruhr, an artificial water support by the water storage management system in the catchment takes place.

In the last two decades some major flood events in the Ruhr catchment occurred [Höfer et al., 2010]. The highest water levels were measured at the turn of the year 1993 to 1994, followed by the flood event in October/November 1998. In August 2007, one of the rare summer floods occurred. The water levels in August 2007 are partly the highest ever measured in the summer half year in the Ruhr catchment. The flood damages at the Ruhr over the last 20 years have been mostly manageable. The reason is that even the main floods have not significantly exceeded the critical design values in the regions with high potentials of loss. In terms of annual return

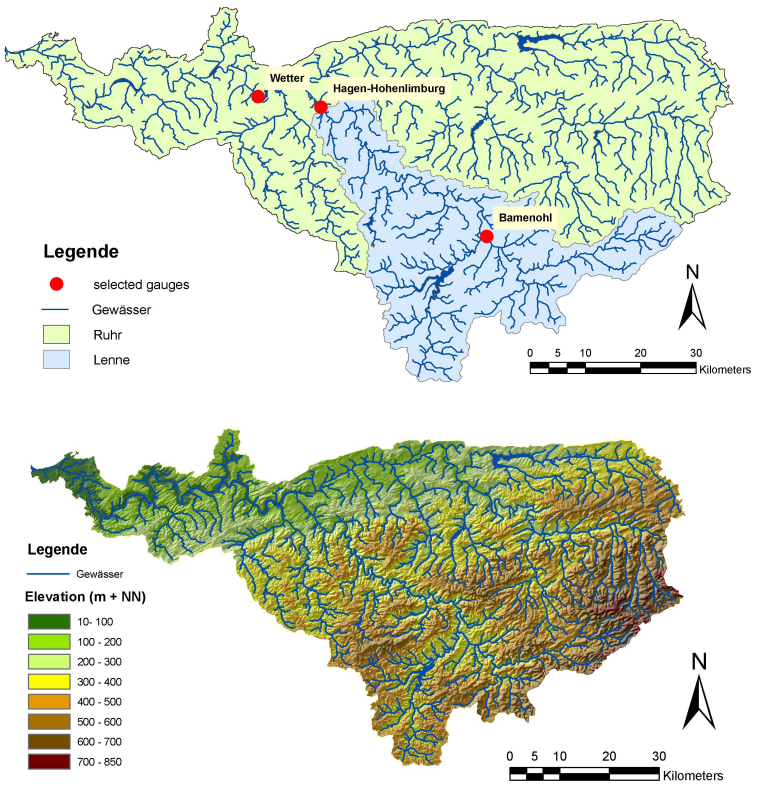

Figure 2.6: Subcatchments of the Ruhr catchment with selected gauging stations (top) and orography of the Ruhr catchment (bottom).

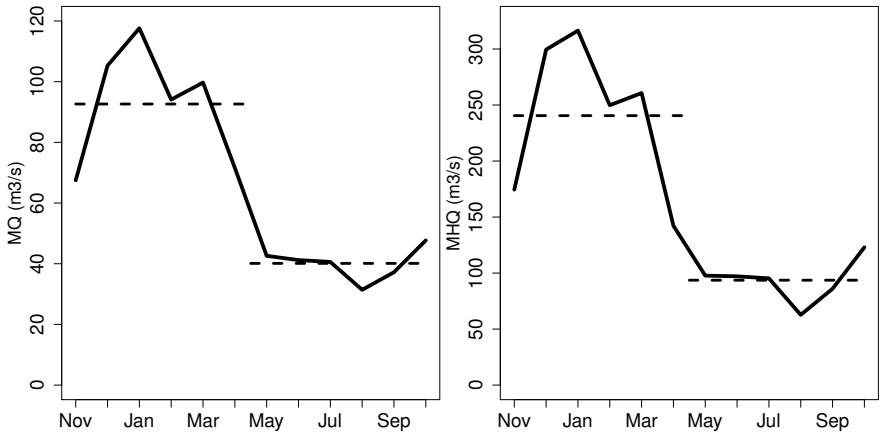

Figure 2.7: Mean monthly discharge (left) and mean maximum monthly discharge (right) for gauging station Wetter, time series 1971-2000.

periods none of the major events in the last two decades exceeded HQ40, i.e. an event that occurs on average every 40 years, at the main gauging station at Ruhr and Lenne.

3 Models and Observations

3.1 Model Chain

The atmosphere is a chaotic dynamical system with interactions on all spatial (and temporal) scales. To assess climate change for a smaller region, one therefore still has to start with the global scale. Computational limitations make it unfeasible to perform high resolution climate simulations for the whole Earth, so instead a method of nesting of regional models within global models is commonly used to bridge the gap in resolution between the GCMs (typically 200 km) and the HMs (here less than 10 km). There are multiple sources of uncertainties in any climate change projection, and the chain of models needed to perform regional assessments introduces further uncertainties.

Fig. 3.1 shows a schematic of the model chain used in this project. The base for any future change assessment rests on an emission scenario. We are here using the so-called SRES scenarios [Nakicenovic et al., 2000] made for IPCC, and since they are all similar in their emission pathways for the next few decades, only one scenario is used. Other emission scenarios can be considered to be small perturbations, and would thus only provide estimates of the natural variability in this case. Two base simulation periods are used: the period 1971–2000 for the control simulation, and 2021–2050 for the future A1B scenario.

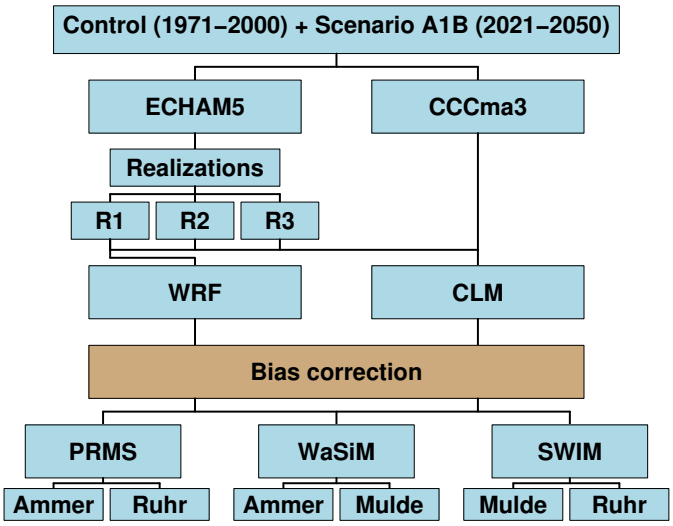

Figure 3.1: Schematic of the model chain used in the project "Flood Hazards in a Changing Climate"

Two GCMs from the IPCC-AR4 ensemble of simulations are used for further downscaling. One is the ECHAM5/MPI-OM [Röckner et al., 2003] model from MPI-M in Hamburg, and the other the CCCma3 model [Scinocca et al., 2008] from Environment Canada. As was shown in the regional climate change chapters of the IPPC-AR4 report [Christensen et al., 2007], there is a large discrepancy in the climate change signal resulting from different GCMs for central

Europe. It is therefore crucial to use multiple models for this kind of assessment. The GCMs used are two of the globally better performing models of the IPCC-AR4 ensemble [Reichler and Kim, 2008]. For the ECHAM5-MPI/OM model, a set of three different realizations, i.e. simulations with different initial conditions and therefore different temporal evolution, was used. These simulations encompass the natural variability of the atmosphere, which is a first step in analyzing the significance of a climate change signal.

To downscale the GCM simulations to a horizontal resolution of about seven kilometers suitable for HMs, two different RCMs are used: CLM [Doms and Schättler, 2002] by IMK-TRO and WRF [Skamarock et al., 2008] by IMK-IFU. Details on the models are given in Berg et al. [2011b]. The reason for using more than one RCM is similar to the use of different GCMs; different parameterizations and physical schemes can provide different results, each being equally plausible. The influence of the RCM is therefore assessed in this step.

Both GCMs and RCMs produce some kind of bias in their simulations, which can cause problems when coupled to an HM [Wilby et al., 2000]. A bias correction methodology was developed for the project and applied to each of the RCM simulations to alleviate some of these problems. The methodology and its application is explained in Chapter 3.5.

The last step of the model chain are the HMs: WaSim from IMK-IFU, SWIM from GFZ, and PRMS from IWG. The HMs are described in Chapter 3.3. The decision was taken that each of the HMs should perform simulations for two catchments, so that each catchment is simulated by two HMs. In total, an ensemble of 10 simulations is available for each catchment.

3.2 Atmospheric Models

An overview of the atmospheric models is given in Table 3.1. The base of the climate projections are two GCMs, namely the CCCma3 and ECHAM5. These global numerical models include representations of the physical processes of the atmosphere, cryosphere, oceans and land surface. The model simulations follow a procedure of an initial spin-up of the full system over several thousand years, until a quasi-stable equilibrium (there are always oscillations around the equilibrium state, i.e. natural variability) between the ocean and atmosphere is reached. At this time, an emission scenario simulation (starting with the well known early industrial emissions of the 20th century) is introduced to the model. This will cause the model to leave its equilibrium and follow the climate change scenario. Depending on the time the emission scenario is introduced to the model, it will be in different natural variability states. This constitutes the difference between the three so-called realizations of the ECHAM5 model simulations in this project. More information on the GCMs can be found in Berg et al. [2011b] and references therein.

Model	Short name	Resolution	Reference
ECHAM5-MPI/OM	E5	T63/L32	Röckner et al. [2003]
CCCma3	C3	T47/L31	Scinocca et al. [2008]
COSMO-CLM	CLM	50 km/7 km	Doms and Schättler [2002]
WRF	WRF	42 km/7 km	Skamarock et al. [2008]

Table 3.1: Short information on the atmospheric models used in the project.

Due to high computational demands, the GCMs are using horizontal resolutions of several hundred kilometers, which is too coarse for this project. A downscaling procedure using dynamical RCMs is therefore applied. The RCMs are run offline within the boundary fields produced by the GCM, a so-called one way nesting. To bridge the resolution gap of several hundred kilometers without too large differences between the resolutions, a double nesting procedure is used:

first, the RCM downscales the GCM data to the coarse nest resolution of around 50 km for all of Europe, and in a second step, the RCM is nested withing the coarse nest and downscales the model fields further to a 7 km resolution, see fig. 3.2. Detailed information on the RCMs (CLM and WRF) can be found in Berg et al. [2011b] and references therein.

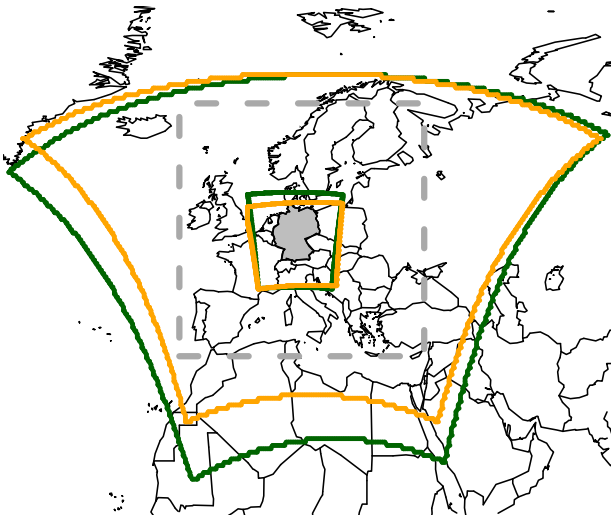

Figure 3.2: Map of the simulation domains indicating the first and second nests of CLM (green) and WRF (orange). Originally in Berg et al. [2011b].

3.3 Hydrological Models

3.3.1 WaSiM-ETH

3.3.1.1 Model description

The water balance simulation model WaSiM-ETH [Schulla and Jasper, 2007] is a deterministic, fully distributed modular model for the simulation of the terrestrial water balance using physically-based algorithms for the vertical fluxes. For instance, soil moisture in the unsaturated zone is calculated with the Richards equation [Richards, 1931] and the potential evapotranspiration according to Penman-Monteith [Monteith, 1975]. Actual evapotranspiration is estimated using a relation between soil moisture and actual capillary pressure. Groundwater fluxes are calculated by a two-dimensional flow model which is dynamically coupled to the unsaturated zone. Other lateral fluxes like direct runoff and interflow are treated in a lumped manner. Surface runoff is routed to the sub-catchment outlet using a subdivision of the catchment into flow time zones. For considering retention, a single linear storage approach is applied to the surface runoff in the last flow time zone. Translation and retention of interflow is treated accordingly. Discharge routing in the river bed channel is based on a kinematic wave approach. The model structure of WaSiM is shown in fig. 3.3. Primary WaSiM was developed for estimating the impact of climate change to an alpine catchment [Schulla, 1997]. In recent years it was also

successfully applied to flood forecast in small and medium sized catchments [e.g. Jasper et al., 2002, Cullmann, 2006, Marx et al., 2006, Pakosch, 2011] and used world wide e.g. in the Middle East or West Africa [Kunstmann et al., 2006a, Wagner et al., 2009].

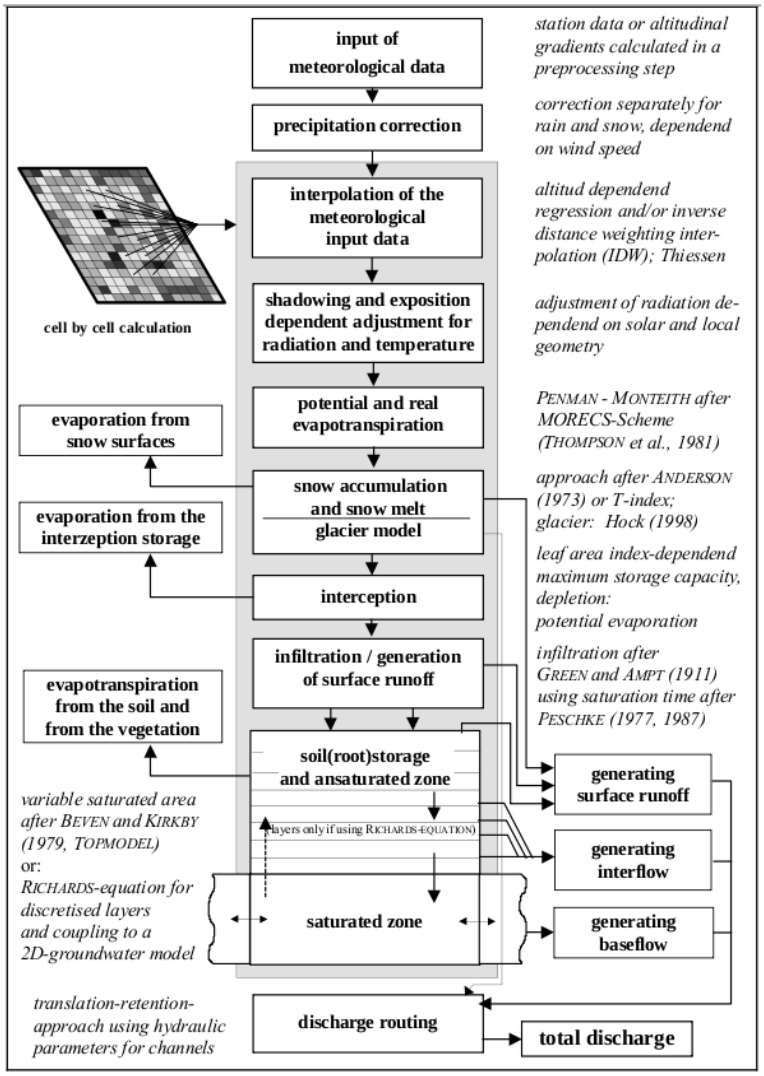

Figure 3.3: Model structure of WaSiM-ETH. Originally in Schulla and Jasper [2007]

3.3.1.2 Data sources and preprocessing

WaSiM is applied for the Ammer and the Mulde catchments. To simulate the water balance and runoff characteristics, WaSiM needs three input data grids describing the area. First, a digital elevation model (DEM) which is available for both catchment areas in a resolution of 100 m. For the Mulde drainage basin the elevation model was aggregated to a 400x400 m grid to reduce computation time. Second, digital soil maps are required at the same resolution as the DEM. Basis for the Mulde catchment is the general soil map of Germany (BUEK 1000), whose soil types were accumulated to 17 representative soils. The soil distribution in the Ammer catchment is based on the geological map of Bavaria (1:500000) [Marx et al., 2006] with resulting 5 soil types. Third, a digital land use map is required mainly for the calculation of evapotranspiration and interception. The land use map of the Mulde catchment results from the CORINE landcover project which includes nine aggregated land use classes. The Ammer catchment is described by

Catchment	Type of data	Description	Sources
Ammer	Met. data	Hourly data of mean temperature, precipitation, solar radiation, relative humidity and wind velocity (2002–2009)	DWD
	Met. data	Daily data of mean temperature, precipitation, sunshine duration, relative humidity and wind velocity (1971–2000)	PIK/DWD
Mulde	Met. data	Daily data of mean temperature, precipitation, sunshine duration, relative humidity and wind velocity (1971–2000)	PIK/DWD
Ammer	Discharge data	Time series of hourly discharge	WWA/HND
Mulde	Discharge data	Time series of daily mean discharge	LfULG
Ammer	Topography	Combination of ERS satellite data, and digital topographic map (1:50000)	RAPHAEL (2000)
Mulde	Topography	DEM Germany 25 m	BKG
Ammer	Land cover data	Landsat-TM data	RAPHAEL (2000)
Mulde	Land cover data	CORINE	EEA
Ammer	Soil data	Geological map of Bavaria (1:500000)	RAPHAEL (2000)
Mulde	Soil data	BUEK 1000 (general soil map of Germany, land use specific version	BGR

Table 3.2: Table of input data sources for the Ammer catchment. *Institute abbreviations: DWD - Deutscher Wetterdienst; DWD/PIK - Data prepared by PIK based on DWD station data [Österle et al., 2006]; WWA - Wasserwirtschaftsamt Weilheim; HND - Hochwassernachrichtendienst Bayern; LfULG - Sächsisches Landesamt für Umwelt, Landwirtschaft und Geologie; BKG - Federal Agency for Cartography and Geodesy; EEA - European Environment Agency; BGR - Federal Institute for Geosciences and Natural Resources.*

nine land cover types generated from Landsat-TM data [Marx et al., 2006].

All input data used for the simulations with WaSiM are shown in Table 3.2. To utilize the information of the DEM, a topographical analysis is necessary. This is carried out using the preprocessing tool TANALYS. It calculates slope, exposition, flow directions, flow accumulation and the river network. In a second step, the catchment is divided into subcatchments.

3.3.1.3 Model calibration

For the Mulde basin, corrected measured meteorological data of the DWD were used to calibrate the model on a daily time step. Station data of precipitation [mm], air temperature [$^{\circ}C$], global radiation [Wh/m^2], relative humidity [-] and wind velocity [m/s] were used. The catchment area with about 6200 km^2 was divided into 11 subcatchments with sizes between 350 and 1000 km^2, namely Niederschlema, Chemnitz, Wechselburg, Hopfgarten, Borstendorf, Lichtenwalde, Niederstriegis, Nossen, Erlln, Golzern and Bad Düben. The calibration period covers the years 1980–1995 with the first year for model initialization. Time series of daily mean discharge data were provided for a total of 45 gauges by the Sächsisches Landesamt für Umwelt, Landwirtschaft und Geologie. River flow was assumed to be natural and no water management interventions were considered.

For the Ammer catchment, an hourly simulation time step performed better than a daily one

due to the small catchment size and the alpine character. Meteorological data from DWD on an hourly time step were only available for the years 2002–2009, which restricted the calibration to this time period. Discharge data in hourly resolution were provided from the Wasserwirtschaftsamt Weilheim (WWA) and the Hochwassernachrichtendienst Bayern (HND).

The Ammer catchment was divided into ten subcatchments whereof five are needed to regulate the reaction of the lakes Staffelsee and Riegsee. For Lake Staffelsee additionally a reservoir with abstraction rules was interposed. The calibrated and representative gauges are Oberammergau, Unternogg, Peißenberg, Obernach and Weilheim with sizes between 40 and 180 km^2. After the successful calibration of the Ammer catchment for 2002–2009, the setup was transferred to the control period from 1971–2000 using daily mean observed meteorological data. For the ensemble analysis, the results of the regional climate models are then again processed on an hourly time step.

3.3.2 SWIM

3.3.2.1 Model description

The model SWIM [Soil and Water Integrated Model; Krysanova et al., 1998] is a semi-distributed, process based eco-hydrological model. The model also simulates plant growth, nitrogen and phosphorus cycling and erosion, however the nutrient cycling and erosion modules were inactivated in this study in order to reduce computation time. The spatial discretization of SWIM is based on subcatchments, which are further subdivided into hydrologic response units (HRUs). The HRUs are areas with the same soil type, land cover, and elevation zone and are assumed to behave hydrologically similar. The model operates on a daily time step.

In the following a brief overview of the approaches for the representation of hydrologic processes implemented in SWIM is given. For a more detailed model description the reader is referred to Krysanova et al. [1998] and Krysanova et al. [2000]. State variables considered in the hydrologic module describe storages for snow, interception, soil water (in different layers), shallow and deep ground water, and water in the river. These stores are interconnected via the following processes: Precipitation is considered as snow when the temperature falls below a threshold temperature, and snowmelt is estimated using a modified degree-day method. Interception is simulated with a simple bucket approach. The sum of rainfall and snowmelt minus interception and evapotranspiration is available for surface runoff and infiltration into the soil. Surface runoff is estimated by a modified version of the Soil Conservation Service curve number scheme, where the curve number is adjusted according to the soil moisture. Additionally surface runoff occurs when the soil is saturated. Soil water above field capacity percolates to deeper soil layers and to the groundwater depending on the hydraulic conductivity and available pore volume of the lower layer. If after percolation soil moisture still exceeds field capacity lateral flow occurs. Potential evapotranspiration (PET) is calculated using the Priestley-Taylor method [Priestley and Taylor, 1972]. For the estimation of the actual evapotranspiration (AET) the method of Ritchie is adopted [Ritchie, 1972]. AET is estimated separately for soil evaporation and plant transpiration, and depends on the soil moisture profile, leaf area index (LAI) and rooting depth. Groundwater is simulated in a conceptual way and represented by two linear stores for shallow and a deep groundwater. Surface runoff, lateral subsurface flow and groundwater all contribute to river runoff, which is finally routed between subcatchments using a Muskingum approach.

3.3.2.2 Data sources and pre-processing

The data sources of input data needed for the SWIM model are summarized in Table 3.3. The catchment was subdivided into subcatchments according to the location of gauging stations.

Type of data	Description	Sources
Met. data	Daily data of maximum, minimum and mean temperature, precipitation, shortwave downward radiation and wind	PIK/DWD
Discharge data	Time series of daily mean discharge	LfULG
Topography	Within Germany: DEM Germany 25 m Outside Germany: SRTM DEM, 90 m	BKG NASA
Land cover data	CORINE	EEA
Soil data	BUEK 1000 (general soil map of Germany, land use specific version	BGR
Water management	Daily data of reservoir inflow, reservoir outflow to river, drinking water abstraction	LTV

Table 3.3: Table of input data sources for the Mulde catchment. *Institute abbreviations: DWD - Deutscher Wetterdienst; DWD/PIK - Data prepared by PIK based on DWD station data [Österle et al., 2006]; LfULG - Sächsisches Landesamt für Umwelt, Landwirtschaft und Geologie; BKG - Federal Agency for Cartography and Geodesy; NASA - U.S. National Aeronautics and Space Administration; EEA - European Environment Agency; BGR - Federal Institute for Geosciences and Natural Resources; LTV - Landestalsperrenverwaltung Sachsen.*

Where it was necessary, additional subcatchment outlets were introduced so that subcatchments did not exceed 100 km^2 as climate data are averaged over subcatchments, which resulted in 85 and 221 subcatchments for the Mulde and Ruhr catchments respectively. The land cover classes from CORINE were aggregated to 9 classes (arable, grass, mixed forest, coniferous forest, deciduous forest, wetland, water, bare soil, residential) and intersected with the soil map and a map of 200 m elevation zones to delineate the HRUs.

Time series of meteorological data were interpolated onto a 1 km^2 grid, and again aggregated to subcatchment average mean values. For temperature universal kriging with elevation was applied, precipitation, humidity and radiation were interpolated using the inverse distance weighting method. Precipitation data were corrected for undercatch errors depending on wind speed and the aggregation state of the precipitation [Yang and Ishida, 1999].

Data from the regional climate models provided at a 7 km resolution were first mapped to a 1 km^2 grid using the nearest neighbour method, and then summarised to subcatchment average mean values. Temperatures were also adjusted for elevation differences between the RCM elevation and the 1km grid using lapse rates calculated from the RCM temperature data over the whole catchment area.

In the Mulde catchment daily data for water abstraction from reservoirs was available for ten resevoirs above an ordinary storage of 1 Mm^3 or a flood protection storage of 0.1 Mm^3. As most of the reservoirs are located in upstream catchments, large parts of the catchment are influenced and the abstractions were taken into account during model calibration, where daily abstraction values were subtracted from the calculated river flow. In the Ruhr catchment only frequency distributions of daily abstractions for three locations (upstream of Villigst, upstream of Hattingen and upstream of Muehlheim) were available. During model calibration a constant mean abstraction according to these data was implemented in the model at these locations, but abstractions were stopped if the discharge at that gauge was below the observed minimum flow (period 1961–1990). However, as no scenarios for future abstractions were available and for

better comparability to the other HMs, the results in chapter 4.2 all show simulations without abstractions.

3.3.2.3 Model calibration

The SWIM model was calibrated using the SCE-UA algorithm [Duan et al., 1992, 1993, Duan, 1994] over a period of five years from 1991 to 1995, and 1990 was used for model initialization. The calibration was performed individually for each subcatchment considering 28 subcatchments for the Mulde and 15 subcatchments for the Ruhr. As objective function a weighted sum of Nash-Sutcliffe efficiency, a modified efficiency giving higher weight to flood peaks, and volume bias was applied. In the Mulde catchment further manual fine tuning took place after the automatic calibration. The performance of the model was evaluated visually with respect to daily flows, average and maximum monthly flow regimes, average and maximum annual discharges, and flow exceedance curves.

3.3.3 PRMS

3.3.3.1 Model Description

The Precipitation Runoff Modeling System (PRMS) is an established hydrological watershed and water balance model originally designed by Leavesley et al. [1983] at the United States Geological Survey (USGS). The PRMS is a deterministic, conceptional distributed model with a modular program design. The spatial discretization is implemented with subcatchments and HRUs. PRMS describes the main components of the hydrological cycle with physical laws or physical interpretable empirical relations. The dynamic variables of the hydrologic processes are integrated in different storage modules [Leavesley and G., 1995]. The HRUs are distributed, finite modeling entities and give a homogeneous runoff reaction to hydro-meteorological events. HRUs may be spatially not continuous. Their assignment usually takes common climate, land-use and underlying soil classification into account.

PRMS calculates the energy and water balance for each HRU on a daily time step. The calculation is based on a hydrologic system with the vertical water flow from the atmospheric input over the storage transformation due to vegetation, snow cover and the soil zone as well as the components of runoff generation and evapotranspiration.

Based on meteorological input data PRMS simulates the hydrological system with its relevant processes from the transforming storages of the vegetation canopy (interception, evaporation), snow cover (snowmelt, evaporation) and soil zone (soil moisture, evapotranspiration) to the discharge generating reservoirs for interflow and groundwater (see fig. 3.4).

In PRMS all components of the hydrologic system that are representing the vertical water and energy flows (so called Soil-Vegetation-Atmosphere-Transfer) are simulated on the basis of the spatially distributed HRUs. The parametrizations of the crucial algorithms can therefore be calibrated for each HRU individually.

Interception by the plant canopy is computed as a function of plant-cover density and the storage available on the predominant plant-cover type in each HRU accounting for the different canopy density during summer or winter periods. PET is calculated using the Haude method [Haude, 1958]. AET is estimated as a function of PET, including first interception-evaporation and evaporation from a potential snow cover. Furthermore, the evapotranspiration from a double layer soil zone as a function of available soil water and soil type is used to account for water losses by plant activity (upper and lower soil zone) and by evaporation processes from the upper soil zone. Surface runoff occurs due to infiltration excess. Infiltration into soil proceeds by a contributing-area concept applying a non-linear function of the antecedent soil moisture. Interflow (linear or non-linear) and groundwater (non-linear) are simulated as

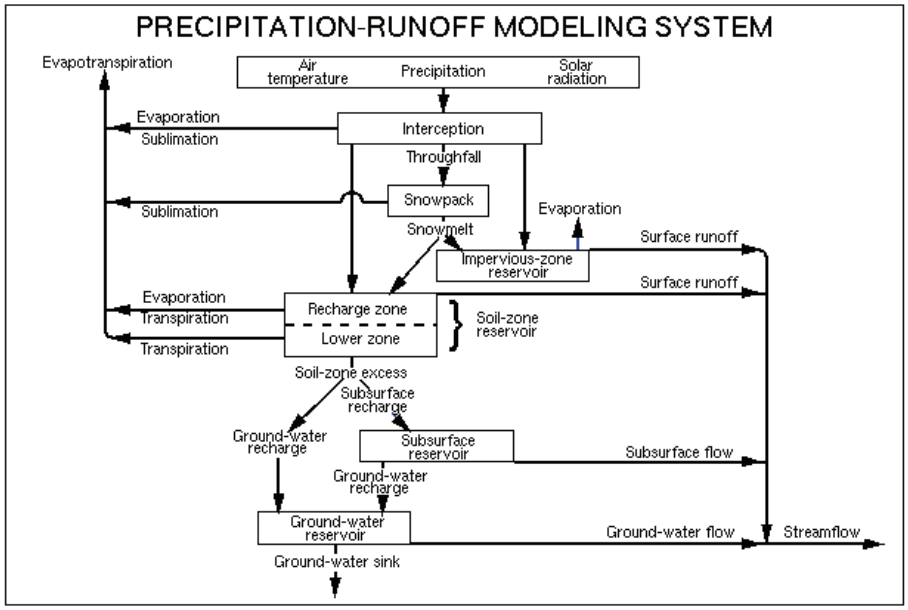

Figure 3.4: The hydrological PRMS model-scheme: as vertically cascading conceptual storages for all relevant compartments and the linking hydrological processes [Leavesley et al., 1983].

conceptual reservoirs linked with each other and with the soil zone, with storage capacities, outflow rates and coefficients determining the dynamics of interflow and groundwater outflow.

To include the translation of the flow parts and the impact of the water resources management systems (e.g. storage and export) in the Ruhr catchment the additional module BEWASYS [Brudy-Zippelius, 2003] is applied. BEWASYS (BEwirtschaftung WAsserwirtschaftlicher SYSteme) is a modular water management model, that allows the balance quantification of natural and artificial water bodies on a daily time step. For the translation the specific times are referred to the actual flow conditions in the HRUs. To handle non-linear correlations between translation time and flow, a stepwise linearisation is adopted. The approximation of the translation time is based on an estimation of the mean time of the flow curve in the channel system [Brudy-Zippelius, 2003].

3.3.3.2 Data sources and pre-processing

The spatial distribution of the Ruhr catchment for the hydrological modeling has to take into account the available gauge stations in the Ruhr basin, the requirements of the HRUs, the basis of any model calculation in PRMS, and a reasonable consideration of significant water management impacts in the BEWASYS add-on. For these purposes the data sources listed in Table 3.4 are used [Brudy-Zippelius, 2003]. The analysis of the Ruhr catchment on that data basis results in a model division of 29 subcatchments and 51 HRUs.

3.3.3.3 Model calibration

The original calibration and validation of the hydrological model system with the water-balance model PRMS and the water management model BEWASYS is performed on the basis of the measurement data (meteorological, discharge, water management) for the hydrological years 1992–1995. Brudy-Zippelius [2003] used a split-sample-test approach. For the primary calibration, the time period 1992–1993 is used and the remaining years 1994–1995 serve as validation

Catchment	Type of data	Description	Sources
Ammer	Met. data	8-hourly data of temperature, precipitation and relative humidity (1990–2001)	DWD
	Met. data	Daily data of mean temperature, precipitation and relative humidity (1971–2000)	PIK/DWD
Ruhr	Met. data	Daily mean and partial, hourly/8-hourly data of temperature, precipitation and relative humidity (1961–1996)	DWD/ Ruhrverband
	Met. data	Daily data of mean temperature, precipitation and relative humidity (1971–2000)	PIK/DWD
Ammer	Discharge data	Time series of daily/partial hourly discharge data (1971–2000/1990–2001)	WWA/HND
Ruhr	Discharge data	Time series of daily/partial hourly discharge data	Ruhrverband, Staatliche Umweltämter NRW
Ammer	Topography	Combination of ERS satellite data, and digital topographic map (1:50000)	RAPHAEL (2000)
Ruhr	Topography	DEM DGM50	Ruhrverband
Ammer	Land cover data	Landsat-TM data	RAPHAEL (2000)
Ruhr	Land cover data	CORINE	EEA
Ammer	Soil data	Geological map of Bavaria (1:500000)	RAPHAEL (2000)
Ruhr	Soil data	Geologic and pedologic maps of NRW	Geologisches Landesamt NRW
Ruhr	Water management	Diverse records and reports	Ruhrverband

Table 3.4: Table of input data sources for the Ruhr catchment. *Institute abbreviations: DWD - Deutscher Wetterdienst; DWD/PIK - Data prepared by PIK based on DWD station data [Österle et al., 2006]; WWA - Wasserwirtschaftsamt Weilheim; HND - Hochwassernachrichtendienst Bayern; EEA - European Environment Agency.*

period. The performance analysis could be performed for up to 31 gauge stations, depending on the available data.

3.4 Meteorological Data Sets

Station observations of temperature and precipitation are available for long time periods. However, the spatial and temporal coverage of stations are not always satisfactory. When validating model simulations to observations, one has to deal with the problem of comparing spatial means over a grid box, which is the model product, to that of point observations which comes from the stations. A commonly used method is to perform gridding of the observational data to the model grid. This can be carried out with various degrees of refinement, but is mainly performed through interpolation. The resulting grid will be dependent on the station density and temporal coverage, and the gridding procedure. In this section we describe and compare different gridded

observational data sets used for the validation and bias correction of the RCM simulations.

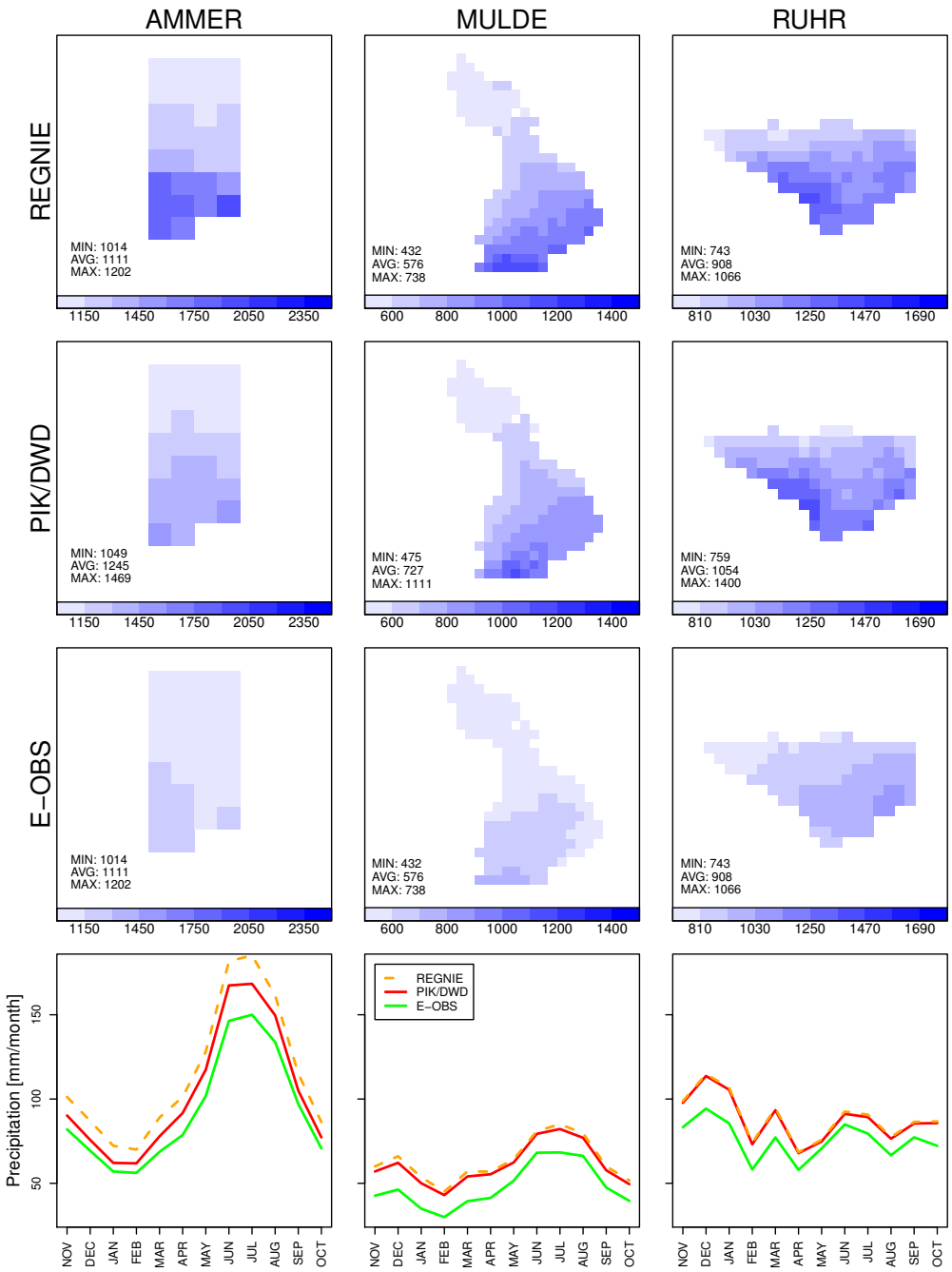

Figure 3.5: Annual mean spatial precipitation distributions (top three rows) for the REGNIE, PIK/DWD and E-OBS data sets. The bottom row shows the annual cycle as monthly means over the catchment areas.

Temperature fields are generally quite smooth, and are therefore less sensitive to the spatial density of the station network. In this project we made use of the E-OBS [Haylock et al., 2008] data set of daily gridded station data for Europe at 50 and 25 km resolution. For validation and bias correction, the data set was first interpolated to the RCM 7 km resolution, and thereafter corrected at each grid point with the standard lapse rate of the atmosphere (6.5 K/km) multiplied

by the difference between the E-OBS and RCM orography. To validate the approach, the data was compared to interpolated station data from GFZ, and only minor differences were found.

Precipitation is a much more heterogeneous variable than temperature, and is therefore much more dependent on spatial coverage of the station data. Three precipitation data sets are investigated here. The first is the REGNIE data set, which is a 1 km gridded product from DWD, which was remapped to the RCM resolution. The second data set is the PIK/DWD interpolated data (directly to the RCM resolution) based on a similar station data network as the REGNIE data, however only using stations that cover the complete control period [Österle et al., 2006]. The third data set is the E-OBS at 25 km interpolated to the RCM resolution. The PIK/DWD and E-OBS data make use of the station data as they are, whereas the REGNIE data set corrects for what is called undercatch. Undercatch is a phenomenon which relates to a deficiency of the station gauges to collect all precipitation, especially under windy conditions [Yang and Ishida, 1999]. The effect is largest when precipitation falls as snow.

Fig. 3.5 shows the mean annual precipitation for the control period at each of the three catchments. There are some minor differences between spatial distribution of the REGNIE and PIK/DWD data sets, but the main distribution is the same. The E-OBS data is much too smooth and does not capture the regional details. The annual cycle, see fig. 3.5, shows that the E-OBS produces lower precipitation amounts than the two others, and that REGNIE is slightly wetter than PIK/DWD. The latter might be due to the effect of under-catch correction.

3.5 Bias Correction Method

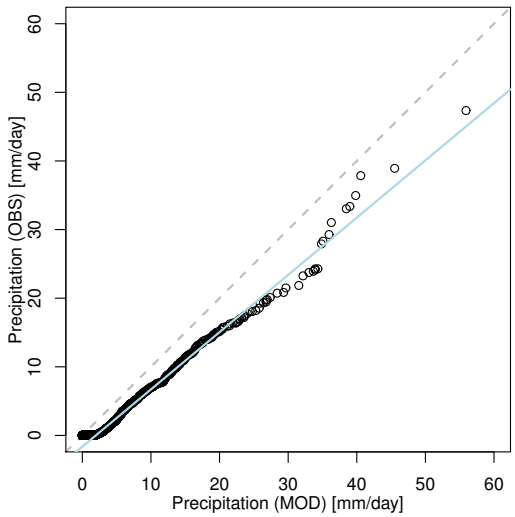

Figure 3.6: Transfer function of a precipitation distribution derived by plotting sorted model data with reference data. A linear approximation to the transfer function is displayed in blue.

HMs are known to be sensitive to bias in the meteorological forcing data [Wilby et al., 2000], partly because they are calibrated with observational station data, and the RCM data must therefore first be corrected for bias. A wet bias in annual precipitation could force the HM into a constantly wet regime, which would have a large influence on the simulated flood characteristics. The bias correction developed within this project takes into account the full distribution of precipitation intensities and temperatures, which also leads to a correction of the mean values [Berg et al., 2011a]. It is here referred to as "histogram equalization" (HE). Other methods, such

as additive removal of the mean bias or scaling of the variable, can produce unwanted effects to the tails of the distribution [Berg et al., 2011a]. Such effects are avoided with the HE approach as it corrects all moments of the distribution.

The HE method can be conceptually explained using fig. 3.6. Given a model and a reference data set of equal length, one can plot them together after sorting the data in increasing order. The result is a perfect empirical transfer function with which one can transfer each single precipitation intensity to the appropriate intensity of the observational data, leading to a perfect agreement between the two distributions. However, such a strict correction only works for data sets of equal length, and for ranges of the distribution which have been observed, so to generalize the function we produce a linear fit to the curve. This was found to be sufficient for most occasions [Berg et al., 2011a].

The Berg et al. [2011a] procedure was applied to the temperature and precipitation results of the fine nest RCM data for each of the catchments using E-OBS data for temperature and REGNIE data for precipitation (see section 3.4). The transfer functions were calculated on a monthly basis.

4 Results

The focus of the project is on changes in discharge, the same focus is therefore also in this chapter. However, to give an overview of the atmospheric driving data and changes thereof, there is a short introductory section (4.1) on the GCM and RCM results at the European and Germany wide scales. More in depth analysis of the atmospheric investigations can be found in the two papers [Berg et al., 2011b] and [Wagner et al., 2011]. In section 4.1.5, the forcing data that are used in the HMs are shown and validated to observational data. The HM results are finally shown in section 4.2 for each catchment.

4.1 GCM and RCM Results

4.1.1 Control

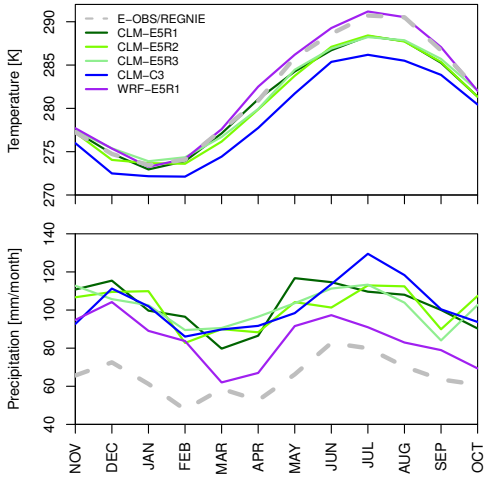

Figure 4.1: Annual cycles of temperature (top) and precipitation (bottom) from the second nest simulations together with observational data for the region of Germany.

An evaluation of the chain of atmospheric models, from the GCM to the coarse nest RCM and finally to the fine nest RCM simulations, was carried out for the variables temperature and precipitation. There are significant biases present for all models of the ensemble, and the biases are often transferred further down the model chain. The CLM simulations have a similar bias as both of the GCMs, i.e. generally cold and wet for central Europe (see fig. 4.3 and fig. 4.4), and thus enlarge the original bias. WRF on the other hand has a warm bias for central-eastern Europe, and thus acts to reduce the original bias of temperature. The CCCma3 GCM has a similar wet bias as the ECHAM5 simulations, but the cold bias is stronger and covers all of Europe. As the RCMs were calibrated in reanalysis driven simulations, the cancellation or amplification of the GCM bias by the RCM is coincidental.

The fine nest simulations follow the bias of the coarse nest simulations, but do not add any significant additional bias. Fig. 4.1 shows the annual cycles of temperature and precipitation

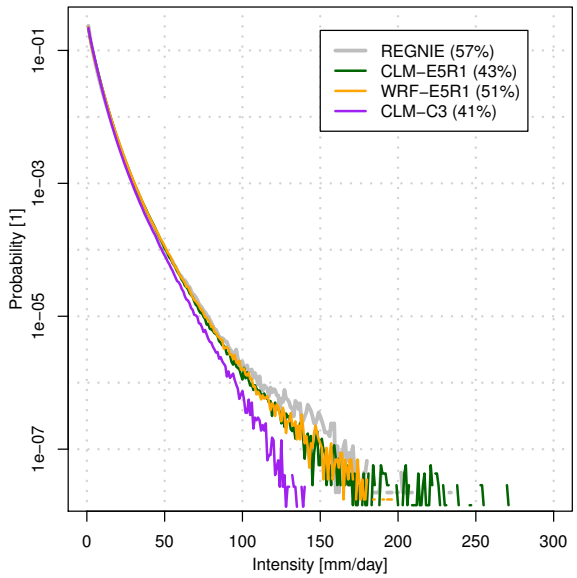

Figure 4.2: Normalised precipitation intensity distribution for the region of Germany of the fine nest. The numbers in the figure legend indicate the dry day probability. Note that only realization one of the ECHAM5 simulations with CLM are shown, for reasons of clarity.

for the ensemble together with the observations. The WRF simulation performs very well for temperature, whereas the CLM simulations with ECHAM5 are cold in winter, and the CCCma3 driven CLM simulation is cold by 2–5 K, with largest bias in winter. For precipitation, the CLM simulations have a wet bias of 40–50 mm/month, whereas the WRF model performs slightly better with 10–40 mm/month wet bias.

The distributions of precipitation intensities of the ensemble are shown in fig. 4.2. All RCM simulations are underestimating the dry day probability, as indicated in the figure legend. A dry day is here defined as a day with less than 1 mm of precipitation. This is due to the so-called drizzle effect of many RCMs, and is particularly strong in the CLM simulations. The low and moderate intensities are overestimated, but the higher intensities are well simulated by all ECHAM5 driven simulations. The CCCma3 driven simulation has problems also for the higher intensities.

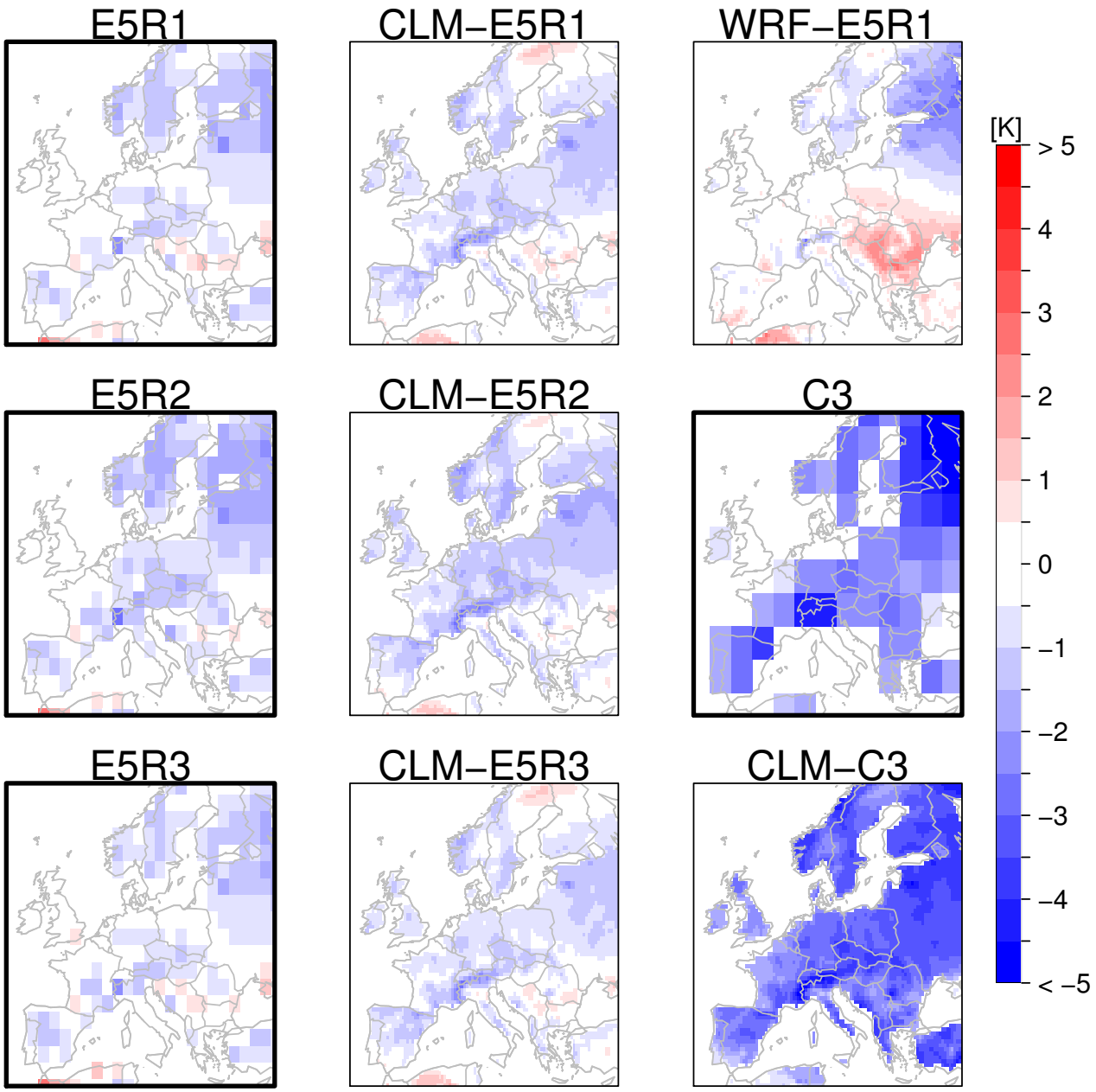

Figure 4.3: Difference maps of annual mean temperature in the control period for the GCM and first nest simulations in comparison to the E-OBS data set. Originally presented in Berg et al. [2011b].

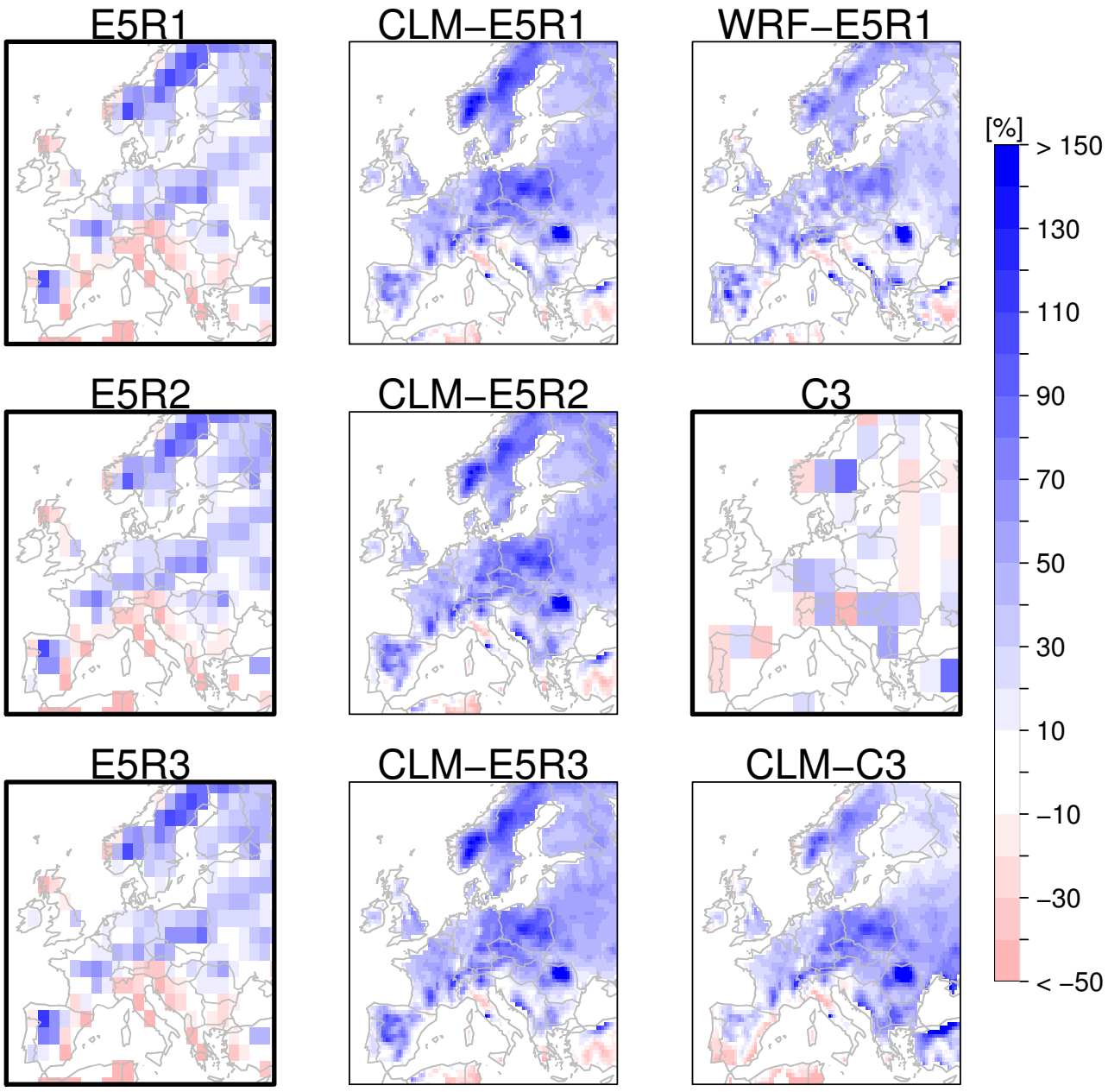

Figure 4.4: Relative difference maps of annual mean precipitation in the control period for the GCM and first nest simulations in comparison to the E-OBS data set. Originally presented in Berg et al. [2011b].

4.1.2 Future Scenario

All GCMs project a significant warming over Europe of about 1–3 K. On the seasonal scale, an increase of mean temperature is present for all applied GCMs and RCMs (not shown). The warming in northern and central Europe is likely to be largest in winter, which agrees with previous results [Christensen et al., 2007]. The RCMs produce similar warmings, however with slightly reduced magnitudes. The patterns and magnitudes vary only slightly between the

ensemble members.

Changes in the seasonal cycle and annual mean temperature averaged over Germany are listed in Table 4.1 for all applied GCM-RCM combinations in the fine nest resolution. Statistically significant temperature changes at 95% confidence level (according to a Student's t test, see Wagner et al. [2011]) are indicated in bold. There is a projected warming for all simulations in all seasons, and consequently also at the annual scale. All annual and most seasonal projected temperature changes are statistically significant. The CCCma3 driven simulation shows a weaker increase in winter, but otherwise similar results as the ECHAM5 driven simulations. The only larger difference between the CLM and WRF simulations driven by the same GCM occurs in summer. In contrast, the selection of the GCM and its initial condition (realization) results in significantly larger differences of projected temperature change for both seasonal and annual averages.

Temperature change [K]	DJF	MAM	JJA	SON	ANNUAL
CLM-E5R1	**1.4**	0.2	**1.1**	**1.5**	**1.0**
WRF-E5R1	**1.6**	0.3	**0.6**	**1.4**	**1.0**
CLM-E5R2	**1.9**	**1.0**	**0.7**	**1.5**	**1.3**
CLM-E5R3	0.7	**0.7**	**0.8**	**1.0**	**0.8**
CLM-C3	**1.0**	**0.9**	**1.2**	**1.3**	**1.1**
Ens. mean	1.3	0.6	0.9	1.3	1.0
Ens. sd	0.5	0.3	0.3	0.2	0.2

Table 4.1: Projected fine nest seasonal and annual mean temperature changes [K] averaged over Germany between 1971 to 2000 and 2021 to 2050 for the CLM (CLM-E5R1-3 and CLM-C3), and WRF (WRF-E5R1) simulations, plus the ensemble mean and standard deviation. Numbers in bold are statistical significant at the 95% confidence level.

The south-north contrast in precipitation changes across Europe, which is described in Christensen et al. [2007], is also indicated by the GCMs applied in this ensemble. The projected changes of the three realizations of ECHAM5 differ in their magnitude, but the overall pattern is the same, see fig. 4.5(left column). For Germany, the different realizations of ECHAM5 produce varying magnitudes of precipitation increase. To assess the projected changes of precipitation in comparison to the natural variability, the change patterns are compared to differences between different realizations, see fig. 4.5. A pattern with similar magnitudes like the projected dipole can be found when studying the differences of e.g. realization three and two for the control period. This means that the projected pattern could arise by chance from natural variability. However, the consistency of the pattern for different GCMs of this and earlier projects indicates that the pattern is significant.

The CLM downscaling of ECHAM5 indicates a similar pattern of changes in annual precipitation, whereas WRF downscaling tends to a slightly positive annual precipitation change. The climate change signal of the CCCma3 GCM is in the same range as that of ECHAM5 realization three, but the CLM downscaling intensifies the climate change signals compared to the CCCma3 GCM. On the seasonal scale, precipitation change patterns for the applied GCMs for winter and autumn are similar to the annual one (not shown). But for spring positive precipitation change signals are also projected for central and eastern Europe except for ECHAM5 realization three. In summer, the projected precipitation decrease signal is more extended in space and magnitude compared to the annual one, except for the WRF simulation which produces an increase in mean precipitation from the north-east of the domain into central Europe. Note, however, that the precipitation is simulated differently by the different models as it is a sum of multiple processes within each single model. Differences in the end result can therefore differ between a

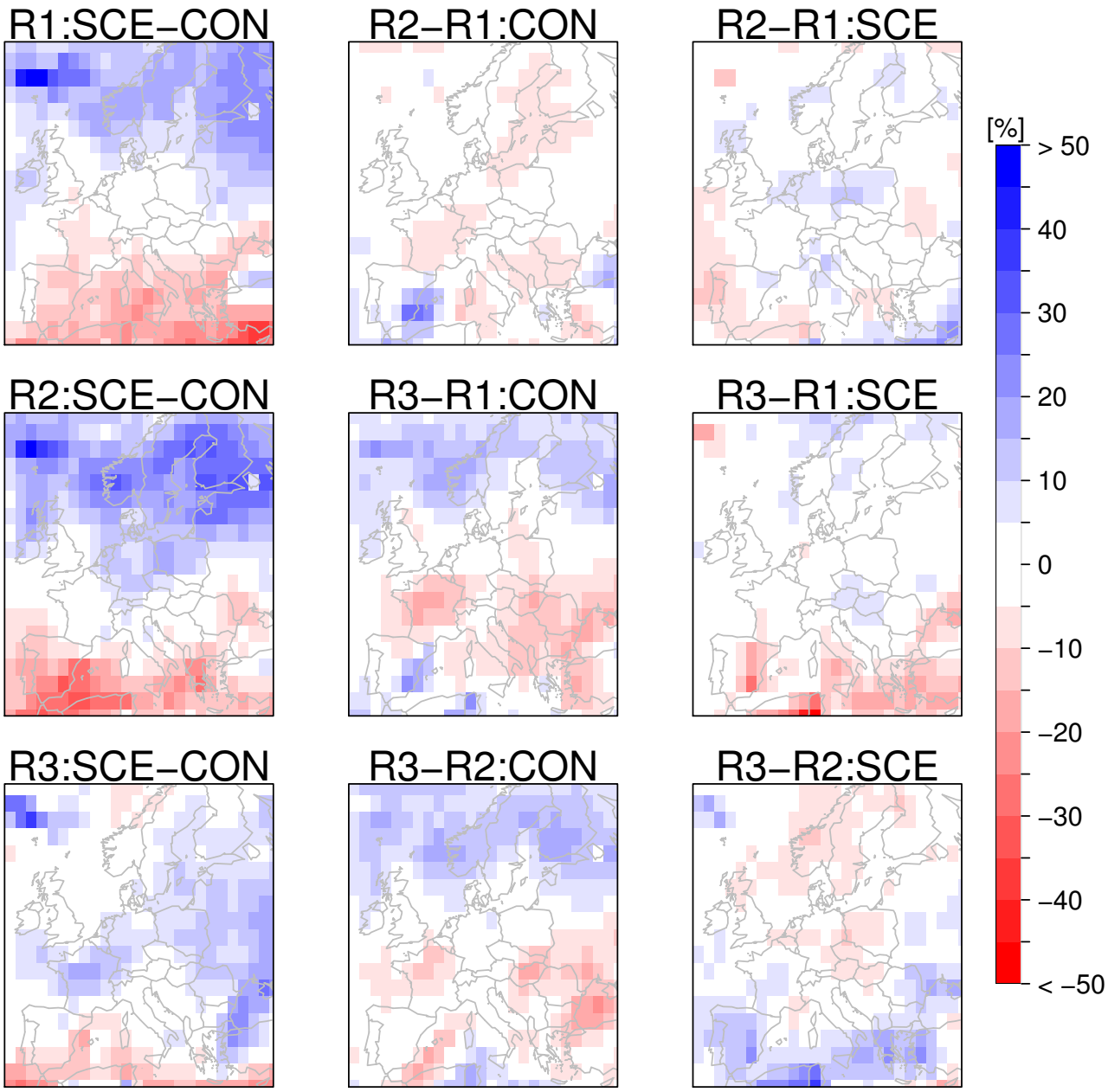

Figure 4.5: Climate change signal in precipitation (relative changes) for the different realizations of the ECHAM5 GCM simulations (left column). The differences between the different realizations for the control (middle column) and future scenario (right column) periods show that the differences are of some ± 10–20 %.

GCM and an RCM due to the parameterizations used, and is not necessarily a result of resolution. The CLM and ECHAM5 uses a more similar parameterization of precipitation, i.e. the Tiedtke scheme [Tiedtke, 1989], and have similar results, whereas the WRF simulation uses the Kain-Fritsch scheme [Kain, 2004], which might explain the different result for summer.

Overall, the GCM and coarse nest RCM analysis shows that the impact of different GCMs

on the simulation results is in the same order of magnitude as the applied initial conditions (realizations) of the GCM. Furthermore, the impact of the RCM on the climate change signal is more dominant for precipitation as compared to temperature, which causes more heterogeneous patterns of the precipitation signal on both seasonal and annual scales, see fig. 4.6.

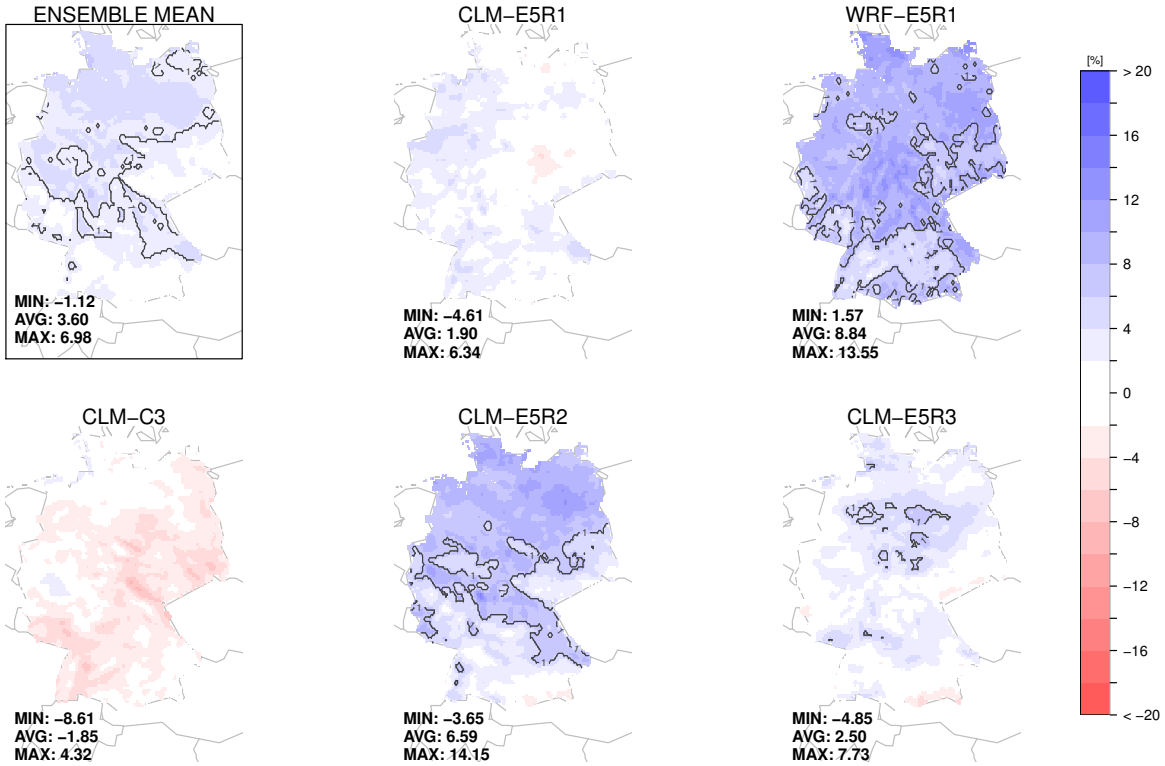

Figure 4.6: Projected annual relative precipitation changes over Germany for the RCM ensemble. Contours delineate regions with statistically significant changes at the 95% level.

Projected changes on seasonal and annual scales averaged over Germany are listed in Table 4.2. The values are highly variable over both season and model. There are a few significant changes for some models in some seasons, but an overall analysis shows that there are no statistically significant changes in mean precipitation for Germany. Comparing the CLM and WRF simulations driven by the same GCM, it is clear that also the RCMs respond differently to the same driving data.

Fig. 4.7 shows the projected changes of the probability density function (PDF) of wet day precipitation intensities, defined as days with at least 0.1 mm of precipitation. Generally, the models show a shift of the PDF toward more extreme values at the cost of the weaker intensities. Similar changes have been shown also for other models in larger ensemble assessments [Boberg et al., 2010]. The intensity distributions of the CLM and WRF models are comparable indicating a decrease of lower precipitation intensities and an increase for higher intensities. The change point is approximately at 6 mm/day. WRF produces slightly higher decreases of lower intensities and higher probabilities in particular for moderate intensities in the range of 10 and 20 mm/day compared to the CLM driven ECHAM5 realization one simulation. Different realizations of the GCM also impact the precipitation PDFs. When the CCCma3 GCM is used as driving model,

Precipitation change [%]	DJF	MAM	JJA	SON	ANNUAL
CLM-E5R1	1.3	5.0	-7.9	9.3	1.9
WRF-E5R1	0.4	**15.9**	6.9	12.9	**8.8**
CLM-E5R2	**12.3**	**12.8**	-0.6	1.8	**6.6**
CLM-E5R3	9.6	-0.7	-5.0	6.0	2.5
CLM-C3	-3.7	6.8	**-8.9**	-1.6	-1.9
Ens. mean	4.0	8.0	-3.2	5.7	3.6
Ens. sd	6.7	6.6	6.2	5.7	4.2

Table 4.2: Projected fine nest seasonal and annual mean precipitation changes [%] averaged over Germany between 1971 to 2000 and 2021 to 2050 for the CLM (CLM-E5R1-3 and CLM-C3), and WRF (WRF-E5R1) simulations, plus the ensemble mean and standard deviation. Numbers in bold are statistical significant at the 95% confidence level.

the projected precipitation PDF differs significantly from the ECHAM5 simulations, however the general trend of a decrease of lower intensities and an increase of higher intensities is also present, but first the magnitude of the projected change is less, and second the change point is shifted to approximately 11 mm/day. The differences in the CCCma3 driven simulation could be due to the bias in the precipitation intensity distribution as presented in fig. 4.7. The shift of the change point is an interesting result in comparison to Boberg et al. [2010], where the change point was found to be remarkably similar between different GCM and RCM combinations.

The analysis of this ensemble in simulating present climate [Berg et al., 2011b] and projected climate changes for Germany [Wagner et al., 2011] have shown the benefit but also remaining uncertainties of the high resolution regional simulations. This means that subsequent climate impact studies, e.g. for the assessment of changes in flood hazard, have to be aware of and cope with these uncertainties. Hence, ensemble approaches are required to include the variations of the projected climate change signals in impact studies.

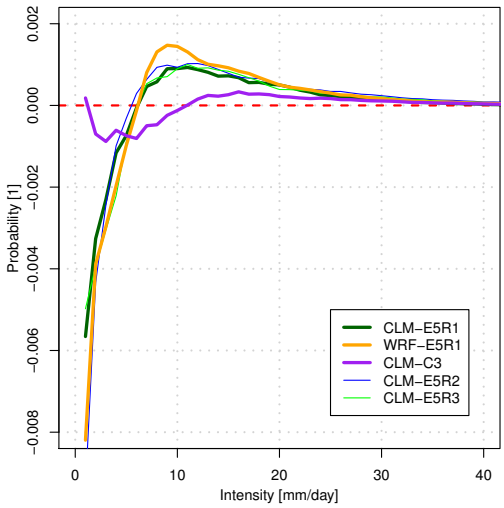

Figure 4.7: Projected change of precipitation PDFs over Germany between 1971 to 2000 and 2021 to 2050 for the (CLM-E5R1-3 and CLM-C3) and WRF (WRF-E5R1) simulations.

4.1.3 Impact of Bias Correction

The most important task of the bias correction is to correct the mean values of temperature and precipitation. However, a more advanced bias correction was applied to the RCM simulations of this project in order to ensure a good distribution of precipitation intensities. The applied method, presented in section 3.5, was investigated in detail in Berg et al. [2011a]. They used a similar observational data set, but applied the correction for an area covering entire Germany and its near surroundings. It was further shown that the HE method performs well in correcting the precipitation distribution, including the dry days. The drizzle effect in the RCM simulations, especially strong in the CLM model, could be corrected well by removing the lowest precipitation intensities. Whether the "correct" events were removed was investigated through the distribution of consecutive dry day periods, see Berg et al. [2011a]. This distribution is close to that of the observations, indicating that drizzle events that shortened the periods for the original simulation were removed correctly. The mean characteristics were corrected almost perfectly, including also the spatial distributions. It was further shown that there is no significant impact of the bias correction on the mean climate change values, but that there are changes in the shift of the precipitation intensity distribution, as shown in fig. 4.8.

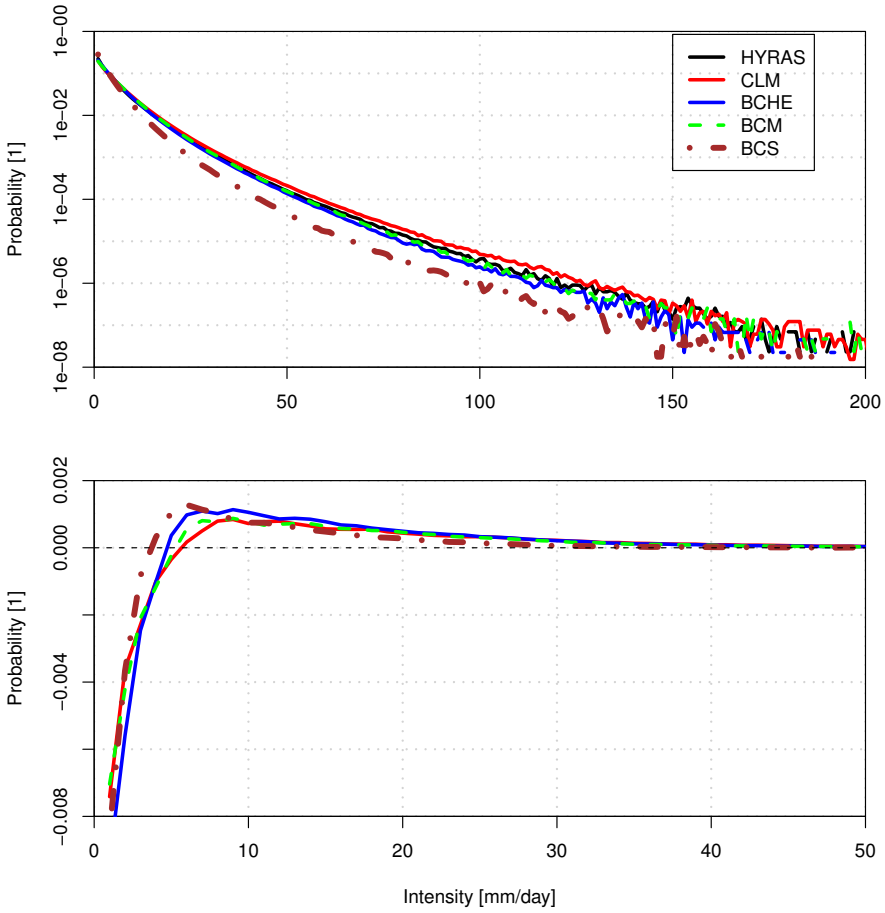

Figure 4.8: Spatially averaged wet day precipitation distributions for the observations (solid black), the original model data (solid red), as well as for the HE method (solid blue), and two other simpler methods (dashed green and dot-dashed brown). Results are presented for the control period (top) and as differences between the future scenario and the control period (bottom). Note the change in the horizontal and vertical scales for the two panels.

4.1.4 Ensemble Analysis

The result for each ensemble member for the changes in mean values of temperature (in degrees) and precipitation (in percent) for entire Germany is shown for each season in fig. 4.9. Confidence intervals were estimated using a bootstrap approach, and are indicated for the 90% level in the figure. There is a clear increase in temperature in all simulations, however the magnitude of the increase varies with the GCM, RCM and season. The precipitation changes are more heterogeneous. Below, the variations in the climate change signals are discussed according to three sources of uncertainty: (i) natural variability, (ii) GCM and (iii) RCM.

The natural variability is here assessed through the three realizations of the ECHAM5 GCM downscaled by the CLM RCM. These are indicated with dark green, blue and light green colours and numbers one to three in fig. 4.9. The largest spread between the simulations is in the winter months (DJF) where the temperature change ranges from about 0.6–1.9 K, and precipitation changes by about 2–12% increase. The spread is lowest in summer, with temperature changes from 0.7–1 K and precipitation changes from 2–8% decrease.

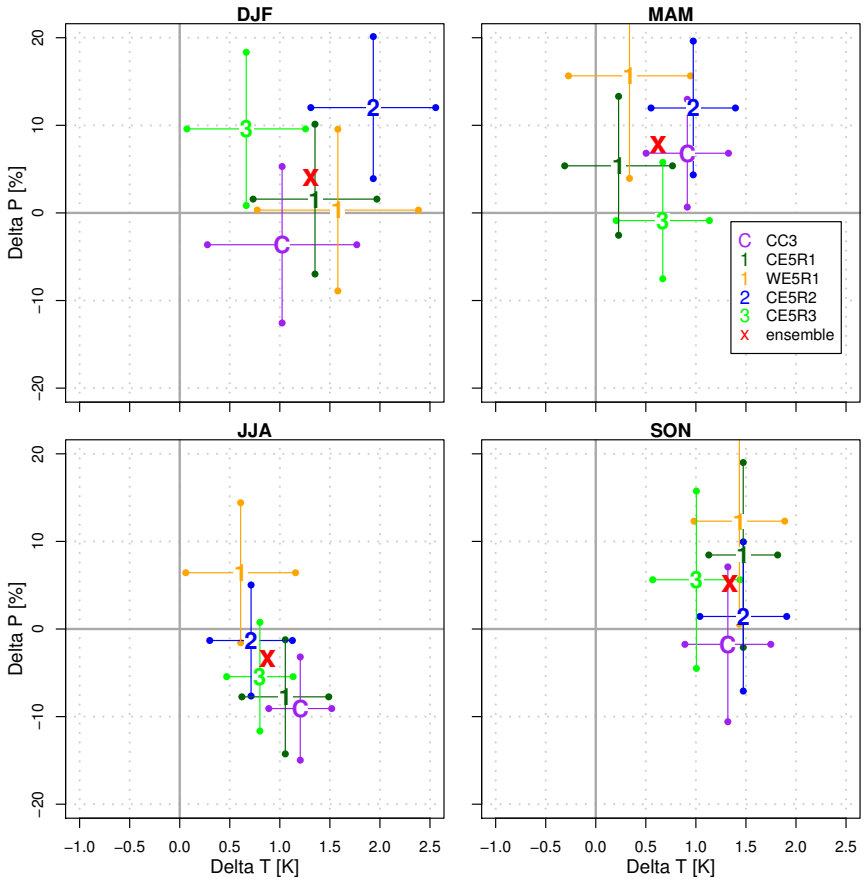

Figure 4.9: Seasonal changes in precipitation (vertical axis, shown in percent) and temperature (horizontal axis, in degrees) for the individual ensemble members. Error bars marking the 90% confidence interval were calculated with a bootstrap approach.

The GCM uncertainty is not well sampled, as only two different GCMs were downscaled, but can be cautiously inferred from the ECHAM5 simulations and the CCCma3 simulation with the CLM (the latter indicated with a purple "C" in the figure). The CCCma3 climate change signal tends to lie inside the temperature range given by the three realizations of the ECHAM5 model,

with an exception for summer where it indicates a higher temperature increase of about 1.2 K. For precipitation, the CCCma3 simulation tends to lie outside the range given by the ECHAM5 simulations, with a decrease in precipitation for all seasons except spring where it agrees with the increase projected by the ECHAM5 simulations.

The RCM uncertainty is shown through the use of the CLM and WRF, both driven by realization one of the ECHAM5 (indicated in the figure by dark green and orange "1"s for CLM and WRF respectively). The trends of the changes in both temperature and precipitation are in the same direction for all months but summer, however with different magnitudes. In summer, the changes in precipitation differ strongly between the two RCMs, with WRF showing an increase of about 7% and CLM a decrease of similar magnitude. This deviation between the RCMs can be traced to differences in the first nest (about 50 km for CLM and 42 km for WRF) of the downscaling procedure, where the WRF model responds differently to the GCM driving data with an increase of precipitation over central to north-eastern Europe (not shown). This deviation of the WRF model from the precipitation simulations of CLM and the driving ECHAM5 model might be due to the convection scheme, which is practically the same for CLM and ECHAM5, while WRF uses a different one, as discussed in Chapter 3.2. The parameterizations of convective precipitation differ between the two RCMs, and this might be the reason for the deviation in the precipitation changes. In Berg et al. [2011] and Wagner et al. [2011], the REMO RCM, forced by the first two realizations of the ECHAM5 model was compared to the CEDIM-ensemble simulations. The spread in the temperature and precipitation changes are similar to that just described when including also this model, however with a larger spread in winter where the REMO simulations show a decrease in precipitation (not shown).

The overall uncertainty from the three sources investigated here indicates possible larger uncertainties from the driving GCM compared to the natural variability, and clear deviations between the RCMs which could be related to specific parameterizations. Temperature shows consistent increases for all simulations and all seasons, but the uncertainties are larger for precipitation and no general conclusions of the change in the mean precipitation is possible from this analysis. Note that the signal would be much clearer if the CCCma3 downscaling simulations would not be part of the ensemble, which shows the importance of including several GCM models in any assessment of this kind.

4.1.5 Meteorological Forcing Data

The topic of the last section was the general characterization of the RCM results for present and future climate. This chapter is meant to be a bridge between the analysis of the HM results in the following part and the previous discussion. The HMs require precipitation, two meter temperature, two meter relative humidity (all HMs), downward short wave radiation at the surface (WaSiM and SWIM) and ten meter wind speed (WaSiM) as meteorological input data. The input data from RCMs and from observations will be discussed and compared for each catchment in the following sections. An analysis of climate change signals at the catchment scale will be shown in order to show the propagation of the change signals through the model chain. Note that it is the bias corrected values of precipitation and temperature that are presented for the RCMs in this section, as these are the ones used as input to the HMs. Precipitation is the main driver of flood discharges for the catchments studied, and therefore a more detailed investigation of the mean monthly precipitation sums are presented, which can be compared to the MQ results of the HMs.

4.1.5.1 Ammer

The base analysis and calibration for the Ammer catchment is carried out with the PIK/DWD station data at a daily time step. However, the small area and fast hydrological response of the Ammer catchment makes a daily time step of the HM almost too coarse. Therefore, the WaSiM model uses an hourly time step and thus requires the additional DWD data set of hourly data.

	Precipitation [mm/month]			Temperature [°C]			ΔPrecipitation [%]			ΔTemperature [°C]		
	Ann.	WH	SH	Ann.	WH	SH	Ann.	WH	SH	Ann.	WH	SH
DWD/PIK	104	77	132	7	1	13	NA	NA	NA	NA	NA	NA
REGNIE	120	91	149	NA	NA	NA	NA	NA	NA	NA	NA	NA
WRF-E5R1	121	89	153	6	0	11	7.3	6.3	8.3	0.8	0.9	0.8
CLM-E5R1	119	90	148	7	1	12	1.6	6.8	-3.7	1.1	1	1.1
CLM-E5R2	125	95	154	6	1	12	0.7	11.7	-10.4	1.4	1.5	1.2
CLM-E5R3	122	95	150	7	1	12	-2.6	-3.4	-1.7	0.9	1	0.9
CLM-C3	122	93	152	7	1	12	1.7	8.3	-4.9	1.3	1.1	1.5
Ens.	**122**	**92**	**151**	**7**	**1**	**12**	**1.7**	**5.9**	**-2.5**	**1.1**	**1.1**	**1.1**

Table 4.3: Annual (Ann.), winter half year (WH) and summer half year (SH) area means of precipitation and temperature in the Ammer catchment, as well as future changes of the variables.

Table 4.3 shows the observational data of the main influencing meteorological variables, together with the RCM simulated data. The DWD/PIK station data within the catchment shows smaller precipitation sums than the gridded REGNIE data, which was used for the bias correction. This means that even after bias correction, the RCM simulations are overestimating precipitation throughout the year in comparison to the station data. The climate change signals are highly variable, as seen in the country wide analysis, but with a general consistency of increases in winter and decreases in summer. These change signals were also projected within previous investigations [Smiatek et al., 2009]. Temperature is close to that observed, and increases by about 1 °C evenly over the year.

	RH [%]			SW radiation [J/cm^2]			ΔRH [%]			ΔSW radiation [%]		
	Ann.	WH	SH	Ann.	WH	SH	Ann.	WH	SH	Ann.	WH	SH
DWD/PIK	80	82	78	1104	710	1498	NA	NA	NA	NA	NA	NA
WRF-E5R1	69	75	63	1253	776	1730	-0.2	-1.1	0.7	-2.3	-3	-1.6
CLM-E5R1	83	84	83	893	647	1140	-0.5	0	-0.9	-2	-5	1
CLM-E5R2	84	84	83	889	633	1145	-0.4	-0.3	-0.6	-1.8	-3.8	0.3
CLM-E5R3	83	84	83	895	626	1164	0	-0.2	0.1	-0.9	-0.3	-1.4
CLM-C3	84	85	84	870	647	1093	-0.4	-0.4	-0.5	-0.6	-2.4	1.1
Ens.	**81**	**82**	**79**	**960**	**666**	**1254**	**-0.3**	**-0.4**	**-0.2**	**-1.5**	**-2.9**	**-0.1**

Table 4.4: Annual (Ann.), winter half year (WH) and summer half year (SH) area means of SW radiation and relative humidity in the Ammer catchment, as well as future changes of the variables.

Of secondary influence to HMs are relative humidity and short wave radiation, which are presented in Table 4.4. WRF is underestimating relative humidity throughout the year, while overestimating short wave radiation. By contrast, CLM is overestimating relative humidity (and

basically lacks an annual cycle), while underestimating shortwave radiation. The CLM result could be related to a problem with too much cloud cover in the model. A slight decrease is projected for both variables, which is fairly consistent among the different ensemble members.

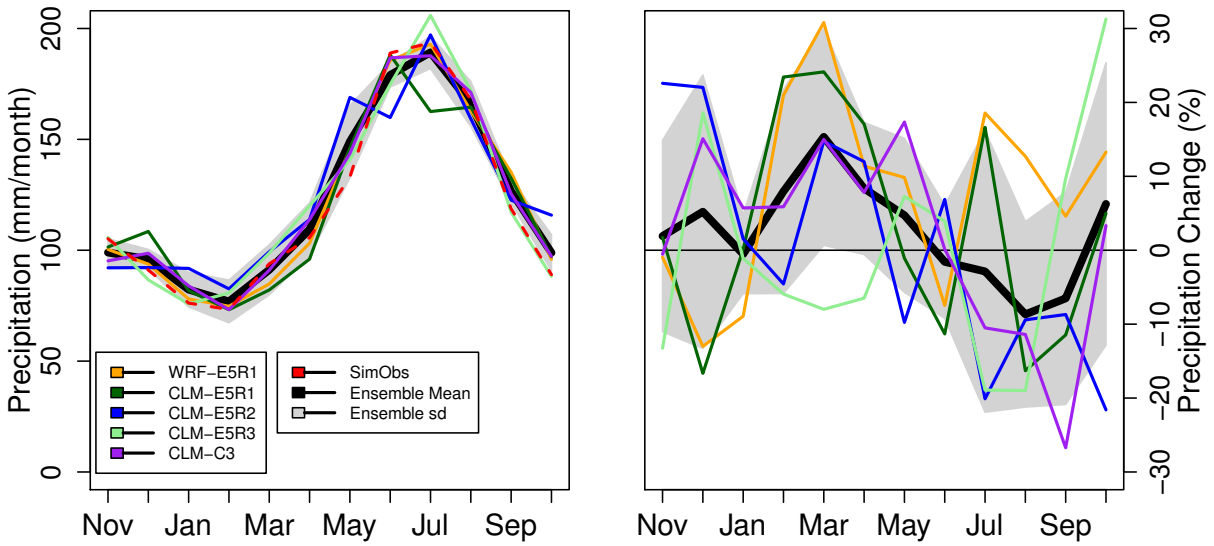

Figure 4.10: Mean monthly precipitation sums in the Ammer catchment for the bias corrected model data in comparison to the REGNIE observations (left), and relative differences between the future and control time periods (right). Shaded areas indicates the enemble spread by one standard deviation.

The annual precipitation in the Ammer catchment is the highest of all selected catchments (up to 200 mm/month, fig. 4.10(left)). The maximum monthly precipitation sums occur during July–August, and the minimum precipitation during January–February. In principle, the RCMs are able to reproduce this annual cycle, although they tend to produce the highest precipitation amount about one month to early, and show a large over prediction in winter (not shown). After bias correction, the annual cycle is well described, and the spread between individual simulations is fairly low.

The relative change between the future and control time periods (fig. 4.10(right)) shows large inter-member variability, but tends to increases in precipitation in spring, and decreases in late summer and autumn. The changes can however not be considered statistically significant.

4.1.5.2 Mulde

The larger Mulde catchment shows a slower reaction to precipitation events than the Ammer catchment, and is therefore simulated with a daily time step. There is one major difference between the SWIM and WaSiM forcing data for Mulde, and that is that the SWIM model is calibrated and validated with undercatch corrected precipitation data. Undercatch is a failure of the precipitation gauges to capture all precipitation when there are e.g. strong winds over the gauge. The undercatch can be estimated for a specific gauge when wind and temperature are known. This was performed with the DWD/PIK data on the input fields for the SWIM model, and showed about a 10% increase in precipitation amounts for winter (where snow worsens the undercatch) and about 7% in summer.

There are similar differences between the REGNIE and DWD/PIK station data for Mulde as for Ammer, i.e. higher precipitation sums for the former, see Table 4.5. The RCMs perform

	Precipitation [mm/month]			Temperature [°C]			ΔPrecipitation [%]			ΔTemperature [°C]		
	Ann.	WH	SH	Ann.	WH	SH	Ann.	WH	SH	Ann.	WH	SH
DWD/PIK	59	52	66	8	3	14	NA	NA	NA	NA	NA	NA
REGNIE	62	55	69	NA	NA	NA	NA	NA	NA	NA	NA	NA
WRF-E5R1	63	55	71	8	2	14	10.1	8	12.1	0.9	1.1	0.6
CLM-E5R1	64	55	73	8	3	14	2.5	8.8	-3.9	1.2	1.1	1.2
CLM-E5R2	63	55	71	8	2	14	7.5	14.6	0.4	1.5	1.8	1.2
CLM-E5R3	64	57	71	8	3	14	0.6	-0.3	1.5	0.9	0.9	0.8
CLM-C3	63	55	72	8	3	14	-2.5	-0.5	-4.5	1.3	1.1	1.5
Ens.	**64**	**55**	**72**	**8**	**3**	**14**	**3.6**	**6.1**	**1.1**	**1.2**	**1.2**	**1.1**

Table 4.5: Annual (Ann.), winter half year (WH) and summer half year (SH) area means of precipitation and temperature in the Mulde catchment, as well as future changes of the variables.

well for temperature and precipitation after the bias correction. Temperature is projected to increase by about 1 °C, and precipitation shows tendencies to increase, although the single members diverge throughout the year.

WRF is underestimating relative humidity in summer, but is close to observations in winter, see Table 4.6. It is overestimating shortwave radiation similarly to the Ammer catchment. CLM also behaves the same as it did for the Ammer catchment, with overestimations of relative humidity, and underestimations of shortwave radiation. The climate change signals show practically no change for relative humidity, but a few percent decrease of shortwave radiation.

The Mulde catchment is the driest of the analyzed catchments. The annual cycle of monthly precipitation (fig. 4.11(left)) is less pronounced than for the Ammer with a secondary maximum in winter. The summer maximum derived from the observations is about 85 mm/month in July. The RCM simulations overpredict the uncorrected precipitation throughout the year, but the shape of the annual cycle is well represented in the ensemble mean (not shown). This holds

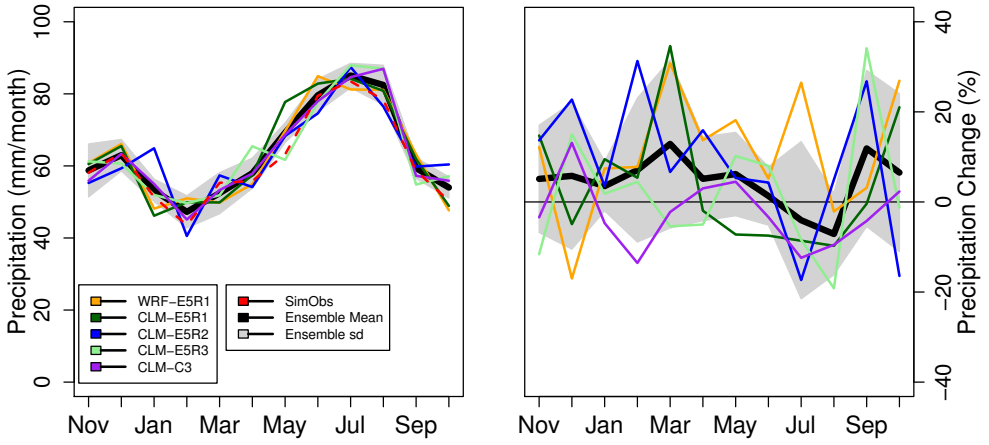

Figure 4.11: Mean monthly precipitation sums in the Mulde catchment for the bias corrected model data in comparison to the REGNIE observations (left), and relative differences between the future and control time periods (right). Shaded areas indicates the ensemble spread by one standard deviation.

	RH [%]			SW radiation [J/cm^2]			ΔRH [%]			ΔSW radiation [%]		
	Ann.	WH	SH	Ann.	WH	SH	Ann.	WH	SH	Ann.	WH	SH
DWD/PIK	78	82	75	998	568	1427	NA	NA	NA	NA	NA	NA
WRF-E5R1	73	82	64	1069	614	1525	0	-1	1	-3.4	-4.9	-1.9
CLM-E5R1	87	88	86	788	541	1034	-0.2	0.2	-0.6	-3.4	-7.8	1
CLM-E5R2	87	88	86	807	539	1076	0.3	0.3	0.3	-5.4	-7.4	-3.4
CLM-E5R3	87	88	86	796	524	1068	0	0.1	-0.2	-2.4	-3.1	-1.8
CLM-C3	87	88	86	801	565	1038	0.1	0.3	0	-2.2	-4.4	0
Ens.	**84**	**87**	**82**	**852**	**557**	**1148**	**0**	**0**	**0.1**	**-3.4**	**-5.5**	**-1.2**

Table 4.6: Annual (Ann.), winter half year (WH) and summer half year (SH) area means of SW radiation and relative humidity in the Mulde catchment, as well as future changes of the variables.

especially for the CLM ECHAM5 simulations. WRF shows a maximum in June and CLM driven by CCCma3 a maximum in August. The spread of the ensemble is smaller than for the Ammer. The bias corrected RCM data stay close to observations.

For the projection period, there is a tendency for a flatter annual cycle. A decrease can be found just in July–August, otherwise the tendency is toward an increase (fig. 4.11(right)). Among the ensemble members WRF predicts an increase most of the year. CLM driven by CCCma3 mostly a neutral to slightly negative change.

4.1.5.3 Ruhr

As for the Mulde, the Ruhr catchment is simulated using a daily time step for both the PRMS and SWIM models. The SWIM model once again uses undercatch corrected data, with similar consequences as described in the previous section.

	Precipitation [mm/month]			Temperature [°C]			ΔPrecipitation [%]			ΔTemperature [°C]		
	Ann.	WH	SH	Ann.	WH	SH	Ann.	WH	SH	Ann.	WH	SH
DWD/PIK	90	94	86	9	4	14	NA	NA	NA	NA	NA	NA
REGNIE	91	95	86	NA	NA	NA	NA	NA	NA	NA	NA	NA
WRF-E5R1	96	103	89	8	3	13	10.5	10.6	10.3	0.8	1	0.7
CLM-E5R1	93	97	89	8	3	13	4	11.5	-3.5	1.1	1	1.2
CLM-E5R2	92	97	87	8	3	13	7.3	16.3	-1.7	1.3	1.6	1.1
CLM-E5R3	93	98	87	9	3	14	2.8	5.6	0	0.9	1	0.8
CLM-C3	93	98	87	8	3	13	0.1	0.2	0	1.3	1.1	1.4
Ens.	**93**	**99**	**88**	**8**	**3**	**13**	**4.9**	**8.8**	**1**	**1.1**	**1.1**	**1**

Table 4.7: Annual (Ann.), winter half year (WH) and summer half year (SH) area means of precipitation and temperature in the Ruhr catchment, as well as future changes of the variables.

Contrary to in previous catchments, the REGNIE and DWD/PIK data in the Ruhr catchment are very close to each other, which could make the validation and control simulations more similar, see Table 4.7. The CLM simulations agree well with the observations after bias correction. The WRF, however, produces a larger overestimation in winter, which seems to be due to the bias correction using a two month running window to calculate the corrections. This

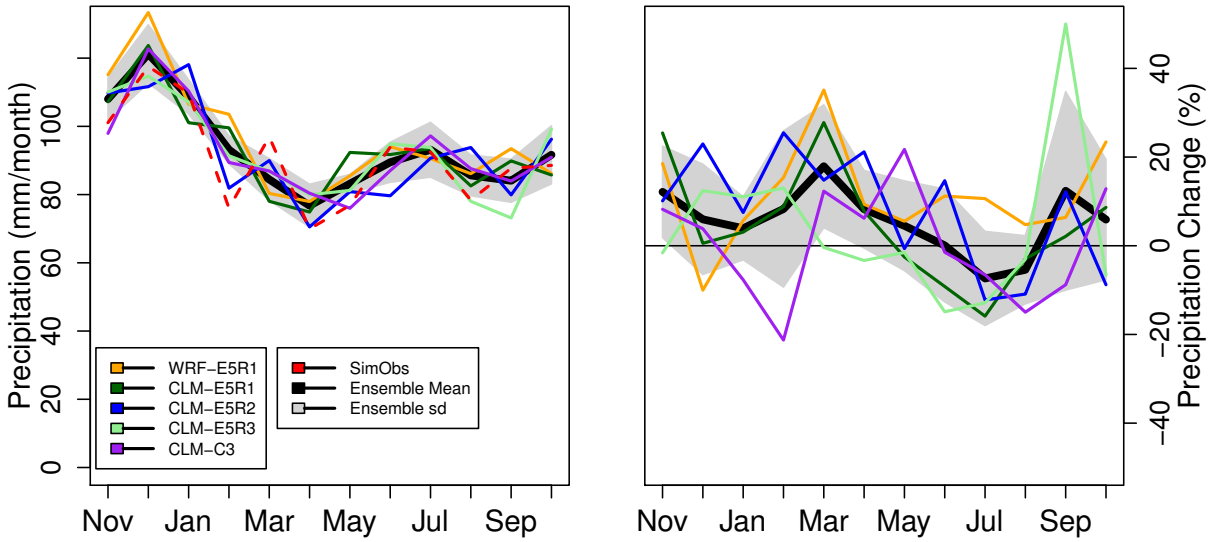

Figure 4.12: Mean monthly precipitation sums in the Ruhr catchment for the bias corrected model data in comparison to the REGNIE observations (left), and relative differences between the future and control time periods (right). Shaded areas indicates the enemble spread by one standard deviation.

causes a low bias in October and January, to reduce the amount of correction for November and December. The climate change signals show a fairly consistent increase in precipitation for winter, but more mixed signals in summer. Temperature is increasing by about 1 °C.

	RH [%]			SW radiation [J/cm^2]			ΔRH [%]			ΔSW radiation [%]		
	Ann.	WH	SH	Ann.	WH	SH	Ann.	WH	SH	Ann.	WH	SH
DWD/PIK	79	82	77	961	554	1368	NA	NA	NA	NA	NA	NA
WRF-E5R1	78	85	71	974	542	1406	0.2	-0.5	0.8	-4.3	-5.9	-2.7
CLM-E5R1	90	91	89	711	473	949	-0.2	0.4	-0.9	-2.8	-8.8	3.2
CLM-E5R2	89	91	88	743	473	1013	0.6	0.7	0.5	-7.3	-9.2	-5.4
CLM-E5R3	89	91	88	727	464	990	0.1	0.3	-0.2	-1.5	-3.1	0
CLM-C3	89	91	88	737	490	985	0.3	0.4	0.2	-3.1	-5.1	-1
Ens.	**87**	**89**	**85**	**778**	**488**	**1068**	**0.2**	**0.3**	**0.1**	**-3.8**	**-6.4**	**-1.2**

Table 4.8: Annual (Ann.), winter half year (WH) and summer half year (SH) area means of SW radiation and relative humidity in the Ruhr catchment, as well as future changes of the variables.

Relative humidity is underestimated by WRF and overestimated by CLM, like for the other catchments, see Table 4.8. Short wave radiation is however fairly close to observations for the WRF model in the Ruhr catchment, while CLM is underestimating it, like for the other catchments. There are practically no projected changes to relative humidity, while short wave radiation is decreasing by a few percent.

The annual cycle of precipitation for the Ruhr catchment (fig. 4.12 left) is weaker than for the other catchments and has a maximum in winter of about 116 mm/month in the observation and a weak secondary June–July maximum (93 mm/month). The simulations are able to reproduce

the shape of the annual cycle but the uncorrected data give too high annual sums in all seasons (not shown). After bias correction, only the WRF model is deviating from the observations, as discussed at the beginning of this section.

Compared to the present day climate, the annual cycle for the future period (fig. 4.12 right) is enhanced in the simulations with a strengthened winter maximum and basically no more secondary summer maximum. The ensemble spread is even smaller than within the control period, especially in summer. The ensemble mean changes are as high as or even higher than the standard deviation during the winter month, due to the small spread. The precipitation increase is up to 20% in March. A decrease in precipitation occurs in July (10%) and August (7%).

4.2 Hydrological Model Results

In the following sections, the results of the hydrological modeling will be discussed. First, the quality of the calibration of each hydrological model will be assessed by means of performance criteria. The most commonly applied method is the Nash-Sutcliffe efficiency (E) [Nash and Sutcliffe, 1970]. Its values range from -∞ to 1, where 1 means a perfect fit of observed and simulated data and 0 means that the simulations are as accurate as the mean of the observations. It is defined as:

$$E_f = 1 - \frac{\sum_{t=1}^{T} \left(Q_o^t - Q_m^t\right)^2}{\sum_{t=1}^{T} \left(Q_o^t - \overline{Q_o}\right)^2} \tag{4.1}$$

where Q_o is observed discharge, Q_m is modeled discharge and t is time. Due to the squared discharge values, this criterion focuses on peak flows.

To have an even stronger focus of model calibration on high flows, a modified Nash-Sutcliffe coefficient (fEff) is used:

$$fE_f = 1 - \frac{\frac{1}{n}\sum_{t=1}^{n} \left(\left(Q_o^t - Q_m^t\right) * Q_o^t\right)^2}{\frac{1}{n}\sum_{t=1}^{n} \left(\left(Q_o^t - \overline{Q_o}\right) * Q_o^t\right)^2} \tag{4.2}$$

To validate the simulated lower flows, the logarithmic Nash-Sutcliffe (lnE_f) criteria is calculated. The volume error, also called Bias (b), compares the simulated sum of discharge with the sum of the observed discharge to calculate whether the entire quantity of runoff is well simulated.

$$b = \frac{\sum Q_m^t}{\sum Q_o^t} \tag{4.3}$$

These performance criteria are calculated for the calibration period, which can be different between the hydrological models and the catchments, and for the validation period as well as for the whole simulated time series.

To represent the results of the hydrological simulations, mean monthly discharge data (MQ) and mean monthly maximum discharge data (MHQ) are shown. To avoid the effects of single outliers, mostly averaged values will be analyzed. In addition, return periods of the annual, winter and summertime maximum floods are shown for observed and simulated discharge output. This is performed with the plotting position method, showing which flood event has the corresponding exceedance probability in years. The plotting positions were defined by first extracting the annual (winter, summer) maxima and sorting from the lowest value with $m = 1$, to the highest value with $m = n = 30$. The return periods are assigned to these values according to

$$RP = \frac{1}{1 - \frac{m}{n+1}}. \tag{4.4}$$

Note that the return values are calculated for the 1971–2000 (or 2021–2050) time period for both model and observational data. They will therefore differ from return values calculated from the complete observational record which is commonly used.

4.2.1 Ammer

4.2.1.1 Calibration and validation

Henceforth, a maximum number of three gauges will be considered for the analysis of the Ammer catchment. The gauge Oberammergau represents the most alpine head basin of the catchment area. Weilheim describes the downstream outlet of the Ammer catchment. As third gauge, Peißenberg is chosen, because it represents the transition from an alpine to a more mountainous landscape.

In a preprocessing step, both HMs use interpolation functions to generate gridded meteorological input fields from observation data. The spatial coverage of the station data within the Ammer catchment is very sparse, especially at the southern alpine part. Recently, a collaborative project of FZ Juelich, KIT, UFZ Leipzig-Halle, DLR, Helmholtz Centre Munich and GFZ, called TERENO was started, with the Ammer catchment being one of four hydrological sites. Within this project, three long term hydrological and meteorological observatories are installed, which will considerably improve the future database [Zacharias et al., 2011]. The calibration with WaSiM for the Ammer catchment, which was performed on an hourly time step for the years 2003–2006, results in satisfying model efficiencies (see Table 4.9). The second hydrological model PRMS used the time period 1991–1996 as calibration period, and a daily time step. The performance criteria are quite good. Overall, the performance criteria indicate a more flood event based calibration of WaSiM with higher values at the modified efficiency and otherwise a more water balance based approach of PRMS with e.g. a better lnE_f and less volume bias. One reason may be the different modeling time steps. Most calibration difficulties are found at the small alpine head basin of the catchment (Oberammergau), but downstream the quality of simulations increases clearly with both WaSiM and PRMS.

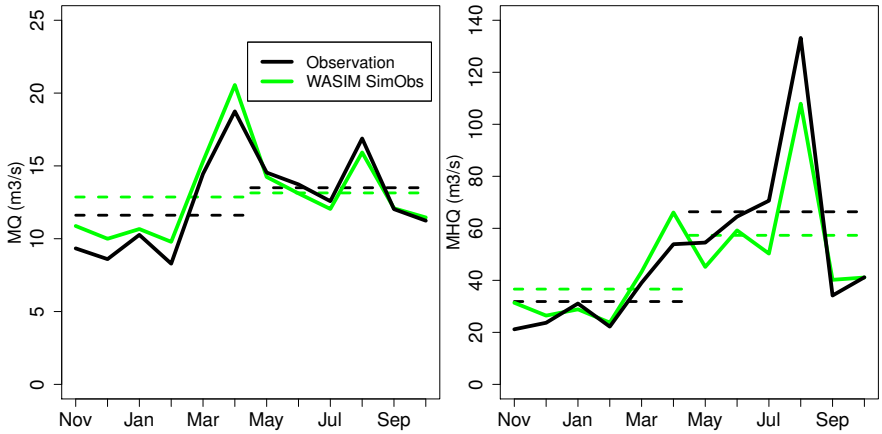

Figure 4.13: MQ and MHQ of the WaSiM validation simulation and observations at hourly time step for the period 2003–2009 at gauge Weilheim. The dashed lines indicate the half-year mean values (colours as in legend).

The MQ at Weilheim for the period of 2003–2009 is characterized by two peak flows, one in spring (April) and one during summer time (August). The annual cycle is well simulated with a small overestimation during winter. Also the mean monthly maximum discharge (MHQ) can be reproduced with WaSiM (see fig. 4.13).

For the common validation period (1971–2000) both hydrological models (WaSiM and PRMS) use a daily time step and for the meteorological observed input the DWD/PIK-Data due to missing hourly data for this period. Noticeable is that the seasonal cycle at the Ammer gauges is different for that period compared to the WaSiM calibration period. The observed discharge data have now a unimodal instead of a bimodal annual regime. The highest measured discharge takes place in July at the gauge Weilheim. Consequently, flow is higher in summer than in winter in the validation period.

In fig. 4.14, MQ and MHQ are shown exemplary for the gauge Weilheim. The characteristics of the annual regime of MQ of both HMs agree fairly well with the observed data. However, both models calculate the highest mean monthly flow ahead of time in April. For MHQ one can see that WaSiM overestimates the high flows strongly in the simulation with a daily time step. PRMS, in contrast, simulates the maximum flows well.

		E_f			fE_f			lnE_f			b [%]		
		all	cal	val	all	cal	val	all	cal	val	all	cal	val
Oberam-	WaSiM	0.54	0.63	0.14	0.95	0.81	1.00	0.33	0.41	-4.86	16	14	155
mergau	PRMS	0.47	0.45	0.48	0.73	0.61	0.73	0.24	0.24	0.24	-11	-12	-11
Peißen-	WaSiM	0.75	0.77	0.73	0.98	0.98	0.90	0.51	0.53	0.48	0	-2	2
berg	PRMS	0.53	0.78	0.50	0.83	0.90	0.83	0.37	0.74	0.36	0	-1	2
Weilheim	WaSiM	0.84	0.87	0.72	0.95	0.95	0.90	0.66	0.71	0.55	3	-2	11
	PRMS	0.70	0.78	0.68	0.78	0.90	0.71	0.72	0.74	0.78	2	-1	3

Table 4.9: Performance criteria for the three selected gauges (Oberammergau, Peißenberg and Weilheim) and the two hydrological models (WaSiM and PRMS), calculated for the complete period 1971-2000 ('all'), and separately for the calibration ('cal') and validation ('val') periods. Note that WaSiM was calibrated with hourly data for the period 2003–2006.

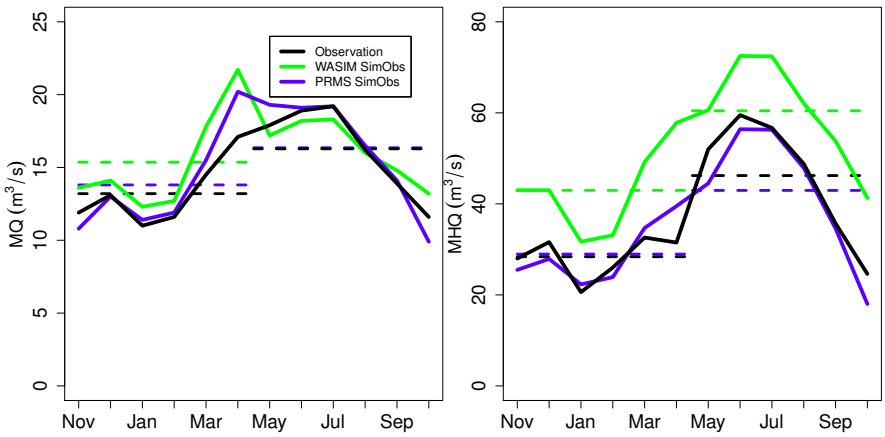

Figure 4.14: MQ and MHQ of the validation simulations at daily time step at gauge Weilheim.

Fig. 4.15 shows the return periods of annual, winter and summer maximum flows from observed (Obs) and simulated discharge (SimObs). The summer floods dominate the characteristics of

the yearly events. The highest discharges during winter are much smaller than in summer. The figure also shows again the overestimation of high flows by the daily based driven WaSiM simulation. PRMS shows a good agreement of simulated and observed data. Although, for shorter return periods over the whole year and for longer return periods in winter there are underestimations. The characteristics of floods in summertime are very well reflected by PRMS.

The severe overestimation of high flows by WaSiM is resolved by simulating the RCM data input in an hourly time step again (like the original calibration from 2003–2006).

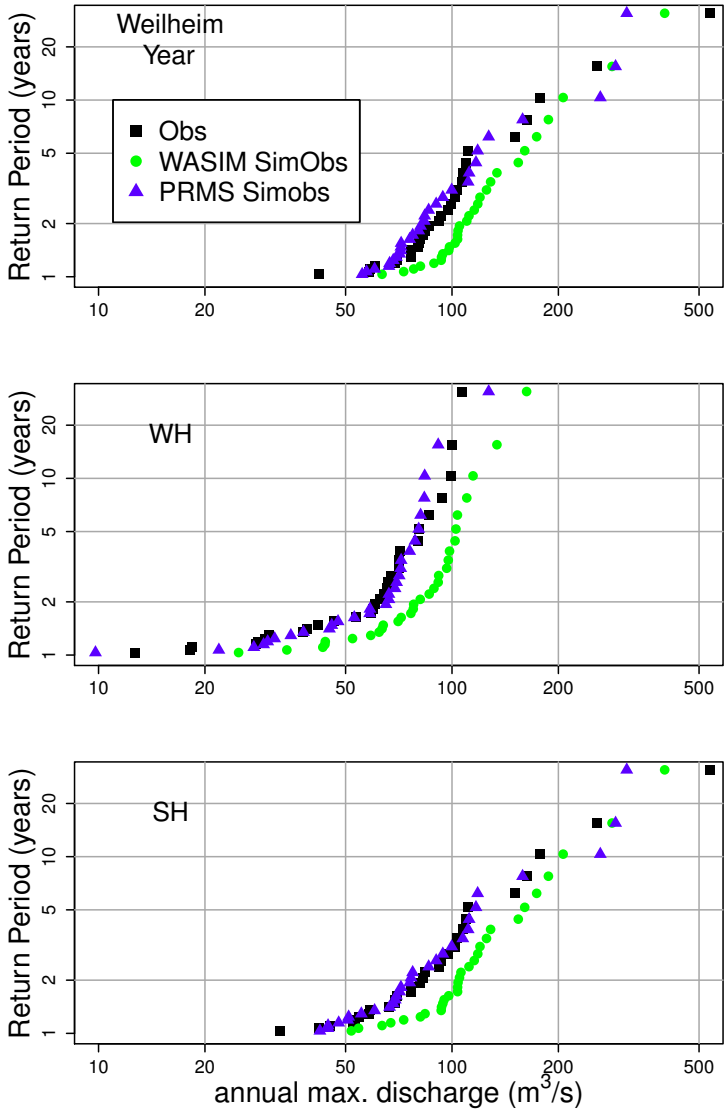

Figure 4.15: Return periods of the validation simulations at gauge Weilheim.

4.2.1.2 Control period

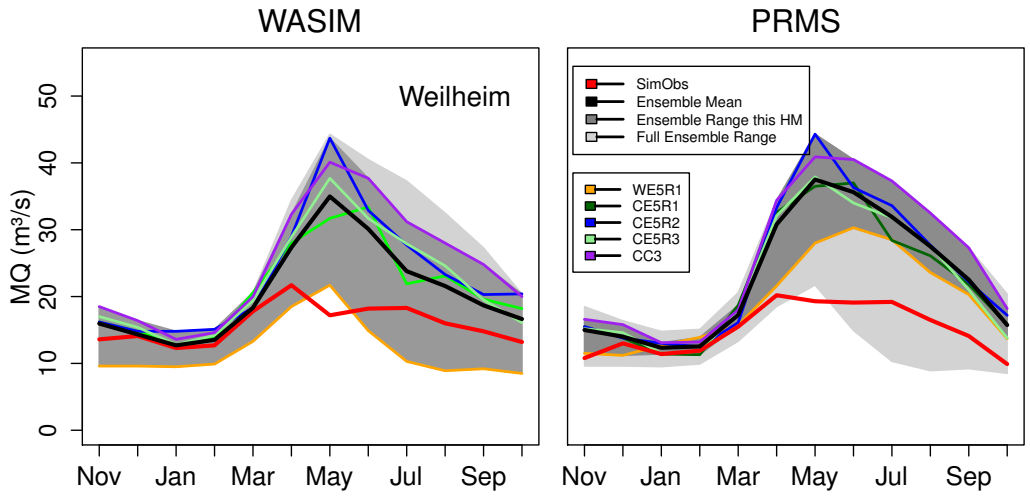

Figure 4.16: MQ of the control simulations at gauge Weilheim. Dark shaded areas indicate the maximum ensemble spread of the HM simulation shown in the plot, and the light shaded areas the other HM.

For the climate change simulations, the hydrological models are driven by RCM simulated meteorological data. Due to the small size and the heterogeneous topography of the Ammer catchment, the hydrological models react sensitively to the different spatial meteorological input data. For the simulations, the hourly time step was applied again for WaSiM driven by RCMs.

Fig. 4.16 shows the range of simulated MQ resulting from the RCM ensemble for both hydrological models, exemplary at the gauge Weilheim. The simulated regime from November until March is close to the SimObs runoff data, but from April to October the results differ considerably. The ensemble minimum is given by the simulations with WRF, the high flows result from the CLM runs. All simulations have a unimodal regime with the peak in May. Both HMs (PRMS and WaSiM) show comparable results, except for the WRF driven simulations. A sensitivity study (see fig. 4.19) has shown strong impact of relative humidity of the RCMs. PRMS shows comparable tendencies, but doesn't seem to react as strongly to the input parameter of humidity as WaSiM does. Remarkable are the large differences between the CLM and WRF driven simulations in spring and summer.

The MHQs, shown in fig. 4.17, are overestimated in summer by both HMs, with higher values of the WaSiM simulations. However, WaSiM achieves even higher values than PRMS. The WRF driven WaSiM simulation underestimates MHQ throughout the year. In contrast, the PRMS simulation with WRF performs well in winter, but overestimates the high flows in summer. The MHQ values of the simulations driven by CLM are overestimated by both HMs. Therefore the range of the ensemble is different between the two HMs. While the simulations with PRMS result in a homogeneous and small spread between the individual RCM members, WaSiM gets a spread up to 50 m^3/s in summer.

The annual 30-year return periods in fig. 4.18 conform to the higher flood events during summer time. Furthermore, the distinct underestimation of discharge by the WRF model and the overestimation of CLM are again apparent. This induces a stretching of the ensemble range, which is more pronounced for WaSiM.

To detect the cause of the large difference of the CLM and WRF based simulations in the Ammer catchment with WaSiM-ETH, as indicated in figs. 4.16 and 4.17, a simple sensitivity test

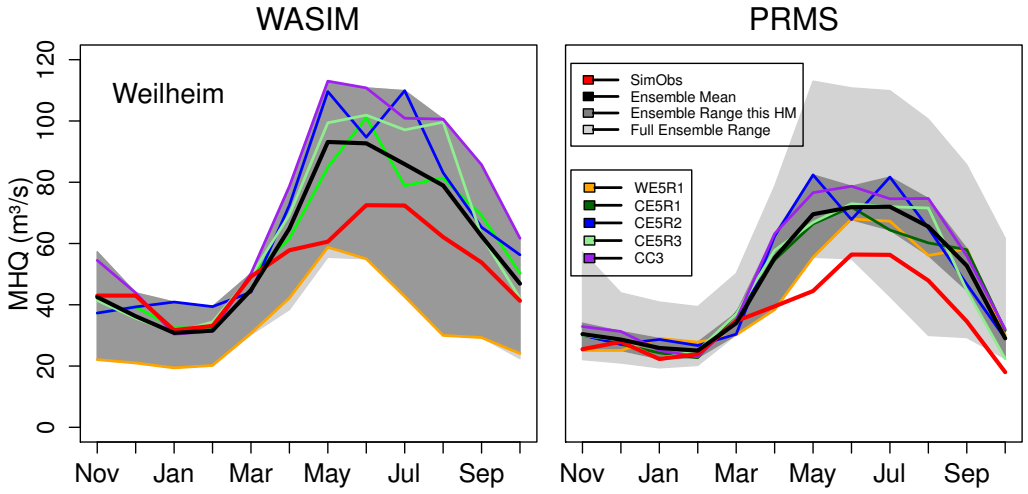

Figure 4.17: MHQ of the control simulations at gauge Weilheim. Dark shaded areas indicate the maximum ensemble spread of the HM simulation shown in the plot, and the light shaded areas the other HM.

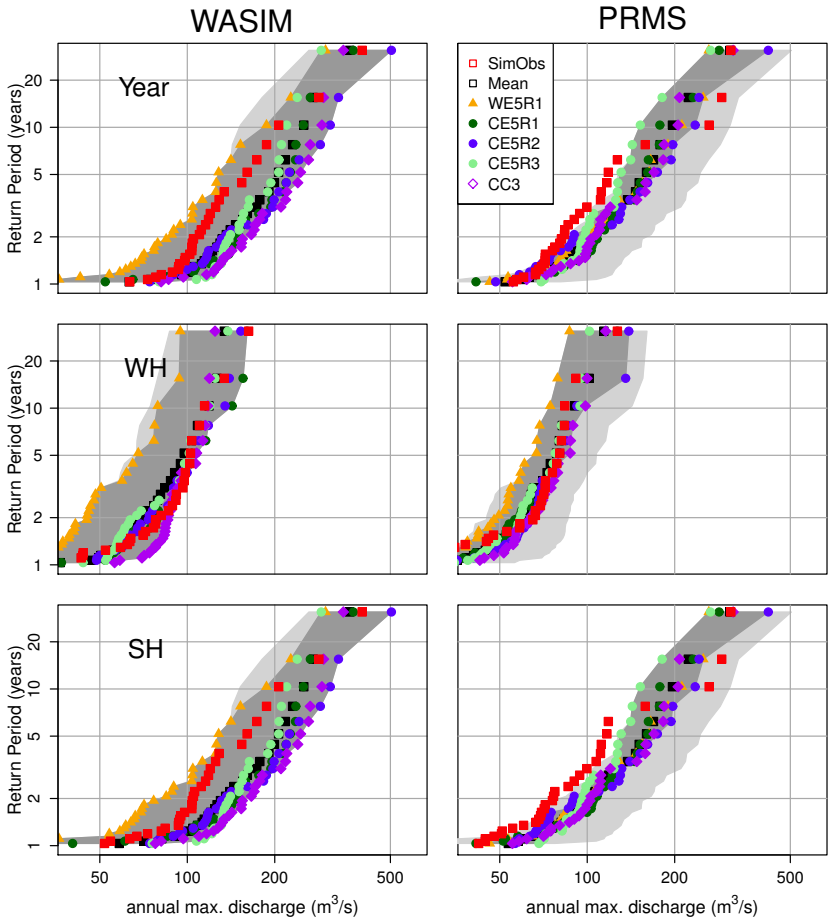

Figure 4.18: Return periods of the control simulations at gauge Weilheim. Dark shaded areas indicate the maximum ensemble spread of the HM simulation shown in the plot, and the light shaded areas the other HM.

was carried out (similar test were carried out for the Ruhr catchment with PRMS with the same results). It showed that the relative humidity (RH) has a large impact on the results. Fig. 4.19 illustrates the results for the sensitivity test with exchanged inputs of relative humidity for CLM (green) and WRF (orange). In this study, the large differences up to 15 m^3/s during summer and autumn in the simulations of the Ammer catchment with WaSiM-ETH can be explained.

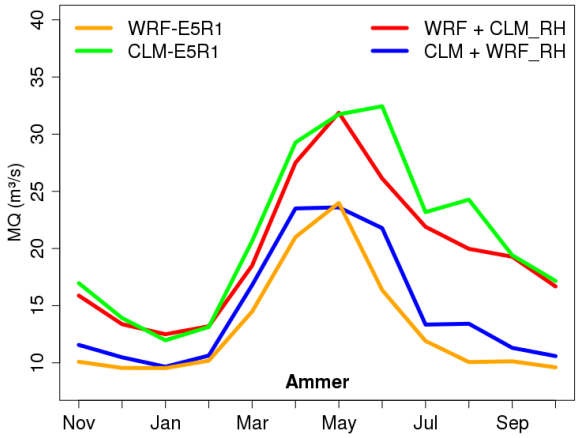

Figure 4.19: Sensitivity test of the influence of relative humidity (RH) to the discharge simulations with WaSiM in the Ammer catchment using CLM and WRF input for the control period.

4.2.1.3 Future period

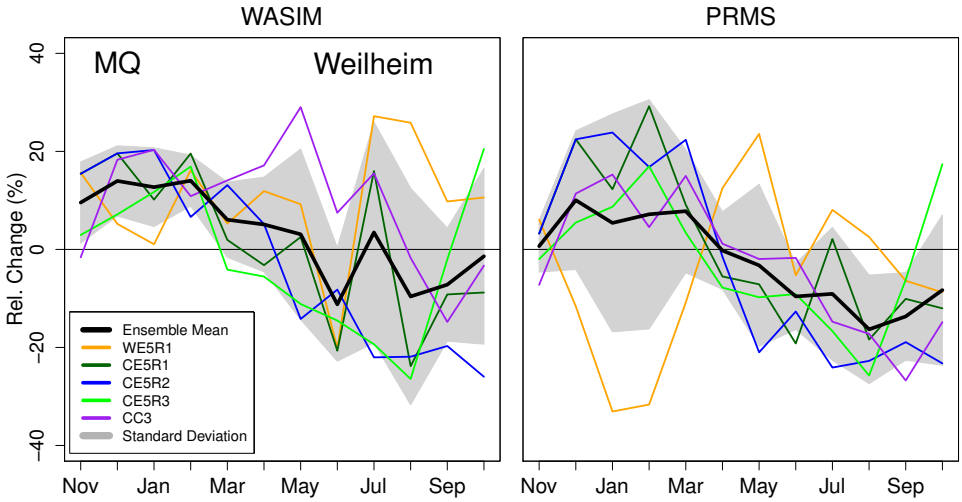

Figure 4.20: Change in MQ between the scenario and control periods at gauge Weilheim. Shaded areas indicate one standard deviation of the ensemble.

The comparison between the control and the future scenario shows tendencies of increasing mean monthly discharge in winter and decreasing discharge during summer (see fig. 4.20). WaSiM shows a clearer trend in winter than in summer, whereas PRMS predicts the decrease in summer more clearly. The spread of the single ensemble members, here indicated by one standard

deviation, is for both hydrological models very large so that an unambiguous statement about a future change in discharge is difficult to make.

It is conspicuous that the WRF-PRMS simulation reacts in the opposite way. The cause for this exceptional reaction in PRMS is not conclusively explained. At this point the WaSiM results are more plausible because they reflect the change in WRF-precipitation input with increasing values all over the year except in December, January and June.

To detect a trend for the MHQ is even more difficult (see fig. 4.22), as the differences of the ensemble members are larger than for MQ. The single ensemble members show in most cases the same discharge tendencies as for the mean monthly discharge.

Changes in return periods, determined by the annual, winter and summer maximum discharge values, show a clearer trend for winter than for summer (see fig. 4.21). Especially for return periods of 5 years and more, both hydrological models predict an increase in winter. For summer, a decreasing tendency is plausible, but the large spread of the single ensemble members makes the changes non-significant. The mean ensemble change covers a range from about -10 to +5% relative change for the future.

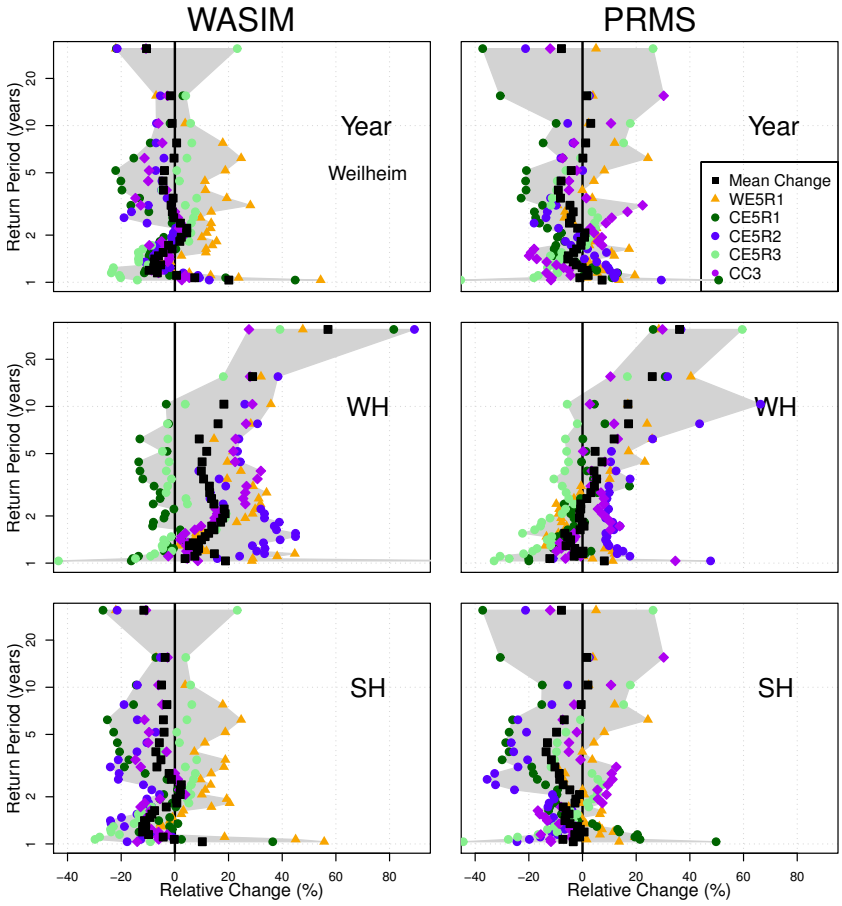

Figure 4.21: Changes in return periods between the scenario and control periods at gauge Weilheim. Shaded areas indicate the min-max range of the ensemble.

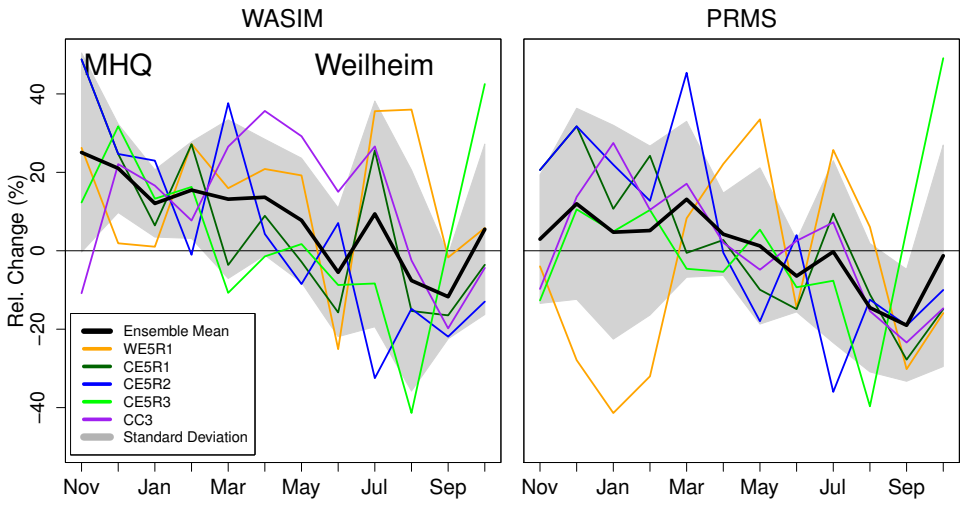

Figure 4.22: Change in MHQ between the scenario and control periods at gauge Weilheim. Shaded areas indicate one standard deviation of the ensemble.

4.2.2 Mulde

4.2.2.1 Calibration and validation

Before using an HM for climate change impact assessment studies, it is necessary to evaluate how the model performs for present conditions. If the HM cannot reproduce the water balance under current conditions, we will trust less in its ability for estimating changes for a future climate, and characteristics of the differences between simulated and observed discharge data have to be taken into account for the interpretation of the results under future climate projections.

The results are shown exemplarily for three selected gauges (for the location of the gauges see fig. 2.4): Bad Düben (6171 km^2) represents the overall catchment, as it is the last gauge with a sufficiently long measured time series before confluence into the Elbe River, Erlln represents a catchment in the middle reaches with a catchment area of 2983 km^2 and Hopfgarten finally represents a smaller catchment (529 km^2) centered in the Ore Mountains. All three gauges have a continuous measured time series of discharge during the period 1971–2000, which has been selected as control period in this study.

		E_f			fE_f			lnE_f			b [%]		
		all	cal	val	all	cal	val	all	cal	val	all	cal	val
Hopf-	WaSiM	0.64	0.63	0.69	0.85	0.86	0.91	-0.08	-0.22	0.08	-11	-12	-10
garten	SWIM	0.72	0.73	0.72	0.86	0.85	0.86	0.62	0.65	0.62	-3	2	-4
Erlln	WaSiM	0.78	0.76	0.86	0.85	0.81	0.90	0.23	0.11	0.38	-17	-19	-15
	SWIM	0.79	0.76	0.80	0.89	0.85	0.89	0.68	0.68	0.69	-4	4	-6
Bad	WaSiM	0.78	0.79	0.82	0.80	0.86	0.94	0.27	0.15	0.41	-11	-12	-10
Düben	SWIM	0.79	0.77	0.79	0.85	0.90	0.85	0.74	0.70	0.74	4	7	4

Table 4.10: Performance criteria for the three selected gauges (Hopfgarten, Erlln and Bad Düben) and the two hydrological models (WaSiM and SWIM), calculated for the complete period 1971-2000 ('all'), and separately for the calibration ('cal') and validation ('val') periods.

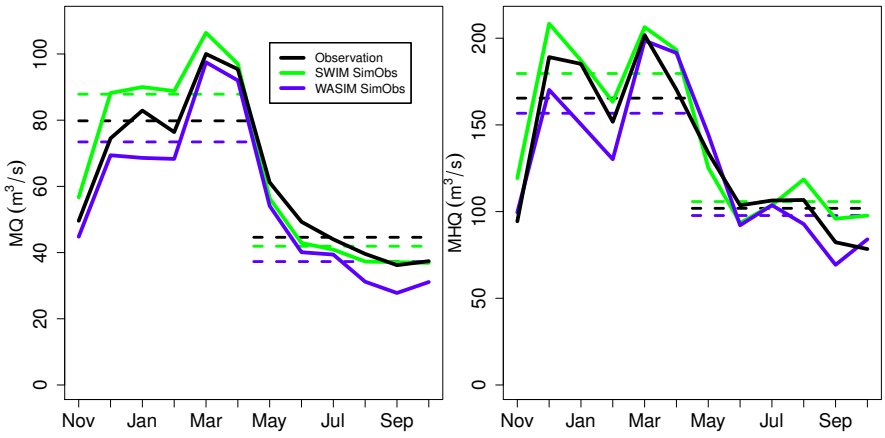

Figure 4.23: MQ and MHQ of the validation simulations at gauge Bad Düben. The dashed lines indicate the half-year mean values (colours as in legend).

Table 4.10 shows the calculated performance criteria for the WaSiM and SWIM HMs. The calibration period for SWIM was 1991–1995, with 1971–1994 and 1996–2000 together used as validation period, whereas the calibration period for WaSiM was 1980–1995, with 1971–1979

and 1996–2000 together used as validation period. With respect to E_f and fE_f values, both models show a good and comparable performance. None of the two models shows a decline in the model performance when moving from the calibration to the validation period. The log efficiency values are lower for WaSiM than for SWIM. As this project concentrates on flood events, the performance with respect to log efficiency values, which characterize the low flow prediction ability, is of minor importance, but it indicates structural problems of the model during low flow conditions. The difficulties of WaSiM during low flow are due to a general underestimation of discharge by approximately 10%, shown by the bias values in the last three columns of Table 4.10. Visual comparisons of simulated and observed daily flows (not shown) supported this, with generally good and comparable performance of the two models.

The results for MQ (fig. 4.23 left) show that the seasonal cycle is generally well represented by both models. While WaSiM underestimates throughout the year, as has also been senn for the volume errors, SWIM overestimates the seasonality, and tends to overestimate in winter and underestimate in summer. Fig. 4.23 (right) shows MHQ, which is also well simulated by both models.

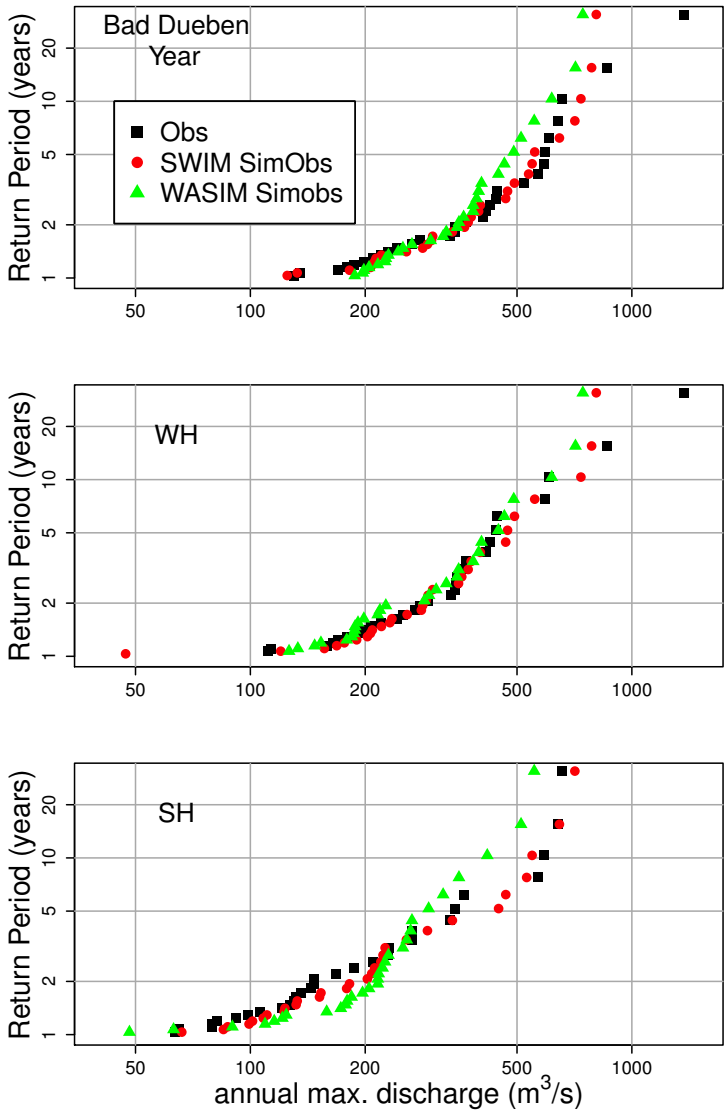

Figure 4.24: Return periods of the validation simulations at gauge Bad Düben.

As for flood frequency analyses usually only the annual maxima or the maxima for the winter and summer half years are extracted, it is important to assess, how well these values can be reproduced. Fig. 4.24 shows empirical flood frequency curves for the annual (top), winter (middle) and summer maxima (bottom). As most annual maximum floods occur in winter, the plots for the annual and winter maxima are very similar, while discharges of the summer maxima are lower. The distribution of simulated maximum winter, summer and annual discharges agrees very well to the observed discharges for both models, except for the one largest value caused by the flood in winter 1974/75. There is a slightly better agreement with discharges simulated by SWIM, particularly in summer WaSiM underestimates flows at higher and overestimates flows at lower return periods.

4.2.2.2 Control period

After demonstrating that both models can reproduce the observed runoff using observed meteorological input, the next step is to evaluate how the models perform with RCM output for the control period used as climate input. Fig. 4.25 shows very noticeable differences between simulated monthly mean discharge with climate input from observations (red line) on the one hand and with climate input from the RCMs from the control period (coloured lines) on the other hand. The climate input from WRF generally results in an underestimation of discharge, while the climate input from CLM mostly results in an overestimation. This overestimation is most pronounced in the summer months from May to October and stronger for the simulations with WaSiM than for the simulations with SWIM.

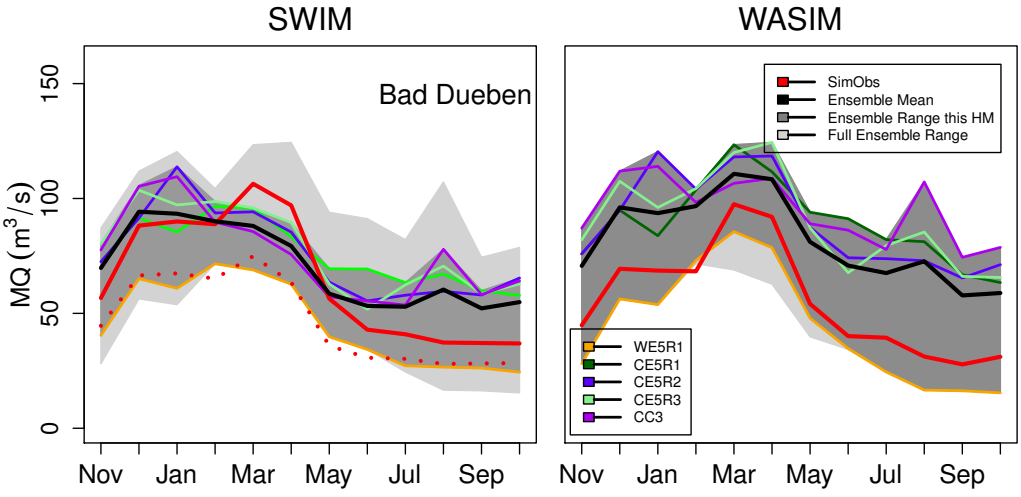

Figure 4.25: MQ of the control simulations at gauge Bad Düben. The dotted red line in the SWIM plot (left) indicates the SimObs curve when no undercatch correction was performed for the calibration data. Dark shaded areas indicate the maximum ensemble spread of the HM simulation shown in the plot, and the light shaded areas the other HM.

The picture is very similar for MHQ (Fig. 4.26). Again we can generally see an underestimation by the simulations with WRF climate input, although there is naturally more scatter for monthly maximum than for monthly mean flows. Average monthly maximum flows are overestimated during the summer months and this overestimation is again stronger for the simulations with WaSiM as compared to the simulations with SWIM.

The next figure (fig. 4.27) shows plotting positions of annual, winter and summer maximum

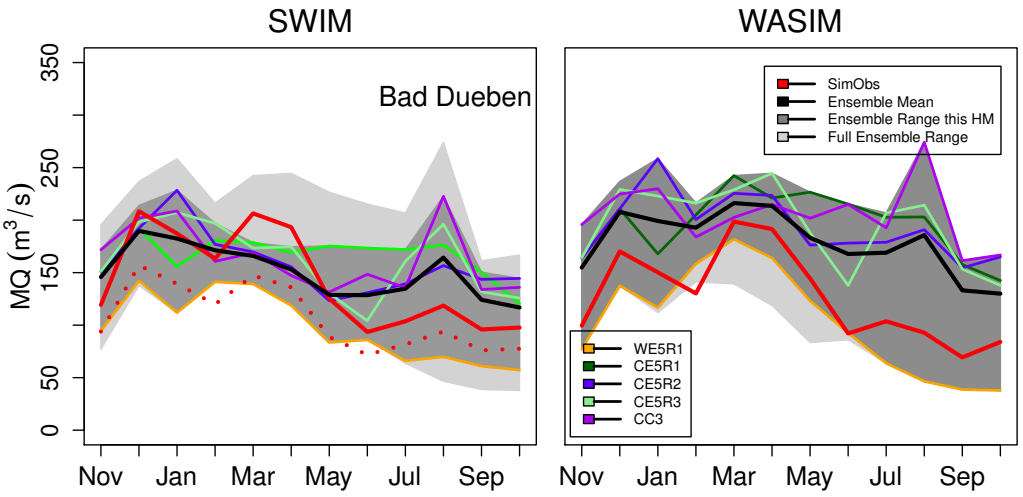

Figure 4.26: MHQ of the control simulations at gauge Bad Düben. The dotted red line in the SWIM plot (left) indicates the SimObs curve when no undercatch correction was performed for the calibration data. Dark shaded areas indicate the maximum ensemble spread of the HM simulation shown in the plot, and the light shaded areas the other HM.

flows simulated with SWIM (left) and WaSiM (right). The values for the summer maximum flows show a larger spread, but the ensemble envelope is consistent with the results for the MQ and MHQ results: an underestimation of the simulations with ECHAM5-WRF climate input and an overestimation of the simulations with CLM climate input, particularly for the WaSiM simulations. For return periods above 5 years the overestimation is lower (WaSiM) or disappears (SWIM). In winter, the range of the different ensemble members is much smaller and the simulations with RCM climate input are much closer to the simulations with observed climate input.

There are several reasons for these deviations between the simulations with observed climate input and climate input from the RCMs. First, WaSiM has been calibrated with observed precipitation without undercatch correction. Since the bias correction was performed with the non-undercatch corrected data, the underestimation of discharge by WaSiM in summer is most likely due to the underestimation of humidity by WRF in summer. WRF underestimates the humidity in summer by about 15% (see Table 4.6). Second, SWIM has been calibrated with observed precipitation with undercatch correction, so that the bias corrected climate input is generally lower than the precipitation during the calibration period. The effect of the undercatch correction on the simulated discharge is demonstrated in fig. 4.25, which also contains a SWIM simulation with observed climate input without undercatch correction (dotted red line). This simulation is very close to the simulation with climate input from WRF. However, there is no stronger underestimation of discharge of the simulation with WRF climate input in summer. This is probably due to a lower sensitivity of SWIM than WaSiM to changes in humidity.

The overestimation of discharge of the simulations with CLM climate input can be attributed to the overestimation of humidity and underestimation of radiation by CLM. CLM overestimates humidity by about 15% in summer and 7% in winter, and it underestimates radiation by about 25% in summer and 5% in winter. The overestimation of discharge shows up stronger in the simulations with WaSiM. In the simulations with SWIM, the factors resulting in a lower discharge (lower precipitation input) and higher discharge (higher humidity and lower radiation)

partly compensate and thus lead to more moderate discharge overestimations using the SWIM than the WaSiM model. A stronger overestimation of discharge by the simulations with CLM climate input during the summer than the winter months is due to (i) a stronger effect of evapotranspiration (which is reduced by the lower radiation and higher humidity) during the summer months, while evapotranspiration is generally only low during the winter months, and (ii) the stronger deviations of the CLM humidity and radiation during the summer than the winter months. The larger range between the different ensemble members for summer than for winter maximum flows might be due to a larger proportion of convective events in summer; convection processes cannot be resolved at a resolution of 7 km, so that the spread of the ensemble might be due to differences in the convection parameterizations between the RCMs.

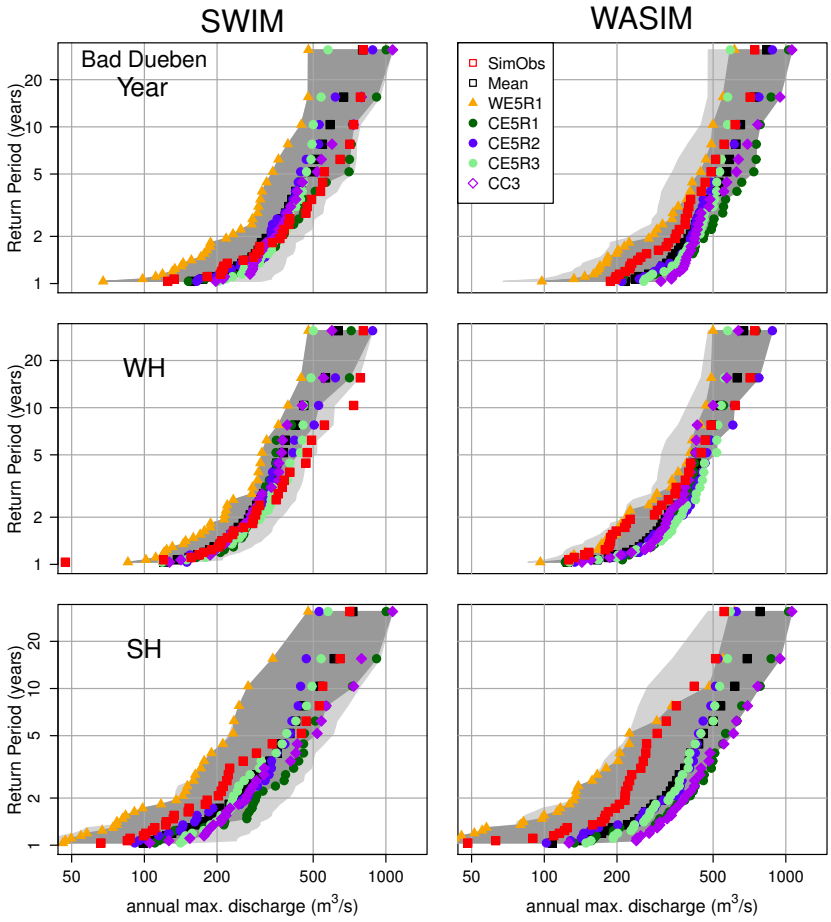

Figure 4.27: Return periods of the control simulations at gauge Bad Düben. Dark shaded areas indicate the maximum ensemble spread of the HM simulation shown in the plot, and the light shaded areas the other HM.

4.2.2.3 Future period

In accordance with the changes for the catchment average precipitation (see Table 4.6), changes in the simulated discharge between the control and scenario period look very heterogeneous for the different ensemble members (fig. 4.28 and fig. 4.29), and there is no overall trend towards increasing or decreasing discharges. The high relative changes of the simulations driven by WRF in particular in summer and autumn are mainly due to the already described underestimation in the control period. For the same ensemble members, the changes are very similar between

the different gauges (not shown) and between the two different hydrological models generally reflecting the precipitation changes. For example, the simulation with ECHAM5-WRF climate input shows an increase in discharge in nearly all months, which is consistent with the change in precipitation for this ensemble member (+11% in winter and +10% in summer). Differences between SWIM and WaSiM in the absolute values of the changes can be explained by the sometimes different base value, e.g. the values of the discharge increases of ECHAM5-WRF in October are larger for WaSiM than for SWIM, which is due to the fact that the average monthly flow in October simulated with ECHAM5-WRF input for the control period is lower for the simulation with WaSiM than with SWIM. Particularly for the average monthly maximum flows the range of the changes is larger in summer than in winter. This is probably related to a larger variability in summer precipitation.

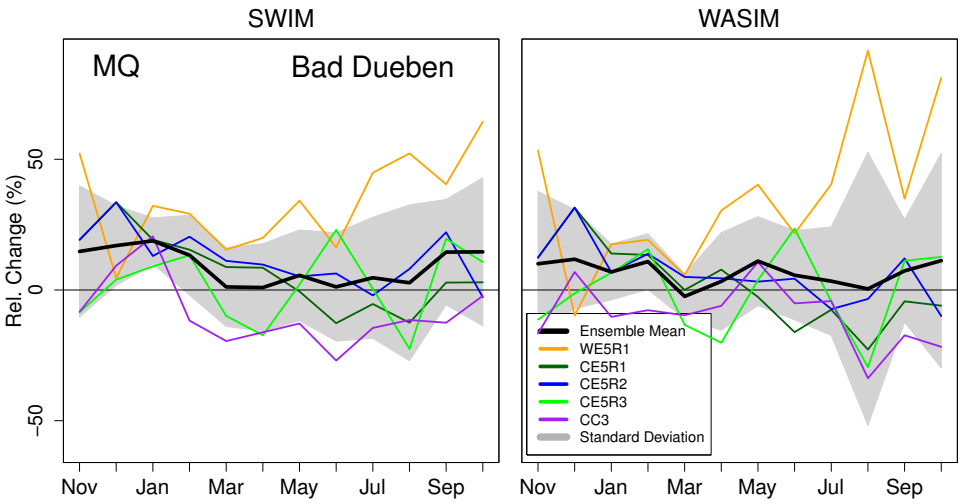

Figure 4.28: Change in MQ between the scenario and control periods at gauge Bad Düben. Shaded areas indicate one standard deviation of the ensemble.

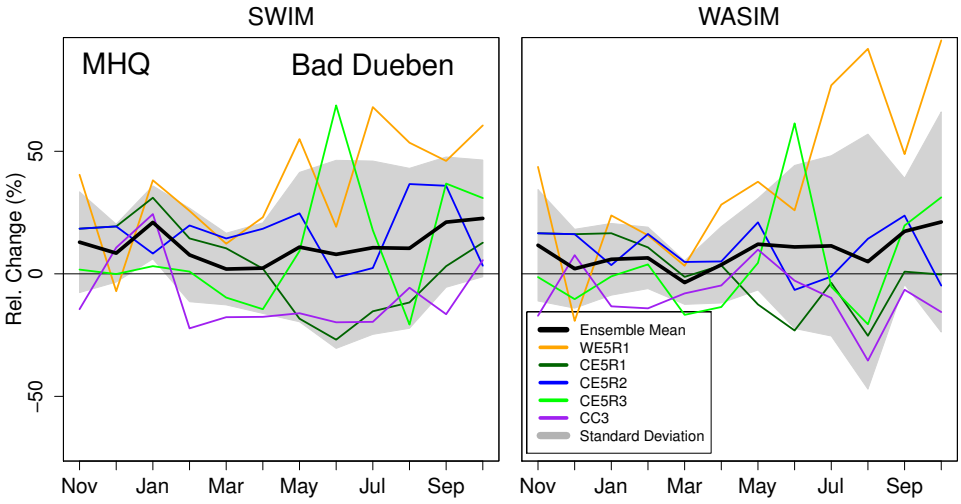

Figure 4.29: Change in MHQ between the scenario and control periods at gauge Bad Düben. Shaded areas indicate one standard deviation of the ensemble.

Looking at changes in return periods (fig. 4.30), again the much larger variability in the summer half year as compared to the winter half year is noticeable. Over all return periods

some ensemble members simulate an increase and others a decrease in the discharge values and the ensemble mean is close to the line of zero change. Only for return periods above five years in the summer half year the ensemble mean shows an increase in discharge, though the variability is very large for these values too and 3–4 ensemble members also show a decrease in summer floods.

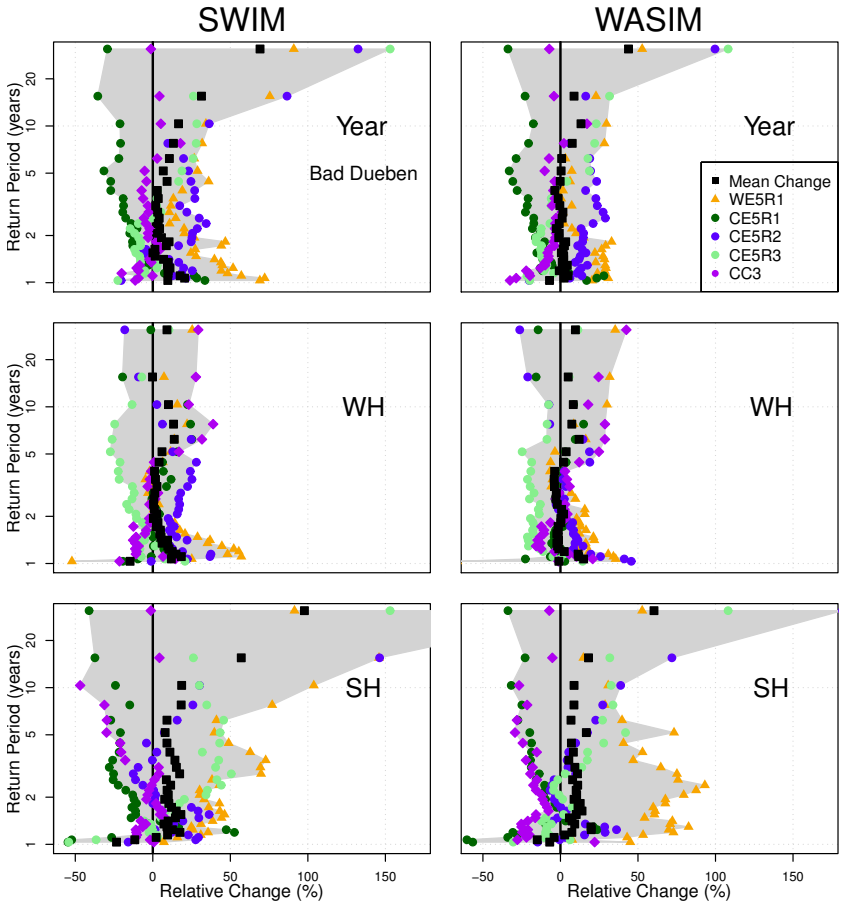

Figure 4.30: Changes in return periods between the scenario and control periods at gauge Bad Düben. Shaded areas indicate the min-max range of the ensemble.

4.2.3 Ruhr

4.2.3.1 Calibration and validation

The original model calibration of the PRMS is the time period 1992–1993. The second hydrological model in the Ruhr catchment, SWIM, uses the period 1991–1995 for the model calibration. The common validation period refers to the time period 1971–2000 (control period). For that purpose the meteorological input data in PRMS is configured with the most available measured station data in the Ruhr basin. On this base of observed data, available for different stations over different time periods, one common spatial dataset for the HRUs of the PRMS model is applied [Höfer et al., 2010] and extended to the necessary control period 1971–2000. The input data for the validation period of the HM SWIM is based on the DWD/PIK-Data as for the Mulde catchment with methods for undercatch correction of precipitation errors (for details see section 3.3.2.2.

Necessary observed data and reliable information about the complex water resources management systems (e.g. export and storage) in the Ruhr basin are not available for the complete validation period. Consideration of these systems are therefore not reasonable in the HMs, and for the further climate scenario simulations assumptions of the management systems in the Ruhr are also not feasible. Of course all observed discharges at the gauge stations include all inter-

		E_f			fE_f			lnE_f			b [%]		
		all	cal	val	all	cal	val	all	cal	val	all	cal	val
Bamenohl	PRMS	0.76	0.84	0.72	0.71	0.71	0.71	0.73	0.88	0.70	1	0	1
	SWIM	0.83	0.86	0.83	0.94	0.95	0.94	0.59	0.69	0.57	-4	0	-4
Hagen-Hohenlimburg	PRMS	0.74	0.80	0.73	0.90	0.92	0.89	0.69	0.74	0.73	10	7	14
	SWIM	0.69	0.74	0.68	0.92	0.93	0.92	0.48	0.55	0.45	7	9	7
Wetter	PRMS	0.73	0.82	0.71	0.91	0.91	0.91	0.69	0.82	0.67	22	15	24
	SWIM	0.82	0.88	0.80	0.94	0.96	0.94	0.67	0.77	0.65	15	16	15

Table 4.11: Performance criteria for the three selected gauges (Bamenohl, Hagen-Hohenlimburg and Wetter) and the two hydrological models (PRMS and SWIM), calculated for the complete period 1971-2000 ('all'), and separately for the calibration ('cal') and validation ('val') periods.

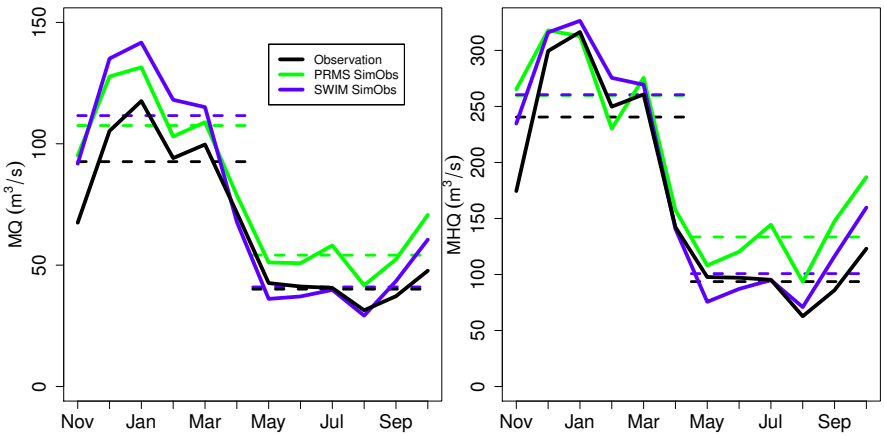

Figure 4.31: MQ and MHQ of the validation simulations at gauge Wetter. The dashed lines indicate the half-year mean values (colours as in legend).

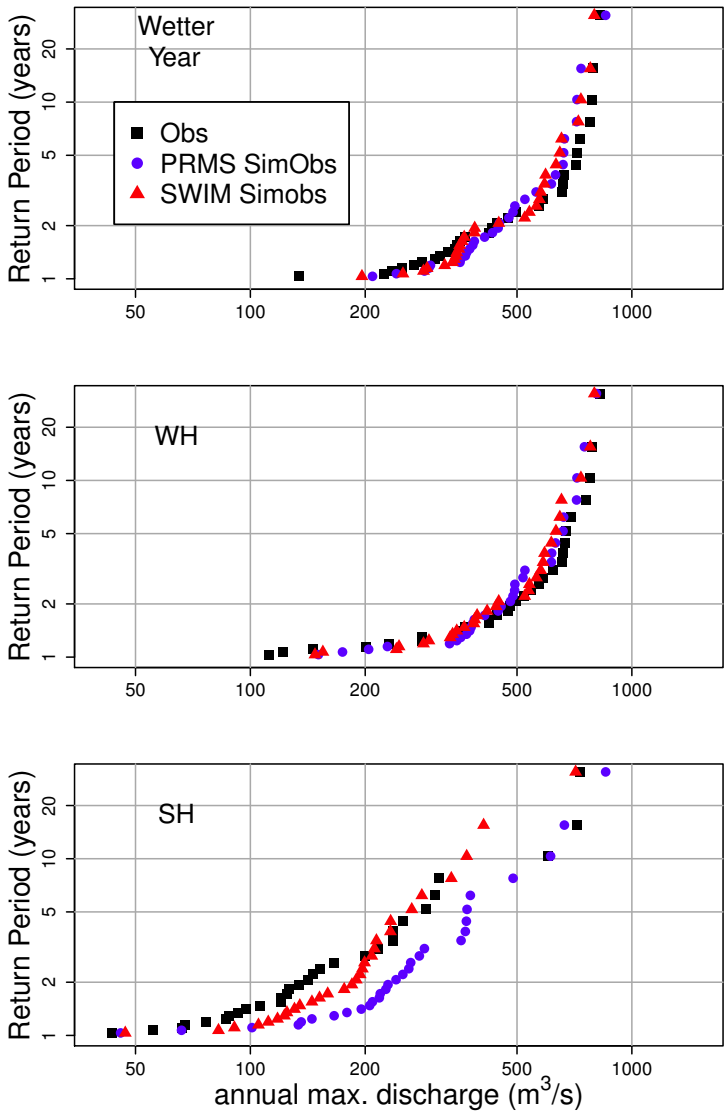

Figure 4.32: Return periods of the validation simulations at gauge Wetter.

ventions of the water resources management system in the Ruhr basin. Therefore, particularly by the comparison of the model data with the observed data over the control time period, this fact is to be taken into account.

The performance of the hydrological models PRMS and SWIM is exemplarily shown for the three selected gauges Bamenohl, Hagen-Hohenlimburg and Wetter. The three gauges have long observed time series of mostly good data quality. The observations at the gauge Bamenohl started in 1972, Hagen-Hohenlimburg in 1977 and Wetter already in 1961.

The performance results are presented in detail in Table 4.11. Both models show good and comparable performance for the control period. The mean E_f of PRMS is 0.84 and for SWIM 0.78. The SWIM model calibration focused more on the flood events, which can be seen in the higher fE_f of 0.93 (PRMS 0.73). The PRMS calibration sets more value on the complete flow spectrum, what is visible in the lnE_f of 0.84 (SWIM 0.52). The volume bias is low for both HMs for the unaffected gauge Bamenohl. Due to the complex water resources management systems, especially the water export, these results are not indicative for the other gauges (Hagen-Hohenlimburg and Wetter).

In fig. 4.31, the mean monthly discharge (MQ) and the mean maximum discharge (MHQ) are shown for PRMS and SWIM at gauge Wetter. The annual regime of both hydrological models (PRMS green and SWIM - blue) agrees well with the observed data (black) at the gauge. The persistent overestimation, especially for PRMS in summer, is mainly due to neglecting the water management in the models.

To evaluate the flood situation in more detail, the return periods of annual, winter and summer maximum flows are shown in fig. 4.32. Both models show good agreement with observations for the annual and winter time. The results of the summer period are again more strongly affected by the water resources management system [Höfer et al., 2010], especially by the operation rules regarding the filling level of the storages, and are therefore difficult to interpret.

4.2.3.2 Control period

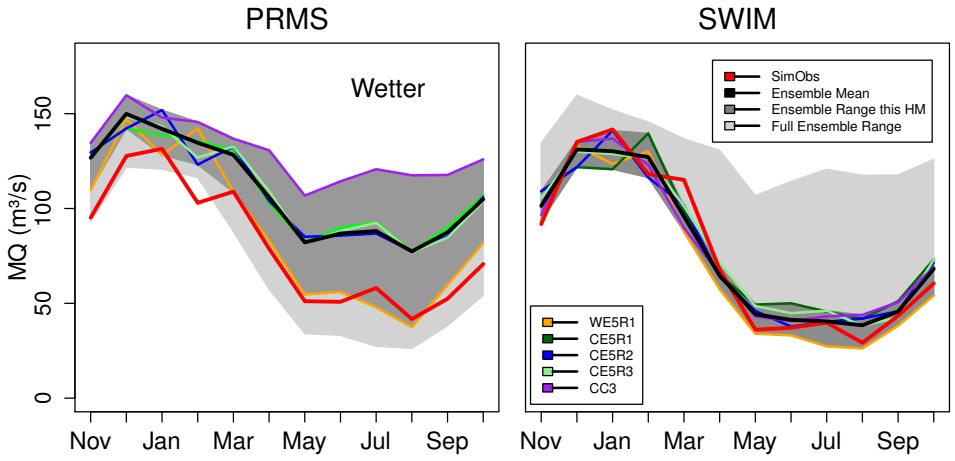

Figure 4.33: MQ of the control simulations at gauge Wetter. Dark shaded areas indicate the maximum ensemble spread of the HM simulation shown in the plot, and the light shaded areas the other HM.

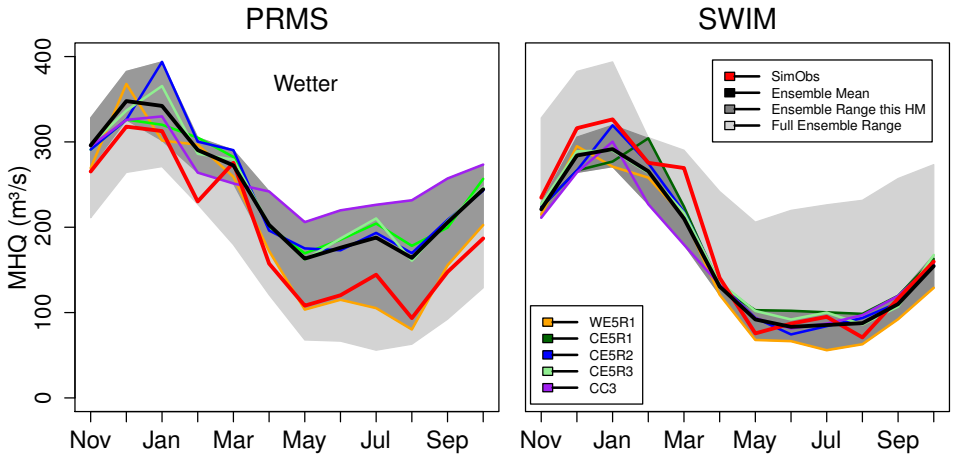

Figure 4.34: MHQ of the control simulations at gauge Wetter. Dark shaded areas indicate the maximum ensemble spread of the HM simulation shown in the plot, and the light shaded areas the other HM.

For the climate change simulations, the hydrological models are driven by RCM simulated meteorological data instead of observed meteorological data. Fig. 4.33 shows exemplary for the gauge Wetter the results of hydrological simulations of MQ. The colours indicate the different meteorological ensemble members (GCM – RCM), left and right marking the different HMs (PRMS left and SWIM right). The black line shows the ensemble mean and grey shadings the ensemble range. Fig. 4.34 shows the results for MHQ.

The ensemble mean of the two HMs follows in general the shape of the observed annual cycle. Noticeable is the different behaviour in summer, although the meteorological model input is the same and the hydrological calibration shows comparable results. This is related to different pre-processing of the input data and different methods and approaches to describe the complex water balance in the HMs. In particular, the concepts for the evapotranspiration differ and use different meteorological input variables.

Fig. 4.35 shows the results for the return periods of the control period for HMs driven by RCM simulated meteorological data, again for the gauge Wetter. In winter, the results are comparable and the ensemble range is narrow. In summer, however, the ensemble spread increases due to larger differences among the hydrological as well as the meteorological models.

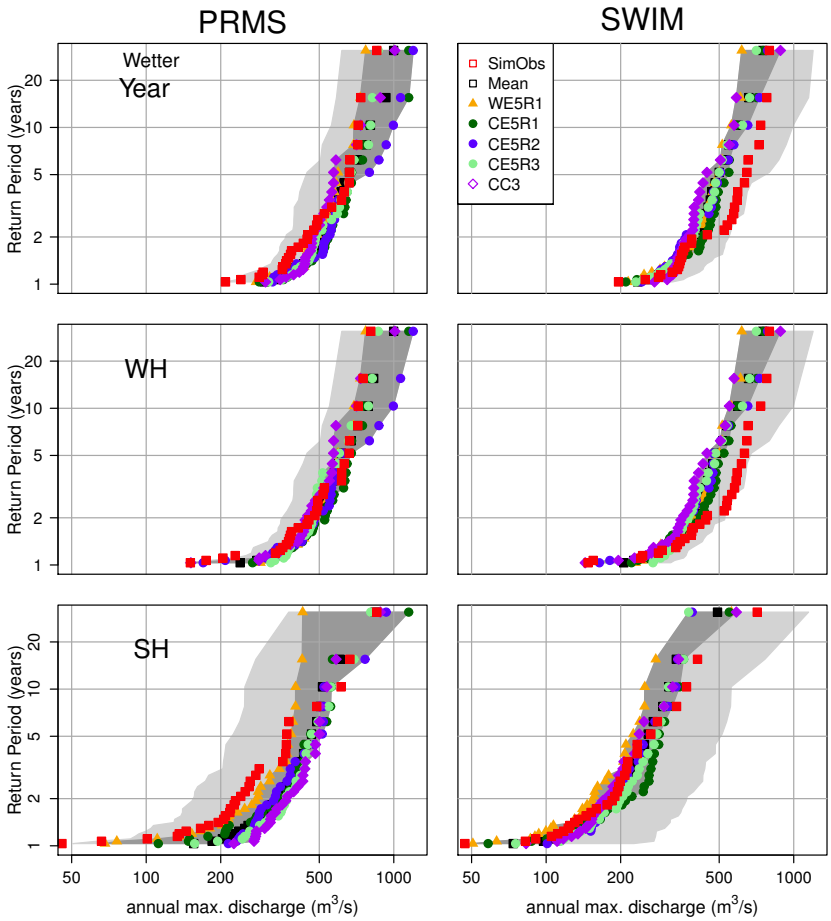

Figure 4.35: Return periods of the control simulations at gauge Wetter. Dark shaded areas indicate the maximum ensemble spread of the HM simulation shown in the plot, and the light shaded areas the other HM.

4.2.3.3 Future period

The impact of a changing climate can be rated by the relative changes between future and control simulation of the ensemble members. Therefore in fig. 4.36 the changes in MQ and in fig. 4.37 the changes in MHQ are presented. The ensemble spread is fairly wide, but a general increase can be inferred for the ensemble mean for most of the year. The HMs show a comparable and quite consistent picture. A clear spread due to natural variability of the climate, characterized by the three realizations of GCM ECHAM5 (green, blue and light green), is visible. The two GCMs ECAHM5 and CCCma3 (purple) show, at least for PRMS, also a different tendency, with an increase in summer and a slight decrease in winter. Most noticeable are however the almost opposite trends in the results for the two RCMs CLM (green) and WRF (orange) in summer. Using the same GCM and realization input, WRF prognoses significantly higher flows compared to CLM, which even projects slight decreases.

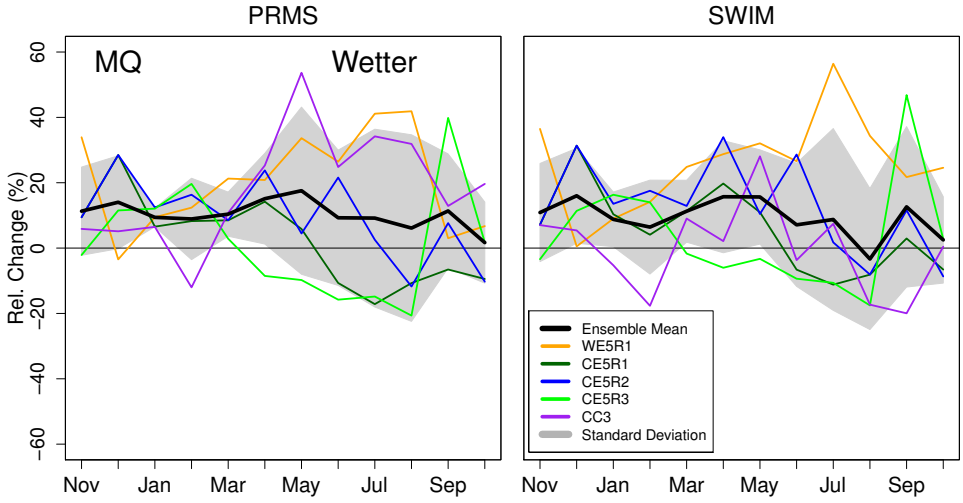

Figure 4.36: Change in MQ between the scenario and control periods at gauge Wetter. Shaded areas indicate one standard deviation of the ensemble.

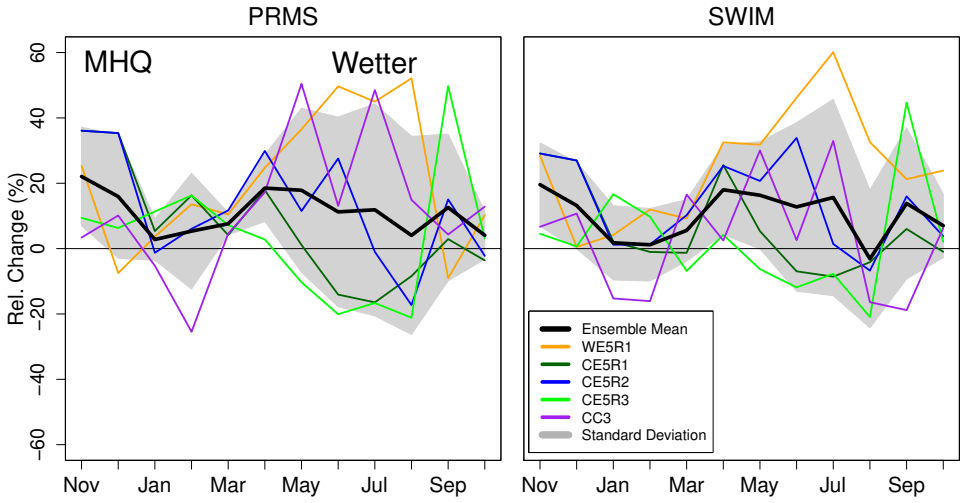

Figure 4.37: Change in MHQ between the scenario and control periods at gauge Wetter. Shaded areas indicate one standard deviation of the ensemble.

Fig. 4.38 shows the relative changes between the future and control scenario referring to the return periods classified in annual, winter and summer maximum flows, again for the gauge Wetter. At the annual scale, there is a quite consistent, albeit slight, increase. Extrapolation and statements for longer return periods are not feasible with the data at hand. On the seasonal scale, we see again that the ensemble spread is larger in summer than in winter.

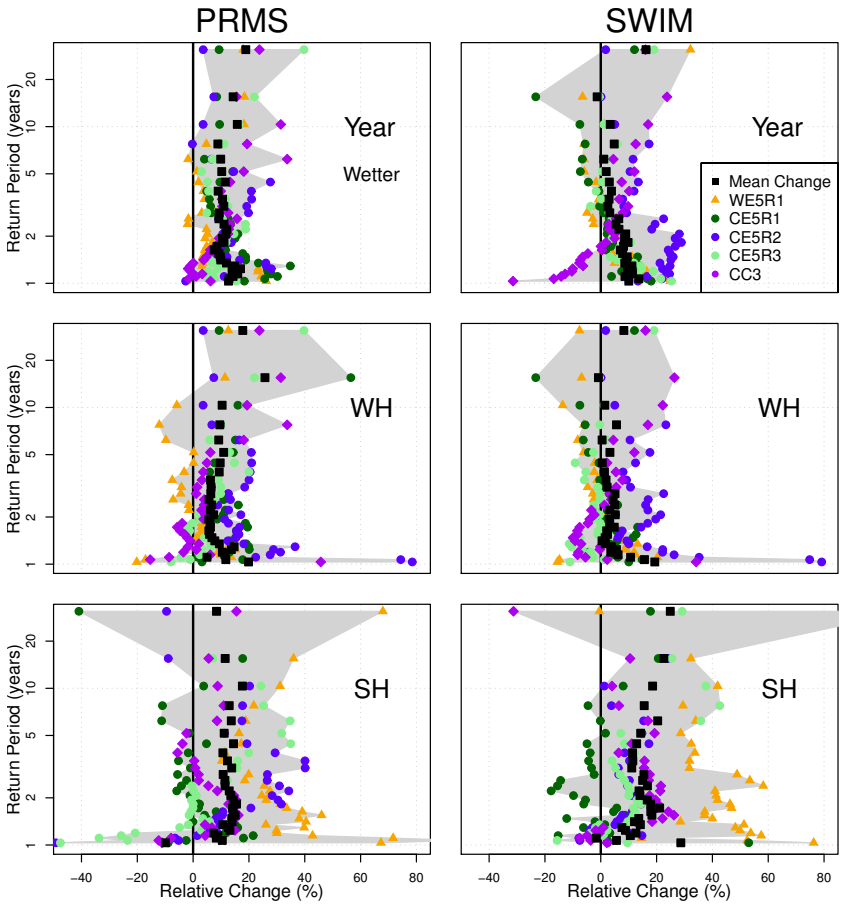

Figure 4.38: Changes in return periods between the scenario and control periods at gauge Wetter. Shaded areas indicate the min-max range of the ensemble.

4.2.4 Overall Results

This chapter discusses the results obtained with the ensemble formed from the combination of GCMs, RCMs and HMs. For each catchment, we have ten ensemble members (five bias corrected RCM simulations: CLM driven by CCCma3 and three realizations of ECHAM5 and WRF driven by ECHAM5 realization one, each of which driving two HMs). In contrast to the previous chapter, we here present the ensemble statistics, and compare the results from different catchments to each other. Results for MQ, MHQ and return values are presented and the focus is on changes between the future and control time periods. The ensemble is characterized in terms of the ensemble mean (all members have equal weight) and the ensemble spread, described by one standard deviation (SD) bounds around the mean.

Fig. 4.39 shows the ensemble mean annual cycle (left) and the changes (right) in MQ for each of the catchments. Averaging over the ensemble has the effect of reducing the variability

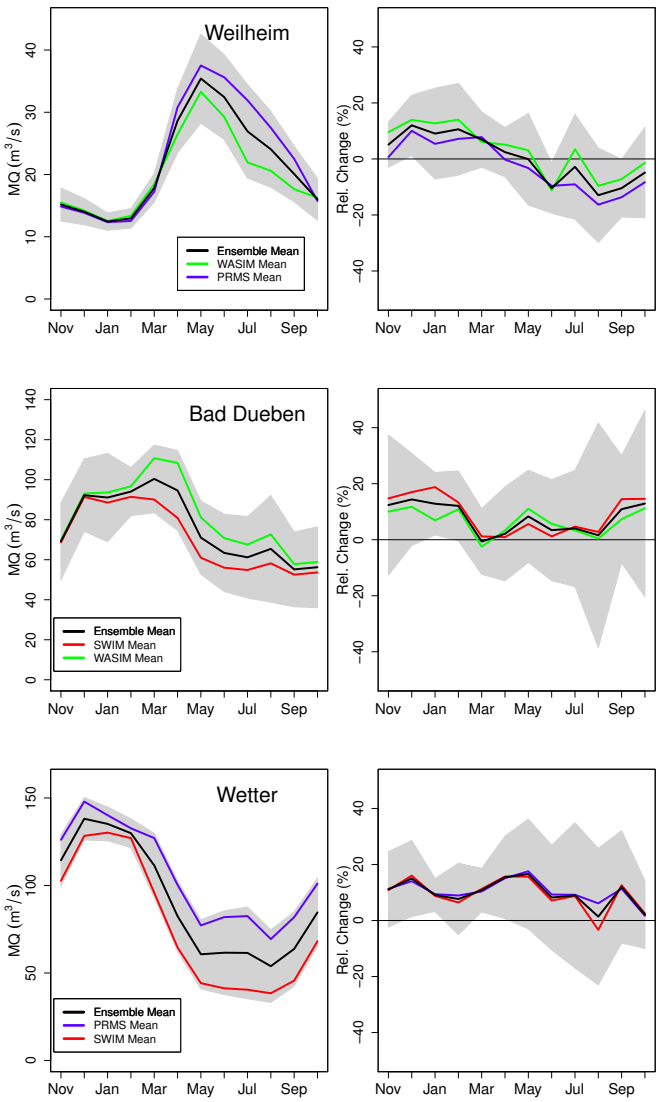

Figure 4.39: MQ for control period (left) and future changes (right) for Ammer (Weilheim), Mulde (Bad Düben) and Ruhr (Wetter). Shaded areas indicate one standard deviation of the ensemble.

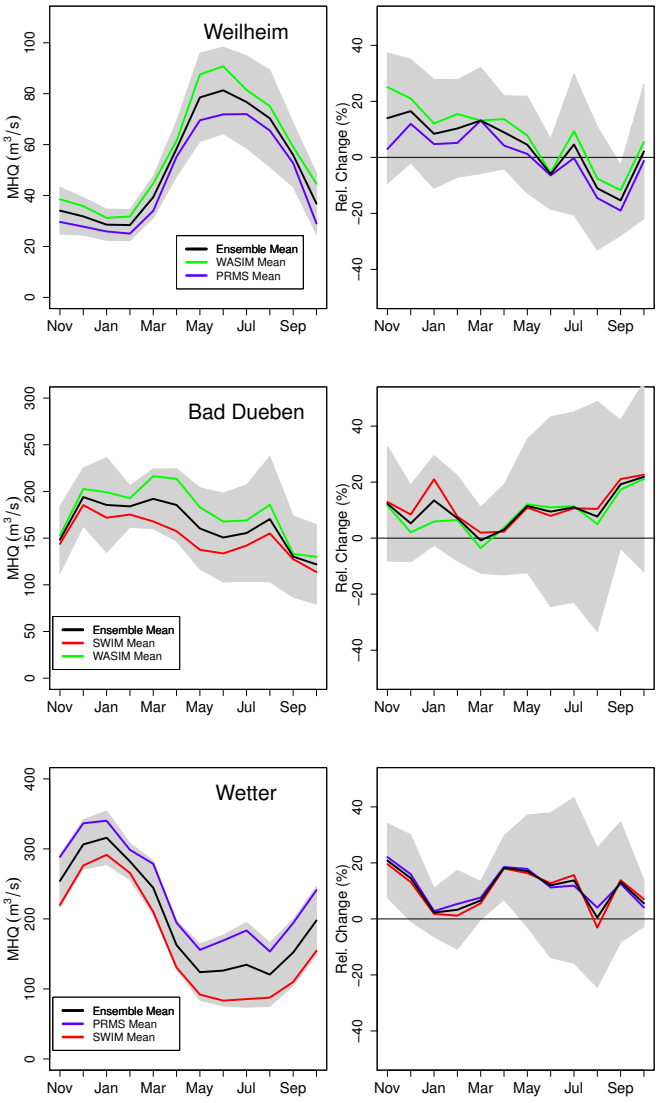

Figure 4.40: MHQ for control period (left) and future changes (right) for Ammer (Weilheim), Mulde (Bad Düben) and Ruhr (Wetter). Shaded areas indicate one standard deviation of the ensemble.

and a clearer pattern emerges. The climate change signal is uncertain, but shows some general features that are of interest. In the Ammer catchment, there is a tendency towards an increase in MQ in winter, and a decrease during summer. The Mulde and Ruhr catchments tend rather to increases during the whole year. Comparing to the changes in precipitation, as presented in section 4.1.5, one notices that the changes in MQ follow almost directly from this. Interestingly, the variability of the ensemble is larger for the Mulde than for the Ammer, although the Mulde catchment is several times larger and would therefore be expected to give a smoother result.

MHQ behaves in many ways similar to MQ, but with a larger variability of the climate change signals, see fig. 4.40.

Concerning return values, fig. 4.41 shows the plotting positions of the return periods for winter and summer half years. Again we see that the variability is larger for the Mulde catchment than for the others during the summer half year. However, besides the large spread, the ensemble result for the full ensemble as well as for each of the HMs separately show large agreement of

increasing discharge for a given return period. This is also true for the Ruhr catchment for all year. The Ammer catchment is a bit different in that the two HMs show larger disagreements on the climate change signal. Especially in winter, the WaSiM model shows practically no changes for the shorter return periods, while PRMS show strong increases in discharge.

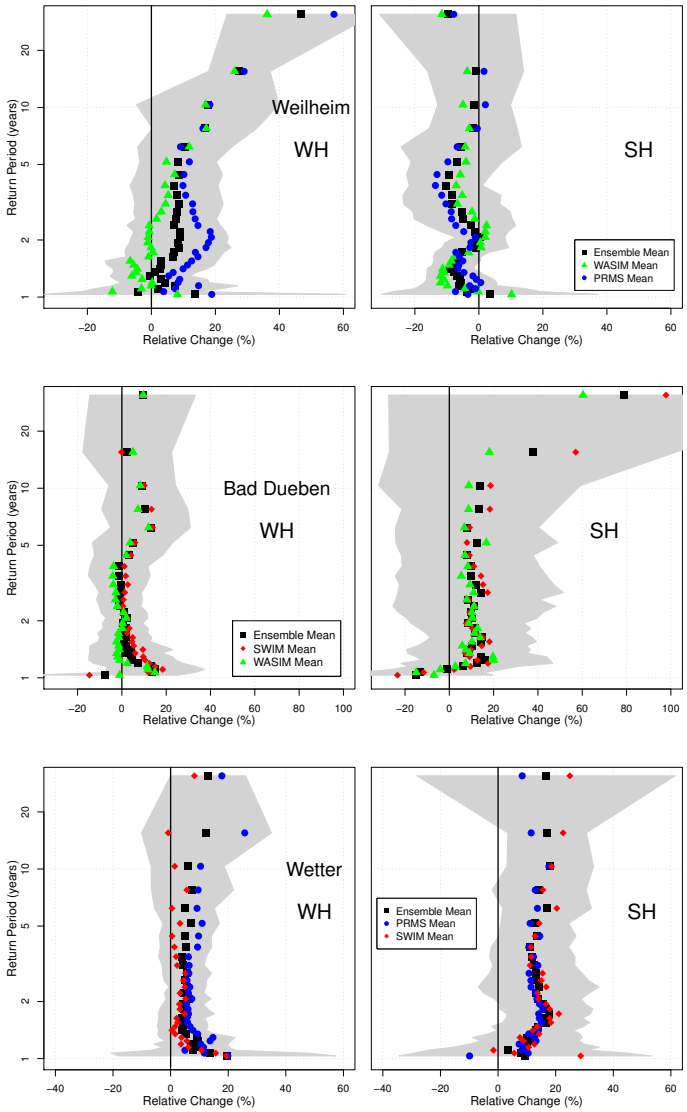

Figure 4.41: Changes in the return periods for winter (left) and summer (right) half years for Ammer (Weilheim), Mulde (Bad Düben) and Ruhr (Wetter). Shaded areas indicate one standard deviation of the ensemble.

4.2.4.1 Analysis of the sources of uncertainty

To assess the sources of the uncertainties in the end results (here the climate changes in MHQ produced by the HMs is studied; the results are similar for MQ) the ensemble is divided into four groups:

- GCM - This group consists of the two CLM simulations driven by different GCMs. However, as three realizations are available for the ECHAM5 GCM, there are three different

possible combinations to use here, i.e. CCCma3 paired with each ECAHM5 realization. The mean of all combinations was used for the assessment here.

- REA - This group consists of the different realizations of ECHAM5 as downscaled with the CLM RCM.
- RCM - This group consists of the WRF and CLM simulations driven by ECHAM5-R1.
- HM - This group consists of the three HMs.

To get a decent statistical sample from the relatively small ensemble, the calculations are performed over all catchments together.

Two standard statistical methods, namely ANOVA and Kruskal-Wallis, are used for testing whether the different groups are statistically different in their MHQ changes. The ANOVA method requires normally distributed data in each group, whereas the Kruskal-Wallis is non-parametric (in the sense that it requires no parameter dependent distribution, however the distributions for the different groups must still have the same kind of distribution). The distribution were found to be approximately normal for each group in WH, and positively skewed in SH. Furthermore, the different groups always produce similar distributions (not shown). This means that both of the statistical tests are applicable to the data at hand.

p-stat.	WH		SH	
	ANOVA	K-W	ANOVA	K-W
GCM	0.11	0.11	0.08	0.09
REA	0.00	0.00	0.19	0.22
RCM	0.37	0.08	0.00	0.00
HM	0.99	0.98	0.26	0.21

Table 4.12: The p-statistics for the ANOVA and Kruskal-Wallis tests applied to the ensemble groups. Here, a low value indicates a more signficant difference between the tested group and the others.

Table 4.12 shows the results of the two tests in the form of p-statistics. A value close to zero means that the group differs significantly from to the others (the null hypothesis of no difference between the tested group and the others can be rejected). Thus in winter, the main uncertainty can be attributed to the natural variability, as simulated with the different realizations, followed by the GCM used. The two statistics agree well on all groups, except for the RCM group which according to Kruskal-Wallis ranks before and for ANOVA after the GCMs. The HMs cannot be considered significantly different from the other groups, i.e. the uncertainty of the end result is not much affected by the HMs. In summer, the RCM group is clearly different from the other groups, followed by the GCM group, and on basically split third place the HM and REA groups.

To summarize, the tests have shown that the uncertainty in the future projections can be attributed mainly to the GCMs and RCMs. The natural variability is a large source of uncertainty for the near future, as it fluctuates at about the same amplitude as the climate change signals. Both the GCM and RCM groups are especially undersampled in this study, but points to important structural uncertainties in the model chain. Note, however, that one should be careful in drawing too strong conclusions from this analysis as the samples for the different group are generally very small. However, this uncertainty attribution is only valid for the climate change signal, which was our primary purpose. For the control as well as for the future period discharges, there is a large contribution of the HMs to the ensemble spread.

5 Discussion and Conclusions

The aims of this project were i) to assess if and how the flood discharges for medium to small size catchment areas in Germany will change in the near future (up to 2050), and ii) what uncertainty is associated with such a statement. We studied three catchment areas, two of them medium sized in low mountain ranges and a smaller one with more alpine characteristics; such catchments react faster to heavy precipitation than large catchments. To reproduce precipitation in a realistic manner (especially summertime convective precipitation), we used two non-hydrostatic RCMs at high spatial resolution (7 km). To quantify the uncertainty of the climate change signal, we used a ten member ensemble, in which the GCM-RCM-HM model chain was built with different GCMs, RCMs and HMs. Although the ensemble used is considered small in comparison to those used for weather prediction, it is one of the largest currently available RCM based ensembles at such a high resolution.

Although the climate change signal is weaker and the 30-year periods make it difficult to consider return periods longer than about 10–20 years, the near future period 2021–2050 was deliberately chosen for its planning relevance and its relative independence from uncertain scenario assumptions about future greenhouse gas emissions. Besides the more scientific result of showing the feasibility and added value of this kind of study, the results for the return periods considered here are of practical relevance to establish flood risk maps for planning and insurance purposes.

According to the ensemble results, the flood discharges remain at the present day level for the near future, or could even increase slightly, notably in the Ruhr catchment. However, single members show a much more pronounced signal.

Increased sophistication and skill of the models (GCMs, RCMs and HMs) can reduce the uncertainties, but only to a certain point; important processes are not sufficiently known, and probably will remain so for the foreseeable future. Multi-model ensembles enable to take this uncertainty into account, but it also requires the willingness and ability to deal with uncertain information.

It must be pointed out that this work was a pilot study combining the investigations of medium to small sized catchments with an ensemble of model chains including high resolution climate models. The study showed the feasibility and — considering the wide range of single results — also the necessity to perform this kind of work. It already indicates trends, but it could be put on a more firm basis and extended in several respects. Some of these are discussed below.

The ensemble: Although the results presented here already give an indication of the future prospects and are certainly much more informative and less error prone than results obtained with only one single simulation, there is a need for a larger and more balanced ensemble. The ensemble used is essentially an ensemble of opportunity, restricted by the availability of suitable GCM data and the need to fit the computing time for quite expensive simulations into the project time frame. The consequence is that the ensemble is quite small and biased towards a specific GCM and RCM. A larger ensemble would provide a better basis for statistical analyses. The majority of the ensemble members is based on ECHAM5 as a driving GCM and CLM as RCM, so it would be important to have more GCMs and RCMs available. Although there are indications that ensembles with about 20 members already capture the main variability, this requires the ensemble to be well distributed. However, such information is not available a priori and can only be ascertained through a larger ensemble size. For GCMs, it can be expected

that more datasets suitable for downscaling will be available in the future; for RCMs, apart from CLM and WRF, not many non-hydrostatic models required for the resolution used (high resolution seems to be a necessary, but not sufficient condition for realistic results at catchment scale) are available. This might be alleviated by using different setups and parameterizations in the available models. It will also be necessary to reduce the biases of the models. A large remaining problem is the required computing time, which considerably reduces the affordable ensemble size. Thus, the main goals should be to derive reliable information from small and possibly biased ensembles, to improve GCMs and RCMs, and to learn to deal with the remaining uncertainty.

Consequences for flood risk: The discharge at gauges varies considerably among the different ensemble members. However, discharge gives no direct information on the size of flooding areas, which is the relevant information in hazard assessments. Obtaining flood risk information requires the discharge information to be fed into hydraulic models, a step which was not included in the present project, but could be carried out with the available data.

Thus, the CEDIM-project "Flood Hazards in a Changing Climate" has shown that there are still large scientific challenges ahead, but at the same time it could already provide valuable information for e.g. water management purposes about trends for the near future, including - very importantly - uncertainty margins. The data produced in the project can be used for further studies, and the methods be applied to other catchments.

Acknowledgement

The authors acknowledge HLRS at the University of Stuttgart for use of the computing facilities under the two projects "High resolution climate modelling" (HRCM) and "High resolution regional climate modeling for Germany using WRF". For access to data records, the following institutions are acknowledged: Deutscher Wetterdienst, Hochwassernachrichtendienst Bayern, Potsdam Institut für Klimafolgenforschung, Ruhrverband, Sächsisches Landesamt für Umwelt, Landwirtschaft und Geologie, Wasserwirtschaftsamt Weilheim.

Abbreviations

AET	Actual evapotranspiration
b	Volume bias
CCCma3	Canadian Center for Climate Modelling and Analysis model version 3
CLM	Climate version of the COSMO (Consortium for Small-scale Modeling) model
DEM	Digital Elevation Model
DWD	Deutscher WetterDienst
NSE	Nash-Sutcliffe efficiency
ECHAM5	GCM model of MPI-M in Hamburg
E-OBS	Gridded observational data set of precipitation and temperature
fEff	Modified Nash-Sutcliffe coefficient
GCM	Global Climate Model (also General Circulation Model)
HE	Histogram Equalization
HM	Hydrological Model
HRU	Hydrological Response Unit
LAI	Leaf area index
MQ	Mean monthly discharge
MHQ	Mean monthly maximum discharge
PIK	Potsdam Institut für Klimafolgenforschung
PIK/DWD	Station data set for Germany
PET	Potential evapotranspiration
PRMS	Precipitation Runoff Modeling System
RCM	Regional Climate Model
R1–3	Marks the different realizations of the ECHAM5 GCM
SH	Summer Half-year
SWIM	Soil and Water Intergrated Model
WaSiM	Water balance Simulation Model
WH	Winter Half-year
WRF	Weather Research and Forecasting model

Bibliography

Arbeitskreis KLIWA. KLIWA (Heft 5) Langzeitverhalten der Lufttemperatur in Baden-Württemberg und Bayern. KLIWA-projekt A 1.2.3: Analyse zum Langzeitverhalten von Gebietsmittelwerten der Lufttemperatur. Technical report, Heft 5. URL http://www.kliwa.de/download/KLIWAHeft5.pdf.

Arbeitskreis KLIWA. KLIWA (Heft 8) Langzeitverhalten der Starkniederschläge in Baden-Württemberg und Bayern, KLIWA-Berichte Heft 8. Technical report, Heft 8. URL http://www.kliwa.de/download/KLIWAHeft8.pdf.

P. Berg, H. Feldmann, and H.-J. Panitz. Bias correction of high resolution RCM data. *J. Hydrol.*, submitted December 2011, 2011a.

P. Berg, S. Wagner, H. Kunstmann, and G. Schädler. High resolution RCM simulations for Germany: Part I - validation. *Clim. Dyn.*, submitted October 2011, 2011b.

S. Beurton and A. H. Thieken. Seasonality of floods in Germany. *Hydrolog. Sci. J.*, 54:62–76, 2009.

F. Boberg, P. Berg, P. Thejll, W. Gutowski, and J.H. Christensen. Improved confidence in climate change projections of precipitation further evaluated using daily statistics from ENSEMBLES models. *Climate Dynamics*, 35:1509–1520, 2010.

H. Bormann, N. Pinter, and S. Elfert. Hydrological signatures of flood trends on German rivers: Flood frequencies, flood heights and specific stages. *Journal of Hydrology*, 404(1–2):50–66, 2011.

Th. Brudy-Zippelius. Wassermengenbewirtschaftung im Einzugsgebiet der Ruhr: Simulation und Echtzeitbetrieb. Technical report, Mitteilungen des Instituts fr Wasserwirtschaft und Kulturtechnik der Universitt Karlsruhe (TH), 2003.

J. H. Christensen, B. Hewitson, A. Busuioc, A. Chen, X. Gao, I. Held, R. Jones, R. K. Kolli, W.-T. Kwon, R. Laprise, V. Magaa Rueda, L. Mearns, C.G. Menndez, J. Risnen, A. Rinke, A. Sarr, and P. Whetton. Regional climate projections. in: Climate change 2007: The physical science basis. contribution of working group I to the fourth assessment report of the intergovernmental panel on climate change, 2007.

O. B. Christensen and J. H. Christensen. Intensification of extreme European summer precipitation in a warmer climate, 2004.

J. Cullmann. *Online flood forecasting in fast responding catchments on the basis of a synthesis of artificial neural networks and process models.* PhD thesis, Technische Universität Dresden, 2006.

R. Dankers and L. Feyen. Climate change impact on flood hazard in Europe: An assessment based on high-resolution climate simulations. *Journal of Geophysical Research-Atmospheres*, 113(D19):17pp., 2008.

G. Doms and U Schättler. A description of the nonhydrostatic regional model LM, part I: Dynamics and numerics. *COSMO Newsletter*, 2:225–235, 2002.

Q. Y. Duan. Optimal use of the SCE-UA global optimization method for calibrating watershed models. *Journal of Hydrology*, 158(3-4):265–284, 1994.

Q. Y. Duan, S. Sorooshian, and V. K. Gupta. Effective and efficient global optimization for conceptual rainfall-runoff models. *Water Resources Research*, 28(4):1015–1031, 1992.

Q. Y. Duan, V. K. Gupta, and S. Sorooshian. Shuffled complex evolution approach for effective and efficient global minimization. *Journal of Optimization Theory and Applications*, 76(3): 501–521, 1993.

H. Feldmann, G. Schädler, H.-J. Panitz, and Ch. Kottmeier. Near future changes of heavy precipitation over complex terrain derived from high resolution RCM ensemble simulations. *Int. J. of Climatology*, submitted, 2011.

C. Frei, R. Schöll, S. Fukutome, J. Schmidli, and P. L. Vidale. Future changes of precipitation extremes in Europe: Intercomparison of scenarios from regional climate models. *Journal of Geophysical Research-Atmospheres*, 111(D6):22pp., 2006.

L. P. Graham, S. Hagemann, S. Jaun, and M. Beniston. On interpreting hydrological change from regional climate models. *Climatic Change*, 81:97–122, 2007.

W. Haude. Über die Verwendung verschiedener Klimafaktoren zur Berechnung der potentiellen Evaporation und Evapotranspiration. *Met. Rundschau*, 11, 1958.

M. Haylock, N. Hofstra, A. M. G. K. Tank, E. J. Klok, P. D. Jones, and M. New. A European daily high-resolution gridded dataset of suface temperature, precipitation and sea-level presssure. *J. Geophys. Res.*, 113:D20119.1–D20119.12, 2008.

J. Höfer, J. Liebert, P. Preuß, J. Ihringer, S. Patzke, and D. Schwanenberg. Hochwasserschutzwirkung der Talsperren im Einzugsgebiet der Ruhr bei ganzjährigem Betrieb unter Berücksichtigung klimabedingter Abflussänderungen einschließlich der konkurrierenden Nutzungen. Mit den Teilprojekten: Ermittlung der Hochwassersicherheit im Ruhreinzugsgebiet (KIT, IWG) und Erweiterung der Klimaanalyse für das Ruhrtalsperrensystem (Deltares). Technical report, Ruhrverband, Essen, 2010.

R. Hurksman, W. Terink, R. Uijlenhoet, P. Torfs, D. Jacob, and P. A. Troch. Changes in streamflow dynamics in the Rhine basin under three high-resolution regional climate scenarios. *Journal of Climate*, 23(3):679–699, 2010.

K. Jasper, J. Gurtz, and H. Lang. Advanced flood forecasting in alpine watersheds by coupling meteorological observations and forecasts with a distributed hydrological model. *Journal of Hydrology*, 267:40–52, 2002.

J. S. Kain. The Kain-Fritsch convective parameterization: An update. *J Appl Meteor*, 43: 170–181, 2004.

A. L. Kay, H. N. Davies, V. A. Bell, and R. G. Jones. Comparison of uncertainty sources for climate change impacts: flood frequency in England. *Climatic Change*, 92(1–2):41–63, 2009.

V. Krysanova, D. I. Muller-Wohlfeil, and A. Becker. Development and test of a spatially distributed hydrological water quality model for mesoscale watersheds. *Ecological Modelling*, 106(2–3):261–289, 1998.

V. Krysanova, F. Wechsung, J. Arnold, R. Srinivasan, and J. Williams. SWIM (Soil and Water Integrated Model), User Manual. Technical report, PIK, 2000.

H. Kunstmann, K. Schneider, R. Forkel, and R. Knoche. Impact analysis of climate change for an Alpine catchment using high resolution dynamic downscaling of ECHAM4 time slices. *Hydrol. Earth Syst. Sc.*, 8(6):1030–1044, 2004.

H. Kunstmann, A. Heckl, and A. Rimmer. Physically based distributed hydrological modelling of the Upper Jordan catchment and investigation of effective model equations. *Advances in Geosciences*, 9:123–130, 2006a.

H. Kunstmann, J. Krause, and S. Mayr. Inverse distributed hydrological modelling of alpine catchments. *Hydrology and Earth System Sciences*, 10(3):395–412, 2006b.

G. H. Leavesley and Stannard L. G. The Precipitation-Runoff-Modeling-System — PRMS. In V.P. Singh, editor, *Water Resources Publications: Computer Models of Watershed Hydrology*, 1995.

G. H. Leavesley, R. W. Lichty, B. M. Troutman, and L. G. Saindon. Precipitation-runoff modeling system. users manual: Report 83-4238. Technical report, U.S. Geological Survey Water-Resources Investigations, 1983.

LfULG. Hochwasser 2002 im Muldegebiet. Technical report, 2009.

A. H. T. Linde, J. Aerts, A. M. R. Bakker, and J. C. J. Kwadijk. Simulating low-probability peak discharges for the Rhine basin using resampled climate modeling data. *Water Resources Research*, 46:19pp., 2010.

R. Ludwig. Die flächenverteilte Modellierung von Wasserhaushalt und Abflussbildung im Einzugsgebiet der Ammer. *Münchener Geographische Abhandlungen*, B32:169pp., 2000.

A. Marx, H. Kunstmann, A. Bárdossy, and J. Seltmann. Radar rainfall estimates in an alpine environment using inverse hydrological modelling. *Advances in Geosciences*, 9:25–29, 2006.

L. Menzel and G. Burger. Climate change scenarios and runoff response in the Mulde catchment (southern Elbe, Germany). *Journal of Hydrology*, 267(1–2):53–64, 2002.

B. Merz, K. Kaiser, O. Bens, R. Emmermann, H. Flühler, U. Grünewald, and J. F. W. Negendank. Klimawandel und Wasserhaushalt. In *Georessource Wasser Herausforderung globaler Globaler Wandel. Beiträge zu einer nachhaltigen Wasserressourcenbewirtschaftung in Deutschland*. acatech/Springer, München/Berlin, 2012.

J. L. Monteith. *Vegetation and the Atmosphere, Vol. 1: Principles*. Academic Press, London, 1975.

N. Nakicenovic, J. Alcamo, G. Davis, B. de Vries, J. Fenhann, S. Gaffin, K. Gregory, A. Grbler, T. Y. Jung, T. Kram, E. L. L. Rovere, L. Michaelis, S. Mori, T. Morita, W. Pepper, H. Pitcher, L. Price, K. Riahi, A. Roehrl, H.-H. Rogner, A. Sankovski, M. Schlesinger, P. Shukla, S. Smith, R. Swart, S. van Rooijen, N. Victor, and Z. Dadi. *Special Report on Emissions Scenarios: A Special Report of Working Group III of the Intergovernmental Panel on Climate Change*. Cambridge University Press, Cambridge, U.K, 2000.

J. E. Nash and J. V. Sutcliffe. River flow forecasting through conceptual models part I a discussion of principles. *Journal of Hydrology*, 10(3):282–290, 1970.

H. Österle, F.-W. Gerstengarbe, and P. C. Werner. Ein neuer meteorologischer Datensatz für Deutschland, 1951-2003. Technical report, Potsdam Institut für Klimafolgenforschung, 2006.

S. Pakosch. *Development of a fuzzy rule based expert system for flood forecasts within the meso-scale Upper Main basin*. PhD thesis, Universität der Bundeswehr München, 2011.

T. Petrow and B. Merz. Trends in flood magnitude, frequency and seasonality in Germany in the period 1951-2002. *Journal of Hydrology*, 371(1–4):129–141, 2009.

T. Petrow, B. Merz, K.-E. Lindenschmidt, and A. H. Thieken. Aspects of seasonality and flood generating circulation patterns in a mountainous catchment in south-eastern Germany. *Hydrology and Earth System Sciences*, 11(4):1455–1468, 2007.

C. H. B. Priestley and J. Taylor. On the assessment of surface heat flux and evaporation using large-scale parameters. *Monthly Weather Review*, 100(2):81–92, 1972.

T. Reichler and J. Kim. How well do coupled models simulate today's climate? *BAMS*, March: 303–311, 2008.

L. A. Richards. Capillary conduction of liquids through porous medium. *Physics*, 1:318–333, 1931.

J. T. Ritchie. Model for predicting evaporation from a row crop with incomplete cover. *Water Resources Research*, 8(5):1204–1213, 1972.

G. Röckner, G. Baeuml, L. Bonaventura, R. Brokopf, M. Esch, M. Giorgetta, S. Hagemann, I. Kirchner, L. Kornblueh, E. Manzini, A. Rhodin, U. Schlese, U. Schulzweida, and A. Tompkins. The atmospheric general circulation model ECHAM 5. PART I: Model description. Technical report, MPImet/MAD Germany, 2003.

G. Schädler, H. Feldmann, H.-J. Panitz, Ch. Kottmeier, and B. Früh. Hochauflösende regionale Simulationen künftiger Starkniederschlagsereignisse in Baden-Württemberg (ReSiPrec). Technical report, IMK-TRO, KIT, 2010. URL http://www.herausforderung-klimawandel-bw.de/images/stories/ReSiPrec_Schlussbericht_Herausforderung_Klimawandel.pdf.

J. Schulla. *Hydrologische Modellierung von Flussgebieten zur Abschätzung der Folgen von Klimaänderungen*. PhD thesis, ETH Zürich, 1997.

J. Schulla and K. Jasper. Model Description WaSiM-ETH. Technical report, ETH Zürich, 2007.

A. H. Schumann. Hochwasserstatistische Bewertung des Augusthochwassers 2002 im Einzugsgebiet der Mulde unter Anwendung der saisonalen Statistik. *Hydrologie und Wasserbewirtschaftung*, 49/4:200–206, 2005.

J. F. Scinocca, N. A. McFarlane, M. Lazare, J. Li, and D. Plummer. The CCCma third generation AGCM and its extension into the middle atmosphere. *Atmos Chem and Phys*, 8: 7055–7074, 2008.

W. C. Skamarock, J. B. Klemp, J. Dudhia, D. O. Gill, D. M. Barker, M. G. Duda, X. Huang, W. Wang, and J. G. Powers. A Description of the Advanced Research WRF Version 3. Technical Report 459, NCAR, Boulder, Colorado, USA, 2008.

G. Smiatek, H. Kunstmann, R. Knoche, and A. Marx. Precipitation and temperature statistics in high-resolution regional climate models: Evaluation for the European Alps. *J. Geophy. Res.*, 114:16pp., 2009. doi: 10.1029/2008JD011353.

K. Sturm, R. Glaser, J. Jacobeit, M. Deutsch, Brázdil R., Ch. Pfister, Luterbacher J., and H. Wanner. Hochwasser in Mitteleuropa seit 1500 und ihre Beziehung zur atmosphärischen Zirkulation. *Petermann Geogr. Mitt.*, 145:14–23, 2001.

S. Taschner. *Flood modelling in the Ammer watershed using coupled meteorological and hydrological models*. PhD thesis, Ludwig-Maximiliansuniversitt München, 2003.

A. H. Thieken, T. Petrow, H. Kreibich, and B. Merz. Insurability and mitigation of flood losses in private households in Germany. *Risk Analysis*, 26(2):383–395, 2006.

M. Tiedtke. A comprehensive mass flux scheme for cumulus parameterization in largescale models. *Mon Weather Rev*, 117:1779–1800, 1989.

S. Trömel and C.-D. Schönwiese. Probability change of extreme precipitation observed from 1901 to 2000 in Germany. *Theor. Appl. Climatol.*, 87:29–39, 2007.

N. Veijalainen, E. Lotsari, Petteri Alhob, and Jukka Käyhköb Bertel Vehviläinena. National scale assessment of climate change impacts on flooding in Finland. *Journal of Hydrology*, 391(3–4):333–350, 2010.

G. Villarini, J. A. Smith, F. Serinaldic, and A. A. Ntelekosb. Analyses of seasonal and annual maximum daily discharge records for central Europe. *Journal of Hydrology*, 399(3–4):299–312, 2011.

S. Wagner, H. Kunstmann, A. Bárdossy, C. Conrad, and R. R. Colditz. Water balance estimation of a poorly gauged catchment in West Africa using dynamically downscaled meteorological fields and remote sensing information. *Physics and Chemistry of the Earth, Parts A/B/C*, 34(4-5):225–235, 2009.

S. Wagner, P. Berg, G. Schädler, and H. Kunstmann. High resolution RCM simulations for Germany: Part II - projected climate changes. *Clim. Dyn.*, submitted October 2011, 2011.

R. L. Wilby and I. Harris. A framework for assessing uncertainties in climate change impacts: Low-flow scenarios for the river Thames, UK. *Water Resources Research*, 42(2):10pp., 2006.

T. Wilby, L. E. Hay, W. J. Gutowski, R. W. Arritt, E. S. Takle, Z. Pan, G. H. Leavesley, and M. P. Clark. Hydrological response to dynamically and statistically downscaled climate model output. *Geophys. Res. Lett.*, 27(8):1199–1202, 2000.

D. Yang and S. Ishida. Bias correction of daily precipitation measurements for Greenland. *J. Geophys. Res.*, 104(D6):6171–6181, 1999.

S. Zacharias, H. Bogena, L. Samaniego, M. Mauder, R. Fuß, T. Pütz, M. Frenzel, M. Schwank, C. Baessler, K. Butterbach-Bahl, O. Bens, E. Borg, A. Brauer, P. Dietrich, I. Hajnsek, G. Helle, R. Kiese, H. Kunstmann, S. Klotz, J. C. Munch, H. Papen, E. Priesack, H. P. Schmid, R. Steinbrecher, U. Rosenbaum, G. Teutsch, and H. Vereecken. A network of terrestrial environmental observatories in germany. *Vadose Zone Journal*, 10(3):955–973, 2011.

O. Zolina, C. Simmer, A. Kapala, S. Bachner, S. Gulev, and H. Maechel. Seasonally dependent changes of precipitation extremes over Germany since 1950 from a very dense observational network. *JGR*, 113:D06110, 2008.

Contact

Center for Disaster Management and Risk Reduction Technology

CEDIM Head Office
Karlsruhe Institute of Technology
Hertzstrasse 16
D-76187 Karlsruhe

Phone: +49 721 608-44436
Fax: +49 721 71173

E-Mail: cedim@gpi.uka.de

For further information about CEDIM and
online map server Risk-Explorer please visit:

www.cedim.de